THE UNIVERSITY OF CHICAGO

CHROMOSOME INVERSIONS AND AVIAN SPECIATION

A DISSERTATION SUBMITTED TO
THE FACULTY OF THE DIVISION OF THE BIOLOGICAL SCIENCES
AND THE PRITZKER SCHOOL OF MEDICINE
IN CANDIDACY FOR THE DEGREE OF
DOCTOR OF PHILOSOPHY

COMMITTEE ON EVOLUTIONARY BIOLOGY

BY
DANIEL MARC HOOPER

CHICAGO, ILLINOIS
AUGUST 2017

In nature, the isolation between
sibling species is seldom absolute.

Jonathan Weiner
Beak of the Finch

Why are inversions not everywhere? One possibility is that they in fact are, and that their frequency has been greatly underestimated.

Mark Kirkpatrick and Nick Barton

Contents

List of Figures

List of Tables

Acknowledgements

My thesis advisor Dr. Trevor Price was an essential guiding force in shaping the development of my research ideas and my approach as a scientist. My seven-year tenure as a member of the Price Lab under his tutelage was instrumental in the successes I have had as a PhD student. I am further indebted to my doctoral thesis committee for their advice and counsel in the development of this research programme – Dr. Andrew Hipp, Dr. Richard Hudson, Dr. Marcus Kronforst, and Dr. Molly Przeworski. The Committee on Evolutionary Biology at the University of Chicago has been a consistently supportive institution to incubate and foster my research ideas. Dr. Mark Kirkpatrick has been a powerful force in motivating my research interests and his feedback on the earlier results of this doctoral work were much appreciated. I was hosted at the Columbia University laboratory of Dr. Molly Przeworski in New York City for four weeks in 2014 in order to learn their bioinformatics pipeline and am additionally thankful for the help of Dr. Sonal Singhal and Dr. Minyoung Wyman while there. The vast majority of labwork for this dissertation occurred at the Pritzker Laboratory for Molecular Systematics and Evolution at the Field Museum of Natural History, Chicago, Illinois, USA. All samples sourced from Australia were brought into the United States through the Birds Division at the Field Museum. I am thus deeply indebted for the assistance from the following members of the Field Museum: Dr. John Bates, Dr. Kevin Feldheim, Dr. JP Huang, Dr. Shannon Hackett, Dr. Ben Marks, and Dr. Erica Zahnle. I must also thank Dr. Molly Schumer and Josh Penalba for their advice with experimental design and laboratory logistics.

Field research was essential for the examination of hybrid zone dynamics and the characterization of inversion polymorphisms in the long-tailed finch system and would not have been possible without the financial, logistical, and materials support of Dr. Simon Griffith. Coping with the daily rigors of working in the Northern Territory was made possible by the countless contributions of Dr. Peri Bolton, Dr. Terry Burke, Kyle Kostrzewa, and Dylan Meyer.

Tissue samples were generously shared for this dissertation from the Kansas University Biodiversity Institute and Natural History Museum and the Australian National Wildlife Collection, Canberra, Australia – Dr. Leo Joseph at CSIRO for sharing such important tissue

samples of estrildid finches. I thank Dr. Nina Bulatova, Dr. Belinda Chang, Dr. Edmundo de Lucca, Dr. Georgy Semenov, Dr. Yuchun Wu, Portia Tang, Iuri Ventura, and the University of Chicago Library for their help in accessing cytological studies not available online. All original artwork used in the figures of this dissertation were painted by the immensely talented Dr. Allison Johnson.

Many institutions and individuals financially supported this work, including: the National Geographic Society (Young Explorers Grant #9270-13), the American Ornithologists' Union Hesse Student Research Award, the Committee on Evolutionary Biology Henry Hinds Fund, the Committee on Evolutionary Biology fund for research in the Pritzker Laboratory for Molecular Systematics and Evolution at the Field Museum of Natural History, the National Science Foundation (DDIG1601323 to Dr. Trevor Price and myself), and the Australian Research Council (DP0881019 to Dr. Simon Griffith).

Many current and former members of the graduate student and post-doctoral community at the University of Chicago were instrumental in the development of this dissertation and in the maintenance of my sanity and good humor: Dr. Natasha Bloch, Dr. Elizabeth Eakin, Dr. Deren Eaton, Dr. Allison Johnson, Dr. Jon Kennedy, Dr. Ellen Leffler, Dr. Daniel Matute, Dr. Darli Massardo, Dr. Wynn Meyer, Dr. Elizabeth Scordato, Dr. Dai Shizuka, Dr. Nicholas VanKuren, Dr. David Wheatcroft, Dr. Erica Westerman, and Dr. Max Winston; Brett Aiello, Hussein Al-Asadi, Shane Dubay, Victoria Flores, Evan Koch, Dallas Krentzel, Simon Lax, Peter Lido, Daniela Palmer, Jenn Stanley, Supriya, and Alex White.

Introduction

Speciation, the process by which new species arise, is associated not only with the accumulation of molecular changes in DNA composition but often also with physical rearrangements in chromosome structure. Chromosome inversions, one common type of chromosomal rearrangement that occurs when a chromosome breaks at two points and the area between those breakpoints is repaired in the opposite orientation, are regularly observed as fixed differences between species and as polymorphisms segregating within species (Hoffmann and Rieseberg, 2008; Faria and Navarro, 2010). Inversions were first discovered by Alfred Sturtevant in 1921 (Sturtevant, 1921) and have since been found to propel the evolution of sex chromosomes (Lemaitre et al., 2009; Wilson et al., 2009; Wright et al., 2014), supergene formation (Kunte et al., 2014; Küpper et al., 2015; Lamichhaney et al., 2015; Tuttle et al., 2015; Kim et al., 2017; Knief et al., 2017), local adaptation (Anderson et al., 2005; Lowry and Willis, 2010; Joron et al., 2011; Jones et al., 2012), and reproductive isolation (Rieseberg, 2001; Noor et al., 2001; Brown et al., 2004; Ayala et al., 2012; Fishman et al., 2013). Despite their evolutionary significance, the widespread presence of inversions is in some ways puzzling, as new rearrangements may be initially disfavored due to structural underdominance in heterokaryotypes, if crossing over within the inverted region during meiosis results in the production of aneuploid gametes (Hoffmann and Rieseberg, 2008; Faria and Navarro, 2010; King, 1993). Reconciling the widespread presence of chromosome inversions with possible selective disadvantages that a new inversion faces remains an unsolved problem and largely motivated this dissertation.

Birds have long been used as models of speciation and are perhaps the best-studied group with respect to how behavior and ecology contribute to population divergence (Price, 2008; Grant and Grant, 2011) but little attention has been given to the role of chromosome rearrangements to bird speciation (Price, 2008; Ellegren, 2010; 2013). Indeed, the gross physical structure of the avian genome is highly conserved with the most easily observed types of macro-rearrangements (fusions, fissions, translocations, etc.), which so often distinguish the karyotypes of species in other taxonomic groups, are relatively rare in birds. As such, karyotype evolution has generally been considered to be an unrelated and unimportant aspect of avian diversification (reviewed in Ellegren, 2010; 2013). Chromosome inversions, however, appear to occur regularly

in birds. Comparative cytological investigations of avian karyotypes regularly detect chromosome inversion differences between and within species based on rearrangement to chromosome banding patterns and/or centromere movement (reviewed in Shields, 1982; Christidis, 1990). Recent comparative genomic analyses of both distantly and closely related avian taxa support the findings of earlier cytological studies in detecting large numbers of inversions differences both pericentric, inversions that include the centromere, and paracentric, inversions that do not include the centromere, in nature (Skinner and Griffin, 2011; Kawakami et al., 2014; Zhang et al., 2014; Singhal et al., 2015).

Why are chromosomal inversions so common? Insights from chromosome inversion polymorphisms, commonly observed in cytological studies (Shields, 1982; Hooper and Price, 2015; Hooper and Price 2017), are limited but revealing as they have only recently been characterized using genomic approaches in three bird species: polymorphic inversions have been implicated as supergenes governing alternative reproductive strategies in all three of which (the ruff *Philomachus pugnax*, Küpper et al., 2015; Lamichhaney et al., 2015; the white-throated sparrow *Zonotrichia albicollis,* Tuttle et al., 2015; and the zebra finch *Taeniopygia guttata*, Kim et al., 2017; Knief et al., 2017). Remarkably, four chromosomes in the zebra finch have chromosome inversions segregating on them and while inversions on the Z chromosome appear to be intimately involved in alternative sperm morphologies (Kim et al., 2017; Knief et al., 2017) the three others upon autosomal chromosomes are of yet undetermined importance (Knief et al., 2016). Moreover, the evolutionary significance of the frequent fixed inversion differences between bird species has remained largely understudied.

Here, I have made efforts in the course of this dissertation in order to better understand the evolutionary dynamics underlying chromosome inversion evolution in birds through i) a synthesis of classic cytological data placed in a phylogenetic context in order to evaluate support for alternative theoretical models of inversion evolution (Chapters 1 and 2) and ii) a genomic assessment of an avian hybrid zone where inversion polymorphism on the Z chromosome may underlie the maintenance of reproductive isolation between hybridizing taxa (Chapter 3).

Background

Study system

The Passeriformes are just one of 39 extant orders of birds yet comprise over half of all avian species diversity, with the ~6000 taxa found in nearly every terrestrial habitat on the planet (del Hoyo, 2011). The radiation has produced a large variety of ecological and morphological types: body size varies >350-fold between the smallest and largest species (4.2 g to 1,500 g) while variation in beak shape and behavior has produced a wide spectrum of feeding morphologies (nectarivores, granivores, insectivores, frugivores, etc.; del Hoyo, 2011; Price et al., 2014). Cytological studies of passerine karyotypes over the past five decades have been conducted for approximately 7% of species (428 of ~6,000 species; see Section 4 below) but this large body of data have not been analyzed holistically in any comprehensive way. In line with the general avian condition, while large macro-rearrangements to karyotype structure, like fusions and fissions, occur quite rarely in passerines, chromosomal inversions have been documented between and within taxa far more frequently.

This dissertation is organized in such a way as to examine support for the general trends of inversion evolution within birds before more explicitly testing these predictions directly. Indeed, I focus on the evolutionary dynamics of chromosome inversion evolution within passerines broadly in order to, first, take advantage of the large body of cytological literature available for them (Chapters 1 and 2) before, second, taking a narrower focus upon an active hybrid zone in a clade of grassfinches (family Estrildidae) where species often show pericentric inversion differences between each taxa (Chapter 3). A major benefit of studying members of the Estrildidae comes from the genomic resources available for the zebra finch, the first passerine to have its genome sequenced and assembled (Warren et al., 2010).

The long-tailed finch (*Poephila acuticauda*) is an Australian grassfinch endemic to the northern tropics and comprises two subspecies that differ in bill color (yellow in western subspecies *acuticauda* and red in eastern subspecies *hecki*) and which hybridize where their ranges overlap in the Northern Territory. Hybrid offspring between subspecies have intermediately colored orange bills (Higgins et al., 2006), intergradation in bill color in the wild is restricted to a

hybrid zone where their ranges meet, and sperm length and shape varies significantly between subspecies (Rowe et al., 2015). Christidis (1986a) on the basis of cytological surveys identified 5 alternative forms of the Z chromosome, products of both pericentric and paracentric chromosome inversion, segregating in a mixed sample of long-tailed finches. An initial assessment of genomic differentiation between members of each subspecies found that while autosomal divergence between taxa is generally low, the Z chromosome is enriched for fixed nucleotide differences (Singhal et al., 2015). Thus, the long-tailed finch provides an ideal system with which to examine the significance of chromosome inversions to the process of speciation. In Chapter 3, I take a reduced representation comparative genomics approach, using samples collected from across nearly the entire range of the species and with special focus on hybrid zone populations of the long-tailed finch, in order to evaluate i) the geographic location and extent of bill color admixture between subspecies, ii) the genomic basis for bill color, iii) which regions of the genome appear to be under selection to prevent hybridization, and iv) whether chromosome inversions show evidence of playing a role in maintaining subspecific divergence.

1 Rates of karyotypic evolution in Estrildid finches differ between island and continental clades[1]

1.1 Abstract

Reasons why chromosomal rearrangements spread to fixation and frequently distinguish related taxa remain poorly understood. We used cytological descriptions of karyotype to identify large pericentric inversions between species of Estrildid finches (family *Estrildidae*) and a time-dated phylogeny to assess the genomic, geographic, and phylogenetic context of karyotype evolution in this group. Inversions between finch species fixed at an average rate of one every 2.26 My. Inversions were twice as likely to fix on the sex chromosomes compared to the autosomes. A high repeat density on the sex chromosomes may increase mutation rates, but other explanations via mutagenic input are not supported, as the number of inversions on a chromosome does not correlate with its length or map size. Inversions have fixed 3.3× faster in three continental clades than in two island chain clades, and fixation rate correlates with both range size and the number of sympatric species pairs. These results point to adaptation as the dominant mechanism driving fixation and suggest a role for gene flow in karyotype divergence. A review shows that the rapid karyotype evolution observed in the Estrildid finches appears to be more general across birds, and by implication other understudied taxa.

1.2 Introduction

Chromosome inversions are often fixed between closely related species as well as found segregating as polymorphisms within species (Coyne and Orr, 2004; Hoffmann and Rieseberg, 2008; Faria and Navarro, 2010). Once established, inversions can foster divergence between populations (Anderson et al., 2005; Lowry and Willis, 2010; Jones et al., 2012) and aid in the

[1] A version of this chapter has been published as: Hooper DM and TD Price. 2015. Rates of karyotypic evolution in Estrildid finches differ between island and continental clades. Evolution 69: 890-903.

speciation process (Rieseberg et al., 2001; Noor et al., 2001; Brown et al., 2004; Joron et al., 2011; Ayala et al., 2013; Fishman et al., 2013; Poelstra et al., 2014) by creating barriers to gene flow through the suppression of recombination and/or the induction of structural underdominance in heterokaryotypes. It remains unclear why rearrangements evolve so frequently in some taxa and by what mechanisms, especially as new inversions are often thought to have deleterious fitness effects due to structural underdominance (Stebbins, 1958; White, 1969; White, 1978; King, 1987; Rieseberg, 2001).

Mechanisms proposed to explain the fixation of novel underdominant rearrangements involve both genetic drift and natural selection. As described by Lande (1979), drift within a deme may counter selection and raise the rearrangement above a frequency of 50%, whereupon selection drives it to fixation. Fixation rate in a species is affected by deme size, but not the total population size of the species. The reason population size does not affect fixation rate is that, after becoming established in one deme, the probability that a rearrangement will fix is equal to the inverse of the total number of demes, but the more demes there are the greater the chance that an inversion becomes established in at least one deme. As in classic models of genetic drift (Kimura, 1962) the two effects cancel out and the fixation rate for a species is approximately independent of its population size, although this result depends on assumptions about population structure and the deme where the rearrangement originated (Lande, 1979; Lande, 1985; Hedrick, 1981; Walsh, 1982; Spirito, 1998). In contrast to the spread of an underdominant rearrangement, if a rearrangement is inherently deleterious its fixation probability within a species should decrease with population size and only realistically occur when population sizes are small (Kimura, 1962; Ohta, 1972; Whitlock et al., 2004).

Chromosome rearrangements may also become established entirely by positive selection. In this case, a rearrangement can spread to fixation if (1) its breakpoints favorably alter gene expression (Wesley and Eanes, 1994; Puig et al., 2004), (2) it increases linkage between epistatically interacting sets of genes (Dobzhansky, 1951), (3) it increases linkage between locally adapted alleles within a population experiencing gene flow from a divergently adapted population (Charlesworth and Charlesworth, 1979; Ortiz-Barrientos et al., 2002; Navarro and Barton, 2003; Kirkpatrick and Barton, 2006; Feder et al., 2011). In this last scenario, gene flow plays a creative role in karyotype evolution because of the selective advantage in keeping locally adapted

alleles together. Adaptive models include those external to the individual, as implied in the mechanisms described above, as well as those resulting from genomic conflicts. For example, meiotic drive may favor the spread of a rearrangement if it is associated with a set of interacting alleles that together affect segregation distortion (White, 1978; King, 1993). Whenever adaptive mechanisms operate, the fixation rate of a novel rearrangement should increase with population size, as the process is mutation-limited. Here, we evaluate fixation rates of large chromosomal inversions in a family of birds, and consider the possible roles of population size and gene flow.

Birds have long been used as models of speciation and are perhaps the best-studied group with respect to how behavior and ecology contribute to population divergence (Price, 2008; Grant and Grant, 2011) but little attention has been given to the possible role of chromosome rearrangements in bird speciation (Price, 2008; Ellegren, 2013). This may be because the gross architecture of avian genomes are conserved, with inter-chromosomal rearrangements such as fusions, fissions, and translocations between species occurring rarely (Takagi and Sasaki, 1974; Griffin et al., 2007; Ellegren, 2010; Ellegren, 2013; Zhang et al., 2014). For example, diploid chromosome number (2N) for birds typically varies between 76 and 80. However, in some clades 2N is much more variable, notably for finches in the genus *Pytilia* (Christidis, 1983), parrots (Nanda et al., 2007), birds of prey (Bed'Hom et al., 2003; de Oliveira et al., 2005; Nanda et al., 2006; Nishida et al., 2008; 2014), and one shorebird, the stone curlew (*Burhinus oedicunemus*; Nie et al., 2009; Hansmann et al., 2009).

In contrast to the general conservation of chromosome number and lack of inter-chromosomal rearrangements, the cytological literature suggests that intra-chromosomal rearrangements, notably inversions, occur more frequently (reviewed in Shields, 1982; Christidis, 1990; Price, 2008, ch. 16; Völker et al., 2010; Skinner and Griffin, 2011; Lithgow et al., 2014, and see Tables 3 and S6). These findings are supported by recent comparative genomics studies that report large numbers of inversions (10s to 100s) between distantly related species (Stapley et al., 2008; Hansson et al., 2009; Aslam et al., 2010; Backström et al., 2010; Kawakami et al., 2014; Zhang et al., 2014). After whole genome alignment Kawakami et al. (2014) identified 140 inversions at a median size of ~2 Mb that distinguish zebra finch (*Taeniopygia guttata*) from collared flycatcher (*Ficedula albicollis*), two species that last shared a common ancestor ~30 Ma

(divergence date inferred from Price et al., 2014). From this, we estimate a fixation rate as fast as one every 0.5 My along the lineage leading to the zebra finch.

Typically a fifth of avian chromosomes are large in size (macro-chromosomes 160-60 Mb) and easily distinguishable cytogenetically. The remaining chromosomes are smaller (micro-chromosomes <40 Mb) and the smallest of these are often indistinguishable using standard cytological approaches (Masabanda et al., 2004; Ellegren, 2013). Here, we examine fixation of large cytologically detectable inversions across 32 species of Estrildid finches (order *Passeriformes*). We use published cytological analyses of the Estrildids, which have described inversion differences between species and polymorphisms within species (Prasad and Patnaik, 1977; Christidis, 1983; 1986a; 1986b; 1987; Itoh and Arnold, 2005). 2N is either 76 or 78 for all Estrildid finches examined except one (the red-winged pytilia, *Pytilia phoenicoptera*, 2N = 56). Seven chromosomes including the Z can be considered macro-chromosomes and the remaining micro-chromosomes. The Z chromosome is the 4th largest while the W is typically 8th in size. The degree of karyotype similarity between species varies considerably and some genera appear to have more labile karyotypes than others (Christidis, 1986a; 1986b). A preliminary analysis using a phylogeny for a subset of the karyotyped Estrildid species estimated that the fixation of cytologically detectable pericentric inversions occurred every 2.92 My along a lineage (Price, 2008, pp. 386-388). We expand on this analysis using a time-dated tree to ask how variation in the rate of inversion fixation differs among chromosomes and is associated with demographic and geographic differences between species.

1.3 Materials and Methods

The family *Estrildidae* contains approximately 140 species distributed across the Old World tropics and southern hemisphere temperate zone (Goodwin and Woodcock, 1982; Sorenson et al., 2004). The Estrildid finches originated in Africa (Sorenson et al., 2004; Sorenson, *pers. comm.*) and their subsequent dispersion and diversification across the Old World have produced 7 discrete radiations that vary extensively in average population size and degree of sympatry between member species (Goodwin and Woodcock, 1982).

1.3.1 Identifying inversions

We primarily use the data of Christidis (1983; 1986a; 1986b; 1987) supplemented by others (Table S1) who describe gross karyotype structure (Tables S2). These authors used Giemsa staining and C- and G-banding techniques to document large inversions, both pericentric (those encompassing the centromere) and paracentric (not encompassing the centromere). Sample size varied across species (maximum of 21 individuals for *Bathilda ruficauda* and just one for three species) with an average of 6.7 karyotyped individuals per taxon (Table S1).

We converted centromere position and banding pattern for the 6 autosomal macro-chromosomes, the 5 largest autosomal micro-chromosomes, and both sex chromosomes into character state data for each species (Table S2). Using published figures, we identified homologous chromosomes between species by chromosome-diagnostic banding patterns and scored them for approximate centromere position (i.e., whether they were metacentric, sub-metacentric, sub-telocentric, or telocentric), following the naming conventions established by Levan et al. (1964). We treated chromosome conformations as distinct when species shared the same general classification (e.g., both were sub-metacentric) but the author of the paper noted that the banding pattern flanking the centromere differed. We identified pericentric inversions between taxa from changes in both the location of the centromere and the orientation of the banding pattern immediately flanking the centromere. We identified paracentric inversions by re-orientation of banding pattern alone. As we detected only three paracentric inversions in our dataset and this is likely to be a significant underestimate of their true diversity (Kawakami et al., 2014; Zhang et al., 2014), we only included pericentric inversions in our analyses. Centromere repositioning can result from processes other than pericentric inversions, such as the redistribution of heterochromatin (Krasikova et al., 2009; Zlotina et al., 2012) and the evolution of neo-centromeres (Marshall et al., 2008). We are able to exclude these alternative explanations because centromere repositioning was matched with inversion of proximal banding patterns.

Six species had pericentric inversions segregating within the individuals karyotyped (Figure 1; Table S2). We did not include them in our analyses because we are only interested in the drivers of inversion fixation. As such, an inversion on a polymorphic chromosome was only

counted as a fixed difference between species if the ancestral conformation, determined by Bayesian approach in SIMMAP v1.5 (Bollback, 2006) – see below, was neither of the forms found segregating.

1.3.2 Phylogenetic Analyses

Several phylogenetic surveys are available (Sorenson and Payne, 2001; Sorenson et al., 2004; Arnaiz-Villena et al., 2009) but there is no complete published phylogeny of the *Estrildidae*. We built a time-dated phylogeny for the 32 karyotyped finches using mitochondrial DNA sequence data from GenBank (Table S3). We dated the tree using the divergence time between the families *Estrildidae* and *Ploceidae* inferred from the multiple fossil-calibrated passerine tree of Price et al. (2014), setting a uniform prior of 17.5-22.1 Ma, based on the 95% confidence limits from the posterior distribution of that tree. Phylogenetic analyses were conducted using BEAST v1.8.0 (Drummond and Rambaut, 2007). Genetic data was sourced from three mitochondrial loci: *cytb* (1143bp), *ND2* (1041bp), and *ND6*+control region (1100bp); and from four nuclear loci: myoglobin (*MG*) exons 2-3, ornithine decarboxylase (*ODC*) exons 6-8, beta-fibrinogen (*FIB5*) exons 5-6, and recombination activating protein-1 (*RAG1*). Data was partitioned by locus, each with its own uncorrelated lognormal relaxed clock, and model of sequence evolution estimated to be the optimal for each locus using Jmodeltest v0.1.1 (Posada, 2008): GTR + Γ + I model for *cytb*, *ND2*, and *ND6*+control region and GTR + I for *MG*, *ODC*, *FIB5*, and *RAG1*. Algorithms were run for 50 million generations and sampled every 5,000 for a total of 10,000 trees of which the first 1,000 were discarded as burn-in. We assessed run length and appropriate sampling for each parameter using Tracer v1.5 (Rambaut and Drummond, 2007). Using TreeAnnotator v1.7.2 (Drummond and Rambaut, 2007), we extracted the maximum clade credibility tree, with associated confidence intervals for median node heights.

1.3.3 Phylogenetic and genomic distribution of inversion fixation

We estimated the ancestral centromere position (up to 4 possible states: metacentric, sub-metacentric, sub-telocentric, or telocentric) for each chromosome at each node in the tree using

SIMMAP v1.5 (Bollback, 2006). To account for phylogenetic uncertainty, we simulated over 1,000 randomly drawn trees from the BEAST output post burn-in. We obtained the posterior probability estimate for each ancestral centromere position for each chromosome at every node. Inversions were inferred to have occurred upon branches where the karyotype of an internal node differed from subsequent nodes or the tips and was supported by a posterior probability, $p > 0.75$. The inferred number of inversions per chromosome was concordant with results from reconstructions based on a maximum likelihood model in Mesquite v2.7.5 (Maddison and Maddison, 2001; results not shown).

We used ancestral karyotype estimates to calculate the total number of inferred inversions that have occurred on each chromosome separately. Here, we had to exclude three chromosomes from a single species (*Pytilia phoenicoptera*) that have fused and thus precluded identification of chromosome homology (Table S2; excluding this species entirely would not affect conclusions). We next assessed the degree to which the genomic distribution of inversions could be explained by mutagenic input. Under the assumption that the inversion mutation rate is constant per DNA base, the probability of a new inversion on a given chromosome or polytene chromosome arm should be proportional to the chromosome's physical size. We also assessed the relevance of a chromosome's map length and GC content based on an alternative process-driven assumption, conditioned on the fact that chromosomal rearrangements are mediated by double-stranded meiotic breaks, that predicts inversions should be proportional to cross-overs (Baudat and de Massy, 2007; de Massy, 2013). Given that at least one cross-over per chromosome arm appears to be required for proper pairing of homologous chromosomes during meiosis, we assessed whether the fixation rate of inversions was constant per chromosome. Finally, as chromosome breakpoints are often enriched in repeat dense regions (Skinner and Griffin, 2011; Kawakami et al., 2014), we assessed whether variation in the number of inversions per chromosome could be explained by variation in repeat density. We estimated chromosome physical size and GC content from the zebra finch genome assembly (Warren et al., 2010), repeat density per chromosome from a RepeatMasker annotation of the zebra finch genome (Smit et al., 1996-2010; http://www.repeatmasker.org), and map distance from two independent zebra finch linkage maps (Stapley et al., 2008; Backström et al., 2010). Using the zebra finch means we are assuming that the general features of the Estrildid finch genome and recombination landscape

(chromosome size, GC content, map distances, and repeat density) are conserved across species. Comparative studies indicate that chromosome size, GC content, and repeat density varies little even between distantly related avian species (Ellegren, 2013; Kawakami et al., 2014; Poelstra et al., 2014; Zhang et al., 2014) and that the recombination landscape has a phylogenetic signal, suggesting our extension of genomic parameters from the zebra finch to a confamilial set is warranted (Dumont and Payseur, 2008; 2011; Smukowski and Noor, 2011). We correlated the number of inversions with chromosome size, GC content, repeat density, and map distance, using each chromosome as a replicate. We subsequently compared alternative mutagenic hypotheses using multiple regression.

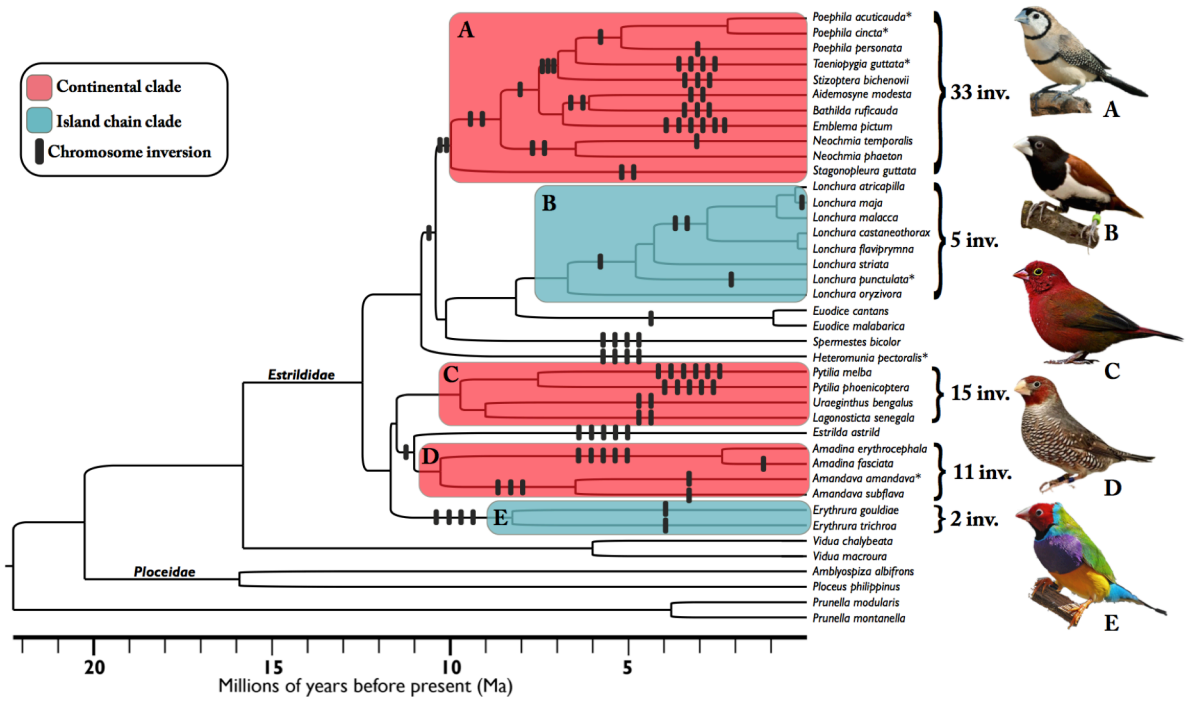

Figure 1 | Phylogeny of those 34 Estrildid finch species with karyotype descriptions. Continental Estrildid clades are boxed in red and island chain clades in blue. The number of pericentric inversions inferred to have fixed, based on ancestral karyotype reconstruction, is shown on each branch. The total number of inversions in the five clades and a species representative are shown to the right of each. The five species with known inversion polymorphisms are labeled with asterisks (e.g. *Poephila acuticauda**). All 5 clades have 100% posterior probability support. From top to bottom: (A) grassfinches – *Stizoptera bichenovii*, (B) munias – *Lonchura malacca*, (C) pytilias, cordon-bleus, and firefinches – *Lagonosticta senegala*; (D) adavats, amadina, and quailfinches – *Amadina erythrocephala*; (E) parrotfinches – *Erythrura gouldiae*.

1.3.4 Chromosome inversion differences between clades

In order to examine the influence of demography and geography on the rate of fixation of inversions, we assigned 27 of the 32 Estrildid finches that have cytological data into 5 clades comprising distinct geographic radiations with complete posterior probability support (Figure 1, Table 1, and Supplementary Figures 1-5). We focus on clades as they represent distinct monophyletic groupings at a deep timeline. Five species were not assigned to any clade because they were either the only species with cytological data belonging to an independent geographic radiation or were singleton species that did not group with other Estrildid species in their region. For example, the black-and-white mannakin (*Spermestes bicolor*) is the single species with cytological data belonging to a clade that radiated after re-colonizing Africa from Asia, precluding an assessment of inversion evolution within this interesting group. M. Sorenson (*pers. comm.)* provided information on the total number and identity of Estrildid species within each clade (i.e. including species without cytological data), based on unpublished phylogenetic results (Table 1). The total number of inversions fixed in each clade was summed across chromosomes. We estimated the fixation rate for the clade as the total number of inversions divided by the total branch length connecting all karyotyped species within the clade. We do not include inversions inferred to have occurred upon the stem lineage of each clade because we are interested only in those inversions that have fixed relative to taxa within each clade. Unlike the extant species we do compare, inferences upon the geographic location, range size, and range overlap of stem lineages are far more uncertain. We also estimated the inversion fixation rate as the total number of inversions divided by the number of nodes, as a measure of the minimum number of speciation events. This may scale with the number of opportunities for secondary contact between partially reproductively isolated forms between which gene flow may promote the spread of an inversion (Kirkpatrick and Barton, 2006).

To assess the relative influences of demography and geography, we extracted species' range sizes and pairwise range overlaps from natureserve.org using the programs Sp and PBSmapping in R (R Core Team 2014; Tables S4 and S5). Each species was scored as continental or island depending on where the majority of their range lay (Tables 2 and S4). Of the 90 species considered within our 5 clades, only 3 had ranges that were between 25-75%

continental (Table S4). Classifying these species alternately as continental or as island did not alter the results in any way. We scored the influence of region (continental vs. island taxa) for each clade as the proportion of species whose ranges were predominately continental.

Across the *Estrildidae*, range size varies by over 3 orders of magnitude from the red-billed firefinch (*Lagonosticta senegala*), the most widely distributed species ($1x10^7$ km^2), to the red-headed parrotfinch (*Erythrura cyaneovirens*), the most narrowly distributed species (3000 km^2, Table S4). We use range size as a proxy for population size and assigned a range size score to each clade based on the average range size of all species within it. Range size generally correlates with nucleotide diversity within species, which is a measure of long-term effective population size (Nevo et al., 1984; Cole, 2003; Leffler et al., 2012). Specifically in the Estrildid finches, estimates of nucleotide diversity are approximately an order of magnitude greater for zebra finch populations upon the Australian continent compared to zebra finch populations upon the Lesser Sunda Islands, consistent with the two order of magnitude difference in their range size (Balakrishnan and Edwards, 2009). It is worth noting that the fixation probability of an adaptive mutation depends on variance in family size (Peischl and Kirkpatrick, 2012) and not N_e per se. Variance in family size is only one of several factors that may cause N_e to differ from N and we have no reason to suspect that variance in family size varies greatly across Estrildid species (Goodwin and Woodcock, 1982).

We define the range overlap of species A with species B as the proportion of species A's range that is shared with B. Species pairs within clades were scored as sympatric if their average range overlap was greater than 15% (Table S5). Each clade was assigned a sympatry score as the proportion of all possible species pairs that were sympatric. Scoring species' distributions as sympatric with an average of 10% or 3% range overlap did not qualitatively change the results for the impact of sympatry on inversion fixation rate.

For each factor (region, range size, and range overlap), we calculated the correlation with inversion fixation rate using clade as the replicate. By studying at the clade level (N = 5), we eliminate possibilities for pseudoreplication as far as possible, but the tests are conservative. We fit a multiple linear regression model using fixation rate as the response variable to determine the extent to which variation in karyotype evolution between Estrildid finch clades is affected by demographic and geographic differences. We focus on the rate of inversion fixation (number of

inversions / total clade branch length connecting karyotyped species) but also consider number of inversions as a function of the total number of nodes in a clade. Neither of the two alternative methods of defining inversion fixation rate correlates with total branch length (both $p > 0.1$).

1.4 Results

The time-calibrated phylogeny for those Estrildid finches with cytological data is presented in Figure 1. Our topology matches that of Sorenson et al. (2004) and an unpublished topology of all Estrildid species (Sorenson, *pers. comm.*) for all shared nodes. Cytological sampling of each of the 5 fully-supported clades (Supplementary Figure 6), as determined from a phylogeny of all Estrildids (Sorenson *pers. comm.*), averaged 38% (minimum of 13% in the firefinches, pytilias, and waxbills – clade D – and maximum of 86% in the grassfinches – clade A, Table 1).

The average rate of pericentric inversion fixation across all 32 karyotyped species is one inversion fixed every 2.26 million years (199 My total tree branch length / 88 inferred inversions). The rate varies considerably among clades (Table 1). For example, gross karyotype has changed as fast as one inversion fixed every 175,000 years of evolution (5.72 inversions per million years, Figure 1, clade A) within the Australian grassfinches but has remained identical for over 11 million years of evolution between two species of Indo-Malayan *Lonchura* munias (clade B).

1.4.1 Genomic distribution of chromosome inversions

Overall, the rate of inversion fixation differs 13× between the fastest and slowest evolving chromosomes (Table 2). The number of inversions across the 11 autosomes departs from a Poisson distribution (Goodness of fit test, $\chi^2_{10} = 93.4$) implying that inversion fixation does not occur at equal rates per chromosome. Across the autosomes, the number of inversions per chromosome is not significantly associated with physical size (Pearson's $r = 0.29$, $p > 0.1$), GC content ($r = -0.61$, $p > 0.1$), or map length regardless of linkage map used (Stapley et al., 2008: $r = 0.38$, $p > 0.1$; Backström et al., 2010: $r = 0.3$, $p > 0.1$). Inclusion of the Z further weakened any association.

Clade:	Inversion fixation rate (Inv/My)	Number of inversions	Combined branch length (My)	Species karyotyped (Total species)	Crown age (Ma)	Proportion continental species	Avg. Range Size (10^6 km^2)	Proportion sympatric*
A) Grassfinches	0.502	31	61.72	11 (14)	7.5	0.93	1.5 ($5x10^{-2}$ - 6.3)	0.57
B) Munias	0.176	4	22.66	6 (26)	5.6	0.23	0.99 ($10x^{-3}$ - 7.8)	0.18
C) Pytilias, Cordon-bleus, and Firefinches	0.526	16	30.4	4 (31)	8.5	1.0	2.3 (10^{-2} - 10.3)	0.49
D) Adavats, Amadinas, and Quailfinches	0.545	14	25.68	4 (8)	9.4	1.0	2.7 (0.5 - 4.0)	0.39
E) Parrotfinches	0.137	2	14.59	2 (12)	7.3	0.09	0.26 ($3x10^{-3}$ - 1.6)	0.11

Table 1 | Phylogenetic distribution of chromosome inversions in the *Estrildidae*. *Proportion sympatric is the proportion of all pairs of species within each clade that overlapped in range more than 15%.

The two sex chromosomes have fixed inversions at a rate on average twice as fast as the autosomes (two sample *t*-tests, using the autosomes as replicates: Z chromosome: t_{10} = 7.1, p < 0.01; W chromosome: t_{10} = 5.0, p <0.01). The only significant difference between the autosomes and the Z, with regard to the parameters we examined, is that the Z chromosome has an order of magnitude greater density of repeats than the autosomal average (two sample *t*-test: t_{10} = 37.4, p < 0.01; Table 2). There is currently no comparable estimate for repeat density on the W. The W chromosome, however, stands out when comparing chromosomes by the number of inversions per base pair (Table 2). We observe one inversion fixed for every 2.5 Mb on the W, which is over twice as many as on the Z chromosome or the closest autosome TGU5 (both one for every 5.7 Mb).

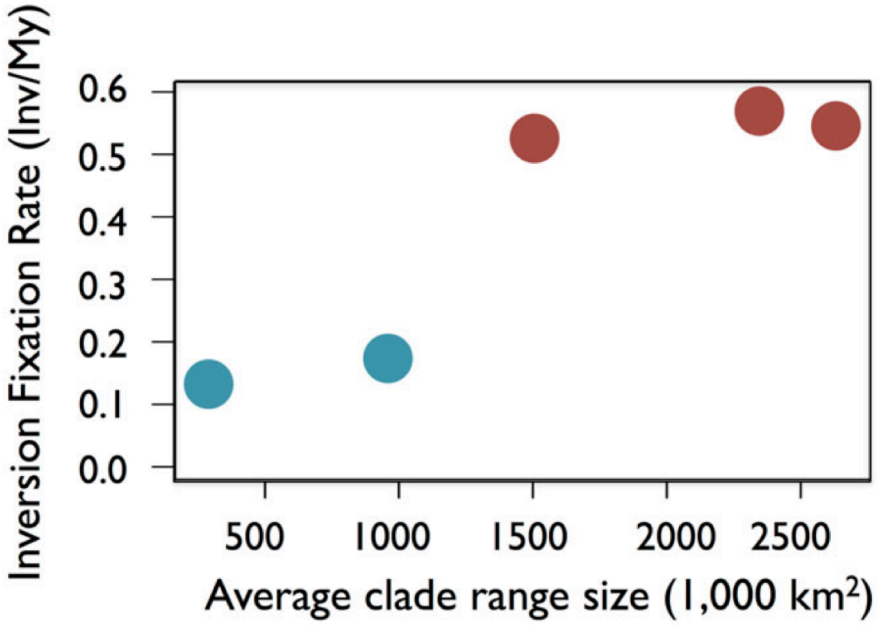

Figure 2 | Rate of inversion fixation (inversions per My) against the average range size of all taxa within each clade. One-tailed Pearson's correlation: r = 0.91, p = 0.02. Continental Estrildid clades are colored in red and island chain clades in blue, as in Figure 1. Clades are arranged from left to right (following Table 1): (E) parrotfinches, (B) munias, (A) grassfinches, (C) pytilias, cordon-bleus, and firefinches, (D) adavats, amadina, and quailfinches.

1.4.2 Rate variation between clades

The fixation rate for inversions is on average 3.3× higher in the three continental than the two island clades (*t*-test: t_3 = 16.9, p < 0.01) and is significantly correlated with the proportion of species within clades that have continental distributions (N =5, r = 0.99, p < 0.001). Continental taxa have on average larger ranges and a higher percentage of sympatric species than island taxa (Supplementary Figures 1-5). Both average range size (N =5, r = 0.91, one-tailed p = 0.02; Figure 2) and proportion of sympatric pairs (N = 5, r = 0.92, one-tailed p = 0.01) are significantly correlated with inversion fixation rate. In a multiple regression on inversion fixation rate, the partial regression coefficients of range size and proportion of sympatric pairs are both significant (range size: p = 0.042; proportion sympatric: p = 0.037), suggesting that both contribute independently.

Chromosome ID	Size (Mb)	Map Length (cM)*	GC Content (%)	Repeat Density (%)	Inversions
TGU2	156.4	34.7 (76)	39.0	0.38	3
TGU1	118.6	63.7 (70)	39.2	0.23	8
TGU3	112.6	22 (69)	39.4	0.38	8
TGU1A	73.7	63.3 (91)	39.7	0.14	9
TGU4	69.8	31.9 (18)	39.2	0.28	10
TGU5	62.4	89.8 (64)	40.8	0.12	11
TGU7	39.8	27.8 (41)	41.1	0.14	5
TGU6	36.3	44.6 (60)	41.6	0.19	4
TGU8	28.0	44.9 (47)	41.3	0.05	4
TGU9	27.2	60.5 (52)	43.1	0.15	4
TGU12	21.6	47.5 (34)	43.7	0.07	1
Z	74.6	32.8 (29)	39.2	1.5	13
W	27.0	-	-	-	11

Table 2 | Genomic distribution of pericentric chromosome inversions. *Map length values are from the framework map for zebra finch given in Table 2 in Stapley et al. (2008) and those shown in parentheses from the framework map for zebra finch in Backström et al. (2010). Chromosome size and GC content values come from the zebra finch genome assembly (Warren et al. 2010). Repeat density was calculated using the RepeatMasker annotation (Smit et al., 1996-2010; http://www.repeatmasker.org) of the zebra finch genome.

Analyses conducted using inversion fixation rate alternatively defined as the number of inversions within each clade divided by the number of nodes in that clade yielded results similar to those reported above, but they were not as strong and not significant at the $p < 0.05$ level.

1.5 Discussion

Previous cytological analyses of karyotype structure in Estrildid finches revealed multiple fixed inversion differences between species (Hirschi et al., 1972; Ray-Chaudhuri, 1976; Ray-Chaudhuri, 1976; Prasad and Patnaik, 1977; Christidis, 1983; 1986a; 1986b; 1987). We found these inversions have accumulated disproportionately on the sex chromosomes and are much more common within continentally distributed clades, which tend to have larger ranges and a higher proportion of sympatric species. Assuming range size correlates with population size, this is not in accord with the expectations for the fixation of underdominant or deleterious rearrangements because these processes should be independent of (Lande, 1979; Lande, 1985; Walsh, 1982; Spirito, 1998) or negatively correlated with (Kimura 1962) a species' population size. Instead, the correlation with range size suggests that inversions have fixed by positive selection (Whitlock et al., 2004; Vicoso and Charlesworth, 2009; Mank et al., 2010b). The positive relationship between range size and inversion fixation rate is present on the autosomes combined (across the 5 clades, $r = 0.82$) and each of the sex chromosomes (Z: $r = 0.44$ and W: $r = 0.84$)

Overall, our results highlight the rapid rate of karyotype evolution in Estrildid finches, with one pericentric inversion fixed every 2.26 My on average. This value is a minimum estimate of the true rate of chromosomal rearrangement. First, many paracentric inversions may have been missed because of the limited number of C- and G- bands per chromosome arm required to infer them and, second, small inversions that cannot be detected cytologically are likely to occur frequently (Kawakami et al., 2014). Paracentric inversions may be less structurally underdominant than pericentric inversions and hence even more likely to fix. This is because, in some groups (e.g. *Drosophila*), crossing over within them produces acentric and dicentric products that are removed to the polar bodies during meiosis (i.e. they do not affect female fertility). Whether similar mechanisms exist in birds is not known. Small inversions may be

subject to similar selective pressures as those examined here but this awaits genomic analysis (e.g. Kunte et al., 2014; Kawakami et al., 2014; Poelstra el al., 2014). We find that degree of sympatry between species is positively associated with the rate of inversion accumulation, even after range size is accounted for, which may be expected if gene flow between incipient species has contributed to inversion fixation, as in models where rearrangements that capture locally adapted alleles are favored (Kirkpatrick and Barton, 2006; Feder et al., 2011). We first consider the genomic distribution of inversions and then the demographic and geographic context of inversion fixation.

We find mixed support for the idea that mutational input has influenced the genomic distribution of chromosome inversions. Chromosome breakpoints are often located within regions that are repeat dense (Skinner and Griffin, 2011; Kawakami et al., 2014) and this appears to be supported by the enrichment of inversions we observe on the sex chromosomes. The repeat density of the Z chromosome is an order of magnitude greater than the autosomal average and has the greatest number of inversions fixed of any chromosome – perhaps suggesting the Z has a greater structural mutation rate. While we do not know the repeat density of the W chromosome, it is also believed to be repeat rich due to the reduced power of selection for fixing DNA replication errors (Dalloul et al., 2010; Völker et al., 2010; Kawakami et al., 2014). Alternative mutagenic explanations for the genomic distribution of inversions, however, bear little support. First, chromosome size is not correlated with inversion fixation rate, which is the naïve expectation if structural mutations have a constant rate per base pair. Second, neither a chromosome's map length nor its GC content are correlated with its rate of inversion fixation suggesting an increased number of cross-overs per se does not necessarily result in an increased rate of inversion fixation. While inversion breakpoints may be more prevalent in areas of high cross-over (Skinner and Griffin, 2011; Kawakami et al., 2014) and inversions originate from errors during meiotic crossing-over, in the Estrildid finches the fixation rate of inversions cannot be explained by differences between the recombination landscapes of chromosomes alone.

These results contrast with a recent comparative genomic survey of inversion differences between the zebra finch and the collared flycatcher, which found a positive correlation between chromosome size and number of inversions (Kawakami et al., 2014). The difference may reflect the level of resolution possible between studies. Our study only considered large pericentric

inversions because of the limitations of the cytological methods used to detect them, while the majority of the inversions found by Kawakami et al. (2014) are small and generally paracentric (median size of 2.62 Mb and 0.78 Mb in the lineages leading to zebra finch and collared flycatcher, respectively). Smaller rearrangements potentially come with both fewer deleterious effects and smaller selective advantages, resulting in a more even distribution across the genome. Our results are perhaps striking because, in contrast to small inversions, large pericentric inversions seem more likely to carry an intrinsic selective disadvantage due to underdominance and thus suggest that selection was critical in driving their fixation.

A strong result in our dataset is that inversions accumulated twice as rapidly on the sex chromosomes as on the autosomes. While meiotic drive on the sex chromosomes (i.e. sex chromosome drive) is often associated with the establishment of inversion polymorphisms it is unlikely to lead to their fixation because of the deleterious effects of high sex ratio skew (Jaenike, 2001). Rather, the scaling of inversion fixation rate on both the Z and W chromosomes with range size suggests positive selection. While a higher mutation rate on the sex chromosomes may contribute (see above), immediate exposure of recessive mutations to selection and the preferential accumulation of sexually antagonistic genes may make for generally fast rates of adaptive evolution (Charlesworth et al., 1987). This "faster Z-effect" is well documented in birds, but has been attributed to the fixation of mildly deleterious alleles by genetic drift rather than positive selection (Mank and Ellegren, 2007; Mank et al., 2010a; Ellegren, 2009; Yan et al., 2010; Zhang et al., 2014). However, explanations crediting the predominant role of drift make several untested assumptions regarding the evolution of sex-biased gene expression and avian effective population sizes (Mank and Ellegren, 2007; Mank et al., 2010a), and so the relative contributions of positive selection and drift need further study. Regarding the relative rate of inversion fixation, because Z-linked genes diverge in function more rapidly than autosomal genes, at any point in time before reproductive isolation is complete an inversion on the Z chromosome should be more likely to capture two or more alleles locally adapted—either to that population's habitat or genomic background—than an inversion on an autosome. Thus, inversions on the Z may be more strongly selected for if gene flow is an important mechanism driving their selective advantage.

The W chromosome has more inversions per Mb than any other chromosome we consider and a fixation rate strongly correlated with average clade range size ($r = 0.84$, $p = 0.038$). This is at first surprising as much of the W is devoid of genic content (in the chicken, of the 1,000 active genes on the Z less than 100 are thought to remain active on the W chromosome, Chen et al., 2012; Moghadam et al., 2012; Ayers et al., 2013; Wright et al., 2014), implying few adaptive advantages for a recombination modifier. However, our results are consistent with recent findings, which show that recombination suppression over large portions of the W has evolved independently and repeatedly in different avian lineages (Wright and Mank, 2013; Wright et al., 2014). Moreover, selection on the W chromosome has played a large role in gene expression evolution, at least amongst chicken breeds (Moghadam et al., 2012). Under positive selection, the fixation rate is $\sim 2N\mu s$, where N is population size, μ is the mutation rate, and s the selective advantage of the heterozygote (Haldane, 1927; Peischl and Kirkpatrick, 2012). This formula assumes that variance in family size is Poisson. Among the three parameters (N, μ, and s), μ and s may help explain the W chromosome's relatively high fixation rate. We can dismiss an explanation based solely on N, as the population size of the W at equilibrium is ¼ that of the autosomes, which should result in a lower fixation rate. While the W chromosome's mutation rate at the nucleotide level is estimated to be significantly lower than on the autosomes, due to its female-restricted mechanism of germ-line transmission (Ellegren, 2013), the structural mutation rate (μ) on the W may be greater because of its elevated repeat density (Dalloul et al., 2010; Völker et al., 2010; Kawakami et al., 2014). While the idea that the high number of inversions on the W is due to its repeat density is plausible, chromosome breakpoints are also more often to be found located in areas that have high recombination rates and a high GC content—both of which are lower on the W than the autosomes (Völker et al., 2010; Kawakami et al., 2014; Ellegren, 2013; Graves 2014). Finally, selection (s) is a composite variable summing across both positive and deleterious effects on fitness. Possibly, s is higher on the W chromosome not because inversions have a greater selective advantage than on the autosomes but rather because the costs of structural rearrangements on the W are reduced.

Species ranges are on average 3.6× larger in continental versus island chain clades and this difference is matched by a 3.3× faster rate of inversion fixation. Adaptive models predict this association, but models where drift operates on structurally underdominant deleterious

rearrangements do not (Lande, 1979; Lande, 1985). The usual explanation for the correlation of population size with fixation rate is that the number of rearrangements (or mutations) arising each generation positively correlates with population size (Kimura, 1962; Whitlock et al., 2004). However, our analyses across chromosomes based on physical and map size, as described above, argue for an important role for selection beyond raw mutational input. Besides coming into contact more regularly, enabling gene flow that promotes the spread of inversions in adaptive models, species on continents with larger ranges are also more likely to encompass a wider variety of landscapes and climates across which selection might favor alternate allelic combinations between populations connected by gene flow. These are the theoretical starting conditions under which a novel rearrangement that captures sets of locally adapted alleles may spread to fixation (Kirkpatrick and Barton, 2006; Feder et al., 2011).

Both the number of inversions and the rate of inversion fixation appear to be correlated with the proportion of sympatric species within Estrildid clades even after accounting for the effects of time and range size. This could be construed as support for inversion fixation as a consequence of gene flow between partially differentiated populations, if extant sympatry between closely related taxa does indeed reflect parapatric divergence. In an extension of the local adaptation model of Kirkpatrick and Barton (2006), chromosome rearrangements are selected to fix between populations upon secondary contact when reproductive isolation is partial but incomplete, and the rearrangement capture two or more incompatibility alleles (Kirkpatrick, 2010). Genome-scale sequence data from recently diverged taxa suggests that gene flow between incipient species occurs regularly during the speciation process (e.g., Jones et al., 2012; Ayala et al., 2013; Lowery et al., 2013; Eaton and Ree, 2013; Cui et al., 2013) but excluding alternative explanations based on incomplete lineage sorting or post-speciation selection has been difficult (reviewed in Sousa and Hey, 2013; Cruickshank and Hahn, 2014).

As in our study, a greater number of chromosome rearrangements have been found in sympatric compared to allopatric taxa in *Drosophila* (Noor et al., 2001), *Helianthus* sunflowers (Rieseberg, 2001), *Anopheles* mosquitoes (Ayala and Coluzzi, 2005), *Agrodiaetus* butterflies (Kandul et al., 2007), and rodents in the families *Cricetidae* and *Muridae* (Castiglia, 2014). One hypothesis, as stated above, is that sympatry reflects historical gene flow between partially reproductively isolated populations that promoted the fixation of these inversions. An alternative

is that the greater number of inversion differences observed between sympatric, relative to allopatric, sister taxa occurs because incipient species are more likely to fuse upon secondary contact when they share karyotype structure (Noor et al., 2001; Rieseberg et al., 2001). Previous studies of the phylogeographic context of rearrangement evolution have not evaluated these alternatives (Ayala and Coluzzi, 2005; Kandul et al., 2007; Castiglia, 2014). If rearrangements accumulate at a constant rate, and incipient species that differ by chromosome rearrangements are more likely to persist upon secondary contact than those that do not differ in rearrangements, then the extent of karyotypic differentiation between sympatric taxa should comprise the upper end of the distribution of karyotypic differentiation between allopatric ones. We do not observe this pattern in the Estrildid finches. Species pairs from island clades, which contain predominately allopatric taxa, have significantly fewer inversions than species pairs from continental clades, which consist of predominately sympatric taxa, regardless of the age of species compared. However, this comparison is confounded with population size. Future examination into the extent of karyotype differentiation between allopatric sister taxa on continents (e.g. the firetails of southwestern and southeastern Australia, gen. *Stagonopleura*), sympatric sister taxa on islands (e.g. the munia species complex of Papua New Guinea, gen. *Lonchura*), and active speciation in hybrid zones should more explicitly elucidate the extent to which gene flow facilitates inversion fixation.

We conclude that karyotype structure across the Estrildid finches is highly variable and appears to evolve rapidly under certain demographic and geographic conditions. Considering that karyotype divergence has been considered unimportant to avian diversification (Ellegren, 2010), one question is whether the Estrildid finches are representative of or an exception to the avian rule. In the following chapter we expand beyond the Estrildid finches to analyze the past six decades of cytological research in passerine birds, the avian order comprising ~60% of all bird species, which suggests that chromosome inversions, while variable in number between families, are a pervasive feature of evolution in birds and often involve the sex chromosomes. The upshot appears to be that the *Estrildidae* are not an exception so much in terms of the raw variation in genomic structure between species as they are an exception with respect to the breadth and intensity of taxa so far examined, likely because many Estrildid species are available from aviculture stocks. Our results suggest that alterations of genomic structure may be as important

to bird speciation as has been proposed for other better-studied taxa (reviewed in Hoffmann and Rieseberg, 2008; Faria and Navarro, 2010). That karyotype evolution by chromosome inversion might be a common feature of avian diversification is an exciting prospect for speciation studies and one that should serve to stimulate future research into the extent of genomic rearrangement between species and the evolutionary context in which these changes occur.

2 Chromosomal inversion differences correlate with range overlap in passerine birds[1]

2.1 Abstract

Chromosomal inversions evolve frequently but the reasons why remain unclear. We used cytological descriptions of 411 species of passerine birds to identify large pericentric inversion differences between species, based on position of the centromere. Within 81 small clades comprising 284 of the species we found 319 differences on the 9 largest autosomes combined, 56 on the Z chromosome, and 55 on the W chromosome. We also identified inversions present within 32 species. Using a new fossil-calibrated phylogeny we examine the phylogenetic, demographic, and genomic context in which these inversions have evolved. The number of inversion differences between closely related species is consistently predicted by whether the ranges of species overlap, even when time is controlled for as far as is possible. Fixation rates vary across the autosomes, but inversions are more likely to be fixed on the Z chromosome than the average autosome. Variable mutagenic input alone (estimated by chromosome size, map length, GC content, or repeat density) cannot explain the differences between chromosomes in the number of inversions fixed. Together, these results support a model in which inversions increase because of their effects on recombination suppression in the face of hybridization. Other factors associated with hybridization may also contribute, including the possibility that inversions contain incompatibility alleles, making taxa less likely to collapse upon secondary contact.

2.2 Introduction

Speciation is associated not only with the accumulation of molecular changes in DNA composition but often also with physical rearrangements in chromosome structure. Chromosome

[1] A version of this chapter has been published as: Hooper DM and TD Price. 2017. Chromosomal inversion differences correlate with range overlap in passerine birds. Nature Ecology and Evolution *In Press*.

inversions, one common type of chromosomal rearrangement, are regularly observed as fixed differences between species and as polymorphisms segregating within species (Hoffmann and Rieseberg, 2008; Faria and Navarro, 2010). Inversions are thought to propel the evolution of sex chromosomes (Lemaitre et al., 2009; Wilson et al., 2009; Wright et al., 2014), supergene formation (Kunte et al., 2014; Küpper et al., 2015; Lamichhaney et al., 2015; Tuttle et al., 2015), local adaptation (Anderson et al., 2005; Lowry and Willis, 2010; Joron et al., 2011; Jones et al., 2012), and reproductive isolation (Rieseberg, 2001; Noor et al., 2001; Brown et al., 2004; Ayala et al., 2012; Fishman et al., 2013). Despite their evolutionary significance, the widespread presence of inversions is puzzling, as new rearrangements may be initially disfavored due to structural underdominance in heterokaryotypes, if crossing over within the inverted region during meiosis results in the production of aneuploid gametes (Hoffmann and Rieseberg, 2008; Faria and Navarro, 2010; King, 1993). Reconciling the widespread presence of chromosome inversions with possible selective disadvantages that a new inversion faces remains an unsolved problem.

Early models of inversion fixation considered how genetic drift might lift an underdominant inversion above 50% frequency in a local deme, after which selection favors its spread (Lande, 1979; Lande, 1985; Hedrick, 1981; Walsh, 1982; Spirito, 1998). This model predicts that inversion fixation rate should be independent of total population size, assuming population structure is similar across taxa (Lande, 1979). Hooper and Price (2015) tested this in the Estrildid finches (family Estrildidae) and rejected it, based on a strong positive relationship between the rate of inversion fixation and range size, assumed to be correlated with population size. More recent models have focused on selection mechanisms in which drift plays no part. An inversion may be adaptive and spread if its breakpoints favorably alter gene expression (Wesley and Eanes, 1994; Puig and Ruiz, 2004) or by meiotic drive if the inversion happens to link alleles that together alter segregation distortion (King, 1993; White, 1978). A major set of models assumes selective advantages of an inversion result from of its effects on recombination (Charlesworth and Charlesworth, 1979; Kirkpatrick and Barton, 2006; Feder et al., 2011; Dagilis and Kirkpatrick, 2016). For example, recombination suppression on the Y (or W in species such as birds in which females are the heterogametic sex) is promoted by accumulation of genes that are beneficial in the heterogametic sex but deleterious in the homogametic sex (Ohno,

1967; Charlesworth, 1991; Charlesworth and Charlesworth, 2000). Gene flow between genetically differentiated populations may also promote recombination suppressors because sets of maladaptive alleles in hybrids are eliminated as a block (Kirkpatrick and Barton, 2006). In this case, genetic differences may reflect local adaptation, genetic incompatibilities, sexually selected traits, and various combinations.

The different models that invoke selection make different predictions that can be tested with comparative analyses. All selection models depend on mutational input, which should scale with population size. However, mutational input should be particularly strongly associated with breakpoint effects and meiotic drive. This is because selective pressures resulting from these mechanisms are less dependent on environmental context and because mutations that produce favorable effects are likely to be rare. Hence, these models predict a strong scaling of inversion fixation with population size. Further, both these models are associated with an unconditional selective advantage, so any gene flow between populations or across the species barrier may destroy differences. On the other hand, in many recombination suppression models gene flow plays a creative role because the fitness of an inversion increases with the proportion of unfit hybrids in a population (Kirkpatrick and Barton, 2006; Dagilis and Kirkpatrick, 2016). Among gene flow models, local adaptation (that is adaptation to ecological factors) predicts associations of ecological differences between taxa with inversion increase, whereas hybridization between incompletely reproductively isolated populations favors an inversion if it captures two or more loci affecting hybrid loss of fitness or an incompatibility locus and a mate choice locus (Charlesworth and Charlesworth, 1979; Kirkpatrick and Barton, 2006; Dagilis and Kirkpatrick, 2016).

Here, we consider the range size of a species to be an estimate of population size (Section 2.3.4), and hence predict range size to be a strong positive correlate in the breakpoint and meiotic drive models. Range overlap between closely related species indicates the potential for hybridization, predicted to be essential in genetic incompatibility models. Across 32 species of Estrildid finches, both range size and range overlap are positively associated with the rate of inversion fixation (Hooper and Price, 2015). However, range size and range overlap are themselves correlated, making it difficult to disentangle their contributions, given the sample size. In this paper we study 411 karyotyped bird species, in order to test the alternatives. Further,

we document widespread occurrence of inversion polymorphisms within species, and consider how the presence of these polymorphisms relates to various alternative models of inversion spread.

The Passeriformes are just one of 39 extant orders of birds yet comprise over half of all avian species, with the ~6000 species found in nearly every terrestrial habitat on the planet (del Hoyo, 2011). The radiation has produced a large variety of ecological and morphological types: body size varies >350-fold between the smallest and largest species (4.2 g to 1,500 g) while variation in beak shape and behavior has produced a wide spectrum of feeding morphologies (nectarivores, granivores, insectivores, frugivores, etc.; del Hoyo, 2011; Price et al. 2014). In contrast the gross structure of the passerine genome does not vary greatly, with diploid chromosome number (2N) falling between 76-80 for 77% of species (Table S1; reviewed in Christidis, 1990). While chromosome fusions, fissions, and translocations are apparently rare in birds, inversions are far more common (Hooper and Price, 2015; Christidis, 1990; Shields, 1982; Price, 2008; Figures 3 and 4). Cytological evidence for the frequent occurrence of inversions in birds is corroborated by recent genomic studies that infer inversion-derived rearrangements both within and between species (Volker et al., 2010; Stapley et al., 2008; Hansson et al., 2009; Aslam et al., 2010; Skinner and Griffin 2011; Zhang et al., 2014; Knief et al., 2016). Here we evaluate the phylogenetic, biogeographical context and genomic distribution of large pericentric inversions (i.e. those encompassing the centromere) on the 9 largest autosomes and the Z chromosome (Tables S1 and S5-8) identified from the cytological literature. We also studied the W chromosome, in which we show movement of the centromere is particularly common. However, it is more difficult to relate centromere movement to an inversion on this chromosome, so we consider it separately.

2.3 Materials and Methods

2.3.1 Identifying inversions

We called chromosome inversions from classic studies of gross karyotype structure that encompass nearly 8% of all passerine species and >50% of passerine families. Of the 428

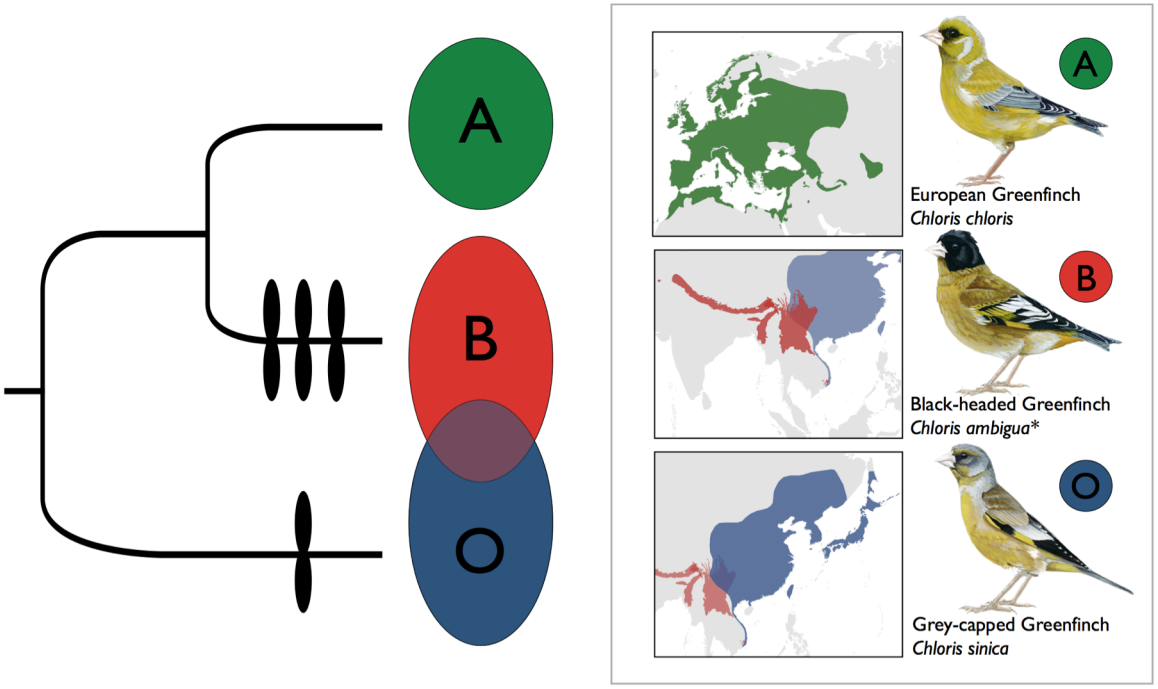

Figure 3 | History of pericentric inversion evolution across greenfinches in the genus *Chloris*. Inversions differences are indicated by black ovals on the branches they are inferred to have fixed. The three members of the black-headed greenfinch species complex (*C. ambigua*, *C. monguilloti*, and *C. spinoides*) are here treated as a single species *C. ambigua* based on the lack of any observed premating isolation where their ranges overlap. Note that *C. chloris* and *C. sinica* actually share an inversion polymorphism on the largest autosome.

passerine species that have had their karyotypes described, we discarded 15 because the cytological data was not of sufficiently high quality to include in this study and two because no suitable genetic data currently exists for them and no tissue materials were available. We analyzed cytological data for the remaining 411 species, representing birds from 59 families (Table S1). Data was sourced from 111 studies that span five decades of cytological research. Methods utilized to describe karyotype varied from simple Giemsa staining to fluorescent *in situ* hybridization with chromosome painting. Sampling rigor varied across studies with respect to the number (average of 7 karyotyped individuals per taxon, range from 1 to 432; Supplementary Figure 5) and sex representation of each species (data from both males and females in 296 of 411 species). Sampling information was not given for 29 species. Due to the considerable heterogeneity in the quality and quantity of karyotype descriptions between species and studies,

we focus on a simple yet powerful trait with which to infer pericentric chromosome inversion differences between and within species: centromere position.

For each species, we converted centromere position for the 9 largest autosomal chromosomes and both sex chromosomes into character state data (Table S1). We scored each chromosome for approximate centromere position (i.e., whether it was metacentric, sub-metacentric, sub-telocentric, or telocentric), following conventions established by Levan et al. (1964). We identified homologous chromosomes between species based upon their physical size, shared banding pattern, and matching chromosome painting as the information was available. When assignment of chromosome homology was not absolute, for instance due to a lack of banding information for similarly sized chromosomes, we conservatively assigned homology in a way that would not result in centromere movement. This was most common for the 2nd and 3rd as well as the 4th and 5th largest autosomal chromosomes, which are of similar sizes (Table 4). However, we treated the centromere position of a chromosome as distinct when species shared the same general classification (e.g., both were sub-metacentric) but the authors noted that the banding pattern flanking the centromere consistently differed. We only include pericentric inversions in our analyses as the cytological data has far less power to identify paracentric inversions (those not encompassing the centromere). Centromere repositioning can result from processes other than pericentric inversion, such as the expansion of transposable elements, the redistribution of heterochromatin (Krasikova et al., 2009; Zlotina et al., 2012), and the evolution of neo-centromeres (Zlotina et al., 2012; Marshall et al., 2008). We found no evidence, however, of these alternative mechanisms of centromere repositioning in the 85 species with banding data available, as centromere movement was supported by inversion of proximal banding patterns. While centromere position for the W chromosome has been recorded for all taxa with females karyotyped, results from this data were analyzed independently in all further analyses as centromere movement on the W chromosome appears to be particularly labile and more likely to result from processes other than chromosome inversion (Rutkowska et al., 2012; Ellegren, 2013).

While the distribution of fixed inversion differences can be used to infer historical patterns of selection, the mechanisms of selection affecting inversions are best studied when rearrangements still segregate in natural populations. We therefore evaluated all species for the occurrence of pericentric inversion polymorphisms and for the presence of inversions present in

different parts of species ranges (Tables S1 and S2). Polymorphisms segregating within populations were often noted in the paper of interest, but the majority of geographic variants are first reported in this study, as they generally depend on comparing different published studies (Supplementary Table 2). Of the 50 total rearrangement polymorphisms identified, two are likely a product of chromosome translocation and three are shared between species – two across three species and one between two species (Table S2).

2.3.2 Phylogenetic analyses

In order to characterize the phylogenetic distribution of chromosome inversion fixation, we built a time-dated phylogeny for the 411 passerine species with karyotype data available. We gathered sequence data from six genes: two mitochondrial: *cytb* and *ND2*, and four nuclear: myoglobin (*MG*) exons 2-3, ornithine decarboxylase (*ODC*) exons 6-8, beta-fibrinogen (*FIB5*) exons 5-6, and recombination activating protein-1 (*RAG1*). Data were primarily sourced from GenBank. For 12 karyotyped species with no or low sequence representation we generated the data ourselves using standard methods (Table S3). Phylogenetic and dating analyses were conducted using BEAST v1.8.2 (Drummond et al, 2012). Sequence data was partitioned by locus, each with its own uncorrelated lognormal relaxed clock, and assigned the optimal-fit model of sequence evolution estimated for each locus using jModelTest v0.1.1 (Posada, 2008). The phylogeny was time-calibrated using 20 fossil calibrations broadly dispersed both in time and topology (Supplementary Figure 1, Table S2). This is the most extensive fossil calibration effort to date within Passeriformes. Each fossil calibration was applied to its corresponding node as a minimum age bound using a conservative uniform prior based on the age of the fossil itself and 80Ma. We ran BEAST for 50 million generations and sampled every 5000 for a total of 10,000 trees of which the first 1000 were discarded as burn in. We assessed run length and appropriate sampling for each parameter using Tracer v1.6 (Drummond et al., 2012). Using TreeAnnotator v1.7.2 (Drummond et al., 2012), we extracted the maximum clade credibility tree, with associated confidence intervals for median node heights (Figure 4 and S2).

2.3.3 Phylogenetic distribution of inversion fixation

In order to map inversion evolution across the phylogeny, we estimated the ancestral centromere position (up to 4 possible states: metacentric, sub-metacentric, sub-telocentric, or telocentric) for each chromosome at each node in the tree by maximum likelihood in Mesquite v2.7.5 (Maddison and Maddison, 2001). We obtained the maximum likelihood estimate for each ancestral centromere position for each chromosome at every node. Inversions were inferred to have occurred upon branches where the karyotype of an internal node differed from subsequent nodes or the tips and was supported by a maximum likelihood, $p > 0.75$. We used this phylogenetic representation of inversion evolution in passerines to investigate the drivers of inversion fixation between species and within the genome. We conducted analyses at two different phylogenetic levels. First, we defined 81 clades in total comprising between 3 and 85 species and, second, we used 47 sister species pairs.

2.3.4 Chromosome inversion differences between clades

We partitioned the phylogeny of karyotyped taxa into 81 clades of closely related species in order to examine the factors associated with broad scale variation in chromosome inversion evolution. Many clades contain additional species that were not karyotyped, and hence not included in the tree, yet these species may influence chromosomal evolution in the focal taxa, e.g. through range overlap. To take this into account, we utilized phylogenies from 55 published family-level studies in order to determine which non-karyotyped species to include in clade level analyses (Table S5). Clades were assigned based on the following grouping criteria: the two most distantly related karyotyped species were less than 15 million years diverged, member species were the result of speciation within a single geographic region (i.e. all clade members speciated in Australia), member species were ecologically similar (i.e. granivores, insectivores, frugivores, nectarivores, or omnivores), a comprehensive family level phylogeny exists to identify non-karyotyped member taxa, and they encompassed at least three species including non-karyotyped taxa. After filtering based on the above criteria, 286 of 411 karyotyped species were assigned to 81 clades (Tables S1 and 5).

We measured variation in karyotype evolution across passerine clades by counting the total number of inversions that had fixed on each chromosome, summing over all branches within the clade. We did not include inversion polymorphisms in this count unless the ancestral conformation of the chromosome polymorphic for an inversion, determined in Mesquite, was neither of the segregating forms. We calculated clade branch length as the sum of branch lengths for species with centromere position scored at each of the 9 autosomes and the Z chromosome. For example, if all species within a clade had complete karyotype records (i.e. centromere position scored for all 10 chromosomes), the branch length value of that clade was the sum of all branches multiplied by a factor of 10. For species missing data for a chromosome, the length of the branch leading to that species was removed from the clade total according to the total number of missing chromosomes (i.e. if a species was missing data at two chromosomes then 2× the branch length to that species were subtracted from the clade total).

We collected range overlap, range size, and body mass data from the complete taxon set for each clade (i.e. including both karyotyped and non-karyotyped species) in order to evaluate the extent to which variation in demography (population size) and speciation history (range overlap) has impacted inversion evolution (Table S5). We extracted range data for all species from natureserve.org using the programs Sp (Pebesma and Bivand, 2016) and PBSmapping in R (Schnute et al., X). We assigned each clade a range size value corresponding to the median range size (km^2) of all member taxa. Median body mass (g) for each clade was calculated from Dunning (1993). We used range size together with body mass in mixed models as proxies for population size based on the positive relationship between the geographic area a species occupies and its nucleotide diversity (Nevo and Ben-Shlomo, 1984; Cole, 2003; Leffler et al., 2012) and the negative relationship generally observed between body size and population density (White et al., 2007). We assigned a range overlap score to each clade based on the proportion of all species pairs whose ranges overlap by >20% (range overlap is the fraction of species A's range that overlaps species B, which typically differs from the fraction of species B's range that overlaps with species A) and/or are known to hybridize in the wild (McCarthy, 2006). We include hybridizing taxa together with taxa whose ranges are sympatric because both imply there is at least the potential for gene flow between taxa. Lastly, we considered a broad role for ecology on chromosome inversion evolution across clades according to the feeding guild used when defining

clades (i.e. clades defined as comprising granivores, insectivores, frugivores, or omnivores; del Hoyo et al., 2011).

The total number of inversions, branch length, range size, and body mass were log transformed, range overlap was arcsine square root transformed, and all variables were centered before analysis (Schielzeth, 2010). We then evaluated the extent to which the number of inversions that had fixed in each clade was associated with branch length, range overlap, range size, body mass, and ecology using generalized least squares to take into account phylogenetic relationships (Grafen, 1989). To do this, we used the NLME package in R (Pinheiro et al., 2014), with the expected error covariance matrix computed based on the phylogenetic distances between clades (Supplementary Figure 3). To assess the relative importance of each factor on the number of inversions fixed in each clade, we compared all possible models and selected the best-fit model based on sample size-corrected information criteria (AICc) using the R package MuMIn (Bartoń, 2013).

2.3.5 Chromosome inversion differences between sister species

We also considered the distribution of inversions between sister species, including both fixed differences and inversions segregating in one taxon but not the other. We determined which karyotyped species pairs were true sisters using the available phylogenetic literature (Table S6). We considered a sister pair to hybridize if they had documented hybrid zones or extensive natural hybridization where they co-occur (McCarthy, 2006). In total, we identified 47 true sisters with both species karyotyped.

For all 47 sister pairs, we calculated the number of inversion differences between them, combined branch length (i.e. twice their time to common ancestry), average range size, range overlap, and whether they are known to hybridize in the wild (12 of 47 pairs do). Inversion difference was scored both as a binary character (no inversions or at least one inversion difference) and as a count (total number of inversion differences). Range overlap was evaluated as a binary character: no overlap or some overlap. We only used this binary categorization because subdividing sisters who overlapped in range into either parapatric (average overlaps of the two species < 20%) or sympatric (>20% overlap) bins did not improve the fit of any model or alter the

results in any way. We used a linear model to examine the interaction between the number of sister pair inversion differences and each factor (age, range size, range overlap, and hybridization) after transforming the continuous character data as described for analysis of clades. Lastly, we assessed whether sister species with overlapping ranges, and the subset of sympatric sisters known to hybridize, are more likely to differ by an inversion than allopatric sisters using Fisher's exact tests.

2.3.6 Triplets

Genetic distance is not time but rather an estimate of time, and one that can come with substantial error (Hudson and Price, 2014). This error can diminish the true contribution of time and elevate the importance of alternative factors (Hudson and Price, 2014). A method to completely control for the potentially confounding influence of time is the use of species triplets (Noor, 1997; Martin, 2015). A triplet consists of a sister species pair (A, B) and a single outgroup taxon (O). Both sister taxa have by definition been separated from the outgroup for the same length of time. If O overlaps B but not A, then the presence of more inversion differences between O and B than O and A gives support for a role of range overlap independent of time (see Figure 3). We assembled a set of species triplets from the phylogeny of karyotyped species and published phylogenies, using the following criteria: both sister species A and B have been karyotyped, A and B are allopatric, and B overlaps in range with O but species A does not. This resulted in just 5 triplets (Table S7). We relaxed the criteria to allow (1) range overlap between A and B and (2) range overlap between A and O so long as they were not sympatric (i.e. ranges overlapped less than 20%) and overlapped in range less than B and O. The average extent of range overlap between species A and O, when they did overlap, was 3× less than the extent of range overlap between B and O. Nineteen triplets were present after applying the relaxed filtering criteria.

We counted the number of inversions inferred to have occurred along the branches leading to species A and B, respectively, based on the distribution of fixed inversions in the complete karyotyped species phylogeny. We also included inversion polymorphisms found in one but not the other taxon. We scored each triplet as follows: more inversions in A than B, more

inversions in B than A, or no difference in the number of inversions between A and B. We evaluated the direction and significance of the relationship between range overlap and inversion evolution across all triplets by applying a signed rank test to those sisters where the number of inversions differed.

2.3.7 Genomic distribution of chromosome inversions

Inversion fixation models that depend heavily on mutational input (e.g. meiotic drive and breakpoint selection) predict a strong correlation with range size but they also predict a strong association with mutation rate. In a final analysis to examine the extent to which inversion evolution is a mutation limited process, we examined the distribution of chromosome inversions across the genome and evaluated the degree to which the number of inversions fixed on a chromosome (Table S8) was associated with four possible mutagenic processes. First, if the mutation rate for inversions is constant per DNA base, the number of inversions should be proportional to chromosome size. Second, because inversions are derived from double-stranded meiotic breaks, the number of inversions on a chromosome could best be predicted by its map length or GC content – features associated with the number of cross-overs per chromosome (Baudat and de Massy, 2007; de Massy, 2013). Third, as inversion breakpoints are often located in repeat-rich regions of chromosomes (Skinner and Griffin, 2011; Kawakami et al., 2014), we tested for an association between the number of inversions and a chromosome's repeat density. Fourth, we asked if the dynamics of inversion fixation on the sex chromosomes and the autosomes differ (Hooper and Price, 2015). Mutation rates on the Z chromosome should be relatively high in birds because the Z spends ⅔ of the time in males, however this mutational advantage needs to overcome the fact that there are only ¾ as many copies of the Z as each of the autosomes (Ellegren and Fridolfsson, 1997; Axelsson et al., 2004).

Primary estimates of chromosome physical size, map length, and GC content were derived from the collared flycatcher genome assembly and linkage map (Kawakami et al., 2014) and chromosome repeat density was estimated from a RepeatMasker annotation of the zebra finch genome (http://www.repeatmasker.org; Smit et al., 2010). We use chromosome size and map length data from the collared flycatcher but obtained identical results when analyses were

repeated using chromosome size and map distance data derived from zebra finch (Backström et al., 2010; Warren et al., 2010) and hooded crow (*Corvus cornix*; Poelstra et al., 2014, Table S10). Comparative genomic studies indicate that chromosome size, GC content, and repeat density are conserved even between species in different avian orders (Zhang et al., 2014; Kawakami et al., 2014; Ellegren, 2013). While the recombination landscape may have phylogenetic signal (Dumont and Payseur, 2008; Dumont and Payseur, 2011; Smukowski and Noor, 2011), recombination hotspots are well maintained in passerines studied so far (Singhal et al., 2015).

We used data from all 411 karyotyped species to examine the correlation between chromosome inversion fixation rate and chromosome physical size, GC content, repeat density, and map length, using each chromosome as a replicate. In order to account for species with missing data we use inversion fixation rate (total number of inversions fixed on a chromosome

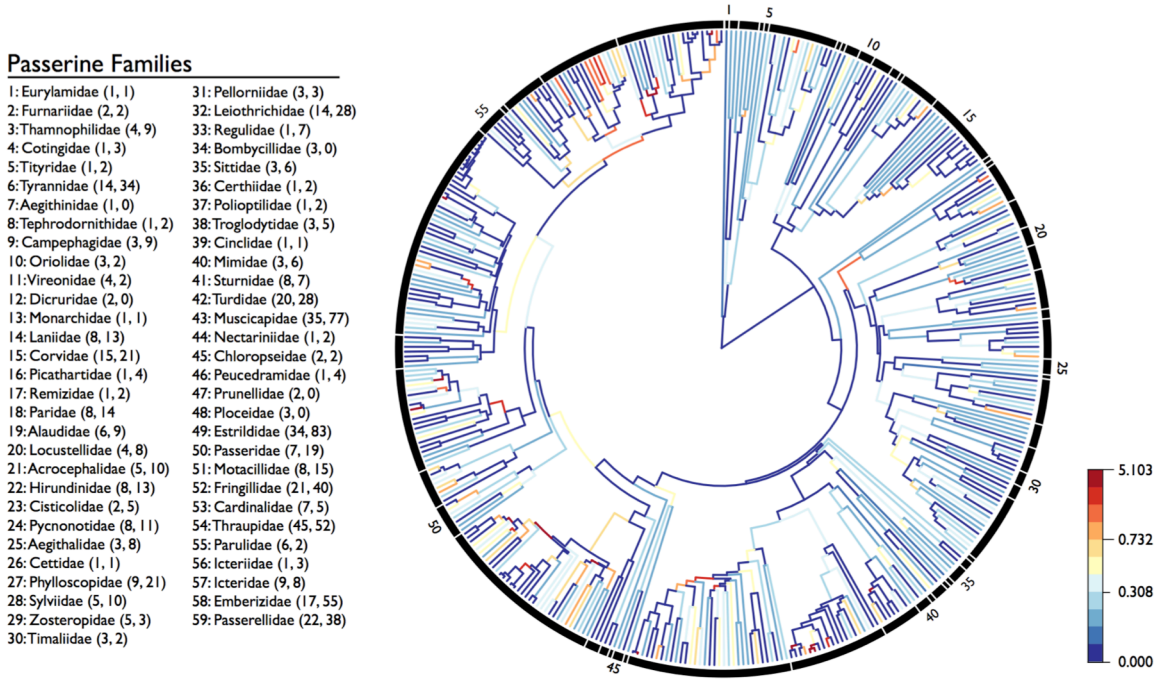

Figure 4 | Pericentric inversion fixation rate variation on the autosomes and Z chromosome combined across the Passeriformes. Passerine families included in this study are shown on the left: numbers within parentheses refer to the number of karyotyped species and number of autosomal and Z chromosome pericentric inversions identified within each family, respectively. Families are ordered clockwise by phylogenetic position in the tree. The time-dated phylogeny for the 411 karyotyped species used in this study is shown on the right. Branches are color-coded according to the inferred rate of pericentric inversion fixation (inversions per My) according to the Jenks natural breaks method where variance within bins is minimized, while variance between bins is maximized.

divided by the combined branch length for all species with data for that chromosome) rather than inversion number (Table S8). Independent variables were log-transformed. We evaluated support for alternative mutagenic hypotheses by comparing between all possible linear models and selected the best-fit model using the R package MuMIn (Bartoń, 2013). Restricting the analysis to the 291 species with complete karyotype data (i.e. documented centromere position for all 10 chromosomes) yielded a similar result (Table S10). Finally, we tested for significant differences in the rate of inversion fixation between the autosomes and the Z chromosome using the 81 independent passerine clades defined above as replicates and paired *t*-tests.

2.4 Results

2.4.1 Rate variation across the phylogeny of passerines

A time-calibrated phylogeny for 411 karyotyped passerine species is shown in Figure 4 and Supplementary Figures 1-3. The topology and divergence time estimates are congruent with recent studies that utilized partially overlapping fossil sets and similar calibration methods (Prum et al., 2015; Claramunt and Cracraft, 2015; Tables S4, S5). Inversion fixation rate varies greatly across lineages (Figure 4). To illustrate extremes, no inversions were fixed over 23.7 My on the lineage leading to the common iora (*Aegithina tiphia*) whereas an inversion on the 6th largest autosome separates the pied wheatear (*Oenanthe pleschanka)* from the black-eared wheatear *(O. melanoleuca*), with a divergence time of ~0.2 My. Thirty-two species (8%) carried chromosomal polymorphisms, and 8 of these had polymorphisms on more than one chromosome (Table S2). This is certainly an underestimate because sample sizes were often small (Methods).

2.4.2 Fixation rate variation across clades, sisters, and triplets

We partitioned the tree into 81 independent clades covering 284 of the 411 species, based on ecology and family membership, and evaluated roles for time, range size, range overlap as well as various ecological variables in accounting for differences in rate of inversion accumulation (Tables S1, S5). Within these clades, we identified 319 autosomal pericentric inversions and 56

Z chromosome rearrangements, which gives an average rate of pericentric inversion fixation across the Z plus autosomes of one every 4.7 million years of evolution. The range was from no inversions fixed over the span of 27.7 My (in the family Dicruridae) to four in 2.2 My (in the genus *Chloris*; Figure 3).

In the clade analysis, range overlap (Figure 5a) and range size (Figure 5b) correlate with fixation rate. The best model predicting the number of inversions fixed in each clade contained just two variables, branch length and the proportion of species with overlapping ranges; median range size drops out. The three top models (ΔAICc <2) had similar AICc scores and model weights. Model averaged results from these top models include clade range size and the interaction between range size and range overlap as additional parameters but only branch length ($p < 0.0001$) and range overlap are significant ($p = 0.002$, Table 3, Table S9.1). Results were consistent regardless of whether we used a more relaxed ΔAICc cutoff to model averaging (models with ΔAICc <4) and alternative minimum range overlap cutoff values (10% or 15% pairwise range overlap) to calculate the extent of range overlap in each clade.

Sister pair analyses support these findings (Figures 5c and 5d). Thirty-eight sympatric sister species were significantly more likely to differ by an inversion than 9 allopatric sister pairs (two-tailed Fisher's exact test: $P = 0.045$; Figure 5c). They also trend towards a greater number of inversion differences than allopatric sister pairs (Mann-Whitney-Wilcoxon test: $P = 0.07$; Figure 5d). However, sympatric sister pairs are older than allopatric ones (3.9 vs 2.5 My to the common ancestor on average; Supplementary Figure 4). In a comparison of general linear models, the best model explaining the presence of inversion differences between sister species contained a single parameter: whether sister species overlapped in range or not ($p = 0.047$; Table 3). Age did not contribute and no alternative models received support with ΔAICc <2 (Supplementary Table 9.2). Results were consistent regardless of whether we used a more relaxed ΔAICc cutoff to model averaging (models with ΔAICc <4). The sample of 12 sympatric sister species known to hybridize in nature are more often differentiated by an inversion than their 9 allopatric counterparts (although this is marginally non-significant; two-tailed Fisher's exact test, $P = 0.087$; Figure 5c), and were estimated to be of similar age (2.5 My for both, although hybridization may have reduced the estimate of divergence time of the sympatric species).

A major issue in the above analyses is whether branch length adequately controls for time. Species triplets consist of a sister pair and an outgroup species, where the outgroup overlaps one of the two sisters but not the other. Comparisons of differences between the outgroup and each sister therefore test for a role of sympatry, with time completely factored out (Noor, 1997; Martin et al, 2015; Hudson and Price, 2014). Figure 3 shows a representative example where inversion differences are associated with geographic overlap with the outgroup. This figure also indicates the only pair of allopatric sister species that differ by >2 inversions, and suggests that overlap with a third hybridizing species may have reduced the power of the previous sister pair analysis.

Results from the triplet comparison support the importance of range overlap (data in Table S7). A conservative triplet set, where the outgroup shows no overlap with one of the two sisters, has little power (N = 5) but in the three triplets that do show differences in inversion accumulation between the sisters, the species overlapping the outgroup has accumulated more inversions. In a relaxed triplet set, in which some degree of range overlap was allowed between the outgroup and both sisters, or between sisters (N = 19), 7 triplets showed no difference in inversion differentiation, 10 showed more inversions in the sister species that overlaps with the

	Clades, N = 81			**Sisters, N = 47**		
Parameter	**Estimate**	**95% CI**	***P***	**Estimate**	**95% CI**	***P***
(Intercept)	0.05	(-1.44, 1.54)	0.87	-0.44	(-2.11, 1.23)	0.601
Range overlap, arcsin	1.57	(0.57, 2.57)	0.002	1.69	(-0.29, 3.65)	0.043
Branch length, log My	0.84	(0.58, 1.09)	< 0.0001	-0.001	(-0.68, 0.68)	0.998
Range size, log km^2	0.13	(-0.14, 0.39)	0.34	0.215	(-0.43, 0.86)	0.517
Range overlap x Range size	0.1	(-0.44, 0.64)	0.72			

Table 3 | Model averaged results for the clade and sister species analyses. For clades, we used phylogenetic generalized least squares to predict the number of observed pericentric inversions. For sisters, we used a generalized linear model with binomial errors to predict the presence/absence of pericentric inversion differences and present the conditional model-averaged results for ΔAICc <4. Approximate 95% confidence intervals are the parameter estimate +/- 2 × standard error. P values for parameter significance were calculated by MuMIn in R (Bartoń, 2013) as the full average of the top models.

outgroup and 2 triplets the opposite pattern (comparing just those 12 triplets with differences, two-tailed sign rank test, p = 0.039). In the triplet analyses, differences in range size between sisters did not predict the number of inversion differences (regression of difference in inversion number on differences in range size, forced through the origin, P > 0.1).

2.4.3 Genomic distribution of chromosome inversions

In order to assess the possibility for mutational input to strongly determine rates of inversion we studied correlates of inversion fixation rate (inversions/My) with chromosome size and genome content, based on assemblies from the zebra finch and collared flycatcher (Table 4). For the full 411-taxa tree rates of inversion accumulation on the autosomes varied fourfold (Table 4). Results

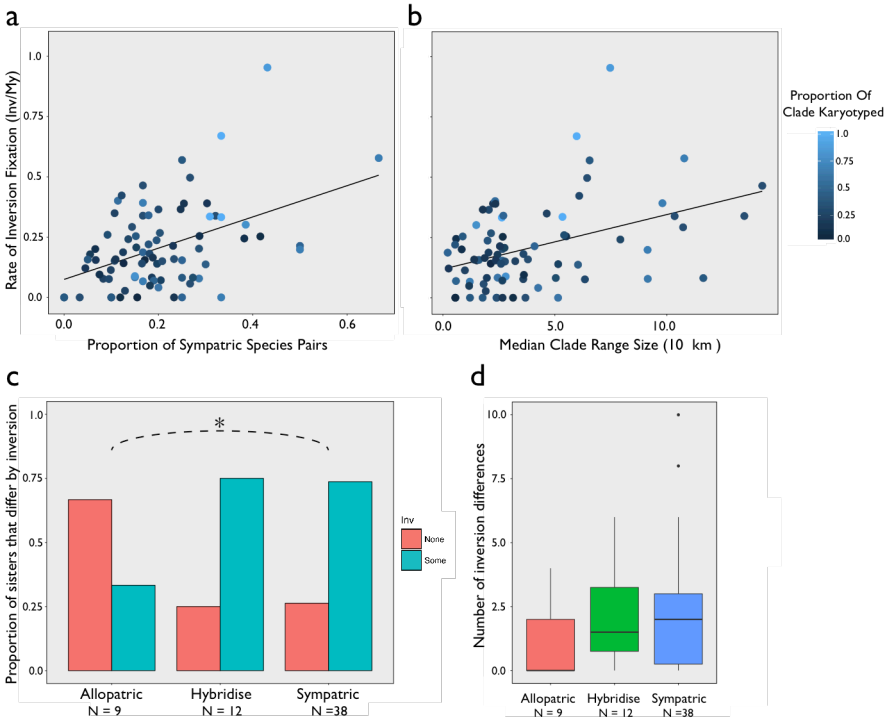

Figure 5 | Pericentric inversion fixation rate within small clades and between sisters. (a and b). Fixation rate across 81 clades, calculated as the total number of inversions on all chromosomes (autosomes and Z) divided by the total clade branch length summed across each chromosome. Each clade is represented by a circle and shaded according to the proportion of total species with karyotype data. (c and d) Sister species sorted into allopatric pairs, sympatric pairs (any amount of range overlap), and the subset of these sympatric sister pairs that are known to hybridize. Variation between sister species groups in (c) the proportion of sister pairs with and without inversion differences and (d) the number of inversion differences between sister species.

were qualitatively identical regardless of whether the zebra finch or collared flycatcher provided chromosome size and map distance data (Supplementary Table 10). The three top models for the autosomes had nearly equivocal AICc scores. The full average of these models included chromosome GC content and repeat density, but neither factor was significant. Results were robust to averaging the six models with ΔAICc <4 (Table S10). Moreover, inclusion of the Z chromosome in these analyses further reduced the fit of any mutagenic model to explain variation in inversion fixation rate between chromosomes.

Despite having fewer genes and a shorter map length than 6 of the autosomes, across the whole tree the Z chromosome has accumulated more inversions than any autosome (Table 4). Compared to the average autosome (but not the fastest autosome) the sex chromosomes evolved faster. When assessed across the 81 clades, inversion fixation rate on the Z chromosome is 1.4× greater than the average autosome (two-sample paired *t*-test with the 81 clades as replicates: t_{80} = 2.1, p = 0.041; Table S8). The genomic distribution of chromosomal variants within species, which includes both polymorphisms within a population and population differences, was in roughly the same ratio: of the 32 within-species pericentric inversion variants, 6 (19%) were on the Z chromosome whereas 10% would be naively expected, given we compared them with 9 autosomes.

We have separated the W chromosome from the main analyses because the genomic make-up of the W chromosome, notably large expanses of repetitive DNA, means that centromere movement may less clearly be related to inversions than on the other chromosomes. Further, a large fraction of the W chromosome is non-recombining implying that inversions within that region would have no affect upon recombination. Despite this, the W showed more centromeric movement than the Z when comparing across clades (paired *t*-test: t_{74} = 2.5, p = 0.013) and its rate of evolution was 2.4× that of the average autosome (t_{74} = 4.1, p = 0.0001). Within species polymorphisms are also common on the W chromosome (11 observed, compared with an average of 3.2 polymorphisms per chromosome for the Z and 9 autosomes, Table S2).

2.5 Discussion

Inversions in birds are common. Large pericentric inversions regularly separate even closely

Chromosome	Size (Mb)	Map Length (cM)	GC Content (%)	Repeat Density (%)	Branch Length (My)	Inversions
1 (FAL2)	157.4	320	39	0.38	4449.2	39
2 (FAL1)	119.8	245	39.2	0.23	4449.2	71
3 (FAL3)	115.7	230	39.4	0.38	4449.2	80
4 (FAL1A)	74.8	230	39.7	0.14	4449.2	108
5 (FAL4)	70.3	175	39.2	0.28	4437.3	104
6 (FAL5)	64.6	172	40.8	0.12	4398.1	79
7 (FAL7)	39.3	125	41.1	0.14	4242.1	48
8 (FAL6)	37.2	122	41.6	0.19	4088.8	35
9 (FAL8)	32	95	41.3	0.5	3973.8	23
Z	59.7*	165	39.2	1.5	4449.2	121

Table 4 | Genomic distribution of chromosome inversions. Autosomes are listed in order of descending size with their presumed homology to the collared flycatcher (*Ficedula albicollis*) genome given in parentheses. Values for chromosome size and map length come from the collared flycatcher genome (Kawakami et al., 2015) while GC content and repeat density come from the zebra finch (*Taeniopygia guttata*) genome (Smit et al, 2010; Warren et al., 2010). Variance in branch lengths by chromosome reflects species with missing data.

related species (e.g. Figure 3). We have restricted our analyses to only those pericentric inversions large enough to be detectable via cytological analysis, which excludes not only all paracentric inversions but also small pericentric inversions, so these counts are surely an underestimate of the true extent of chromosome inversion variation in passerines, as is becoming increasingly clear from genomic studies (Zhang et al., 2014; Kawakami et al., 2014; Singhal et al., 2015; Knief et al., 2016). Large pericentric inversion polymorphisms within species are also common and clearly underestimated by us, as sample sizes were often small. Indeed, twice as many individuals were karyotyped in the 31 passerine species found to have inversions segregating versus the study as a whole (9.9 versus 4.8 individuals, respectively; excluding 3 species of large sample size, Supplementary Figure 5; Table S2).

The main result is that the strongest correlate of inversion fixation after accounting for time, is not range size, but range overlap. Range overlap is pertinent to models of inversion spread because this gives the possibility for hybridization between taxa. F1 hybrids should more rarely recombine parental allelic combinations in the inverted region compared to co-linear chromosomes, with the consequence that fewer backcrosses carry deleterious combinations, whether these deleterious consequences are for ecological reasons, or simply because of genetic

incompatibilities (Kirkpatrick and Barton, 2006; Dagilis and Kirkpatrick, 2016). Secondary contact between long divergent forms is regularly associated with hybridization and genetic exchange (reviewed in McCarthy 2006; Payseur and Rieseberg, 2016). We know for birds that hybrid zones regularly form between taxa that can be millions of years old (Weir and Price, 2011; Table S6), and the generation of complete infertility of hybrids takes a comparable length of time (Price and Bouvier, 2002). Altogether, the evidence suggests that one contribution to the establishment of pericentric inversions in passerines stems from their selective advantage in keeping sets of adapted alleles together. We first consider caveats before returning to the main results.

A major issue is that allopatric sister species may exhibit fewer inversion differences than sympatric sisters due to a lower mutational input, either because they have smaller population sizes or because they are younger. In fact, sympatric sister pairs are of similar range size to allopatric pairs and statistically, we find no evidence that range size is an important contributor to inversion fixation. However, sympatric sister pairs are older than allopatric ones and age differences do correlate with the number of inversions fixed. Nevertheless, all our tests indicate that this is unlikely to completely over-rule a role for range overlap. Two examples illustrate the case for an association between range overlap and inversion fixation. First, tits in the genera *Periparus* and *Pardaliparus* last shared a common ancestor 7Ma (5.2 – 8.9Ma, 95% Highest Posterior Density), have largely allopatric distributions (no pair of species overlap in range more than 20%), and no known inversion differences. In stark contrast, an Asian clade of tits in the genus *Poecile* diverged 4.3Ma (3.1 – 5.6Ma, 95% HPD), are largely sympatric (⅔ of pairs), and the species examined differ by up to seven pericentric inversions (Table S5). A second example comes from greenfinches in the genus *Chloris* (family Fringillidae; Figure 3). Inversion differentiation between *C. sinica* and sympatric *C. ambigua* has outpaced inversion differentiation between *C. sinica* and allopatric *C. chloris*. In both the tits and the greenfinches, a model where gene flow promotes the spread of inversions has additional support because hybridization between overlapping species has been recorded in nature (in the tits, between *Poecile montanus* and *P. palustris*, and in the finches, between *C. ambigua* and *C. sinica*; McCarthy, 2006).

The second issue is whether hybridization promotes inversion fixation or instead incompatibilities associated with inversions prevent sympatric species collapse. In the latter case,

species that overlap in range may show more inversions than allopatric ones because those allopatric forms without inversions have fused on secondary contact. However, this still raises the issue of what forces cause inversions to arise in allopatry, and why they should differentially accumulate incompatibilities. In the model of Navarro and Barton (2003), inversions accumulate incompatibilities because they trap alleles that would otherwise flow across the species border. Therefore, it may be that inversion promotion and inversion preservation are best considered complementary explanations, with both integrally tied to recombination suppression in the face of gene flow.

Further separating the promotion or preservation models is difficult. For example, the relatively large number of inversions on the Z (and likely on the W) may reflect Haldane's rule processes and inversion preservation, because they cut off gene flow through the heterogametic sex early (notably because of recessive incompatibilities exposed in the heterogametic sex, and Z-W interactions; Price, 2008; Turelli and Orr, 2000). But these same processes may select for inversions to increase on the sex chromosomes because they tie together those incompatibilities that are most strongly expressed in young species pairs where hybridization produces at least some fertile F1 offspring. Coyne and Orr (1989) noted that under a model of differential merging, young sympatric pairs should form a subset of the allopatric pairs, which implies that some allopatric pairs should differ in inversions. In our study most young allopatric sisters do not differ in inversions (Supplementary Figure 4). This would appear to support a role for secondary contact in promoting their spread. However, sample size is small (9 pairs of allopatric sisters) and one pair of allopatric sisters does differ by four inversions (3 fixed differences and an inversion polymorphism). This four inversion allopatric pair may therefore be consistent the idea of preservation on contact, but that particular example can be explained away because the outgroup to the sisters hybridizes with the species that has accumulated three of the inversions (Figure 3).

Other processes beyond those associated with recombination suppression surely contribute to inversion accumulation. If gene flow is a frequent event upon establishment in sympatry, and breakpoint selection or meiotic drive has driven accumulation of inversions in allopatry, we have argued that inversions would introgress across the species barrier rather than contribute to species differences. We also suggested that these models predict a particularly strong scaling with population size because they depend on mutagenic input. However, these

predictions assume many other factors are held constant. For example, large inversions capture multiple alleles, possibly including rare deleterious recessives, which would prevent fixation of the inversion despite whatever selective forces favor its increase (Kirkpatrick and Barton, 2006). Further, the rapid movement of the centromere on the W chromosome is most easily explained by high mutagenic input (Materials and Methods). If any of these centromere movements are a consequence of inversions, they are unlikely to be due to recombination suppression, because recombination is already limited to a small pseudo-autosomal region on the W (Singhal et al., 2015). The Z chromosome has a higher inversion fixation rate than any autosome, which may reflect an elevated mutagenic input due to a male-biased mutation rate, as the Z chromosome spends ⅔ of its time in males. However, as noted above, the Z may be particularly likely to accumulate inversions as a consequence of their effects on recombination suppression in hybrid zones, as well as in cases of sexual conflict.

Processes that depend strongly on mutagenic input can be evaluated using information on genome content (Table 4). The distribution of chromosome inversions detected using comparative genomic approaches in birds is positively associated with chromosome size (Zhang et al., 2014; Kawakami et al., 2014) and inversion breakpoints are often located in regions with elevated recombination rates, GC content, and repeat density (Kawakami et al., 2014). These results suggest a role for models where mutagenic input is the rate-limiting factor, such as the breakpoint and meiotic drive models. However, the results were not replicated here, and we found few correlates of genome content with inversion accumulation (although repeat density is suggestive.) A primary reason for the difference between the genomic studies and ours likely resides in the different size classes of inversions considered between studies (Hooper and Price, 2015). Inversions detected from comparing high-resolution linkage maps (Kawakami et al., 2014) or whole genome alignments (Zhang et al., 2014) are capable of finding structural variants orders of magnitude smaller than the exclusively large inversions we identified from cytological data. We suggest that the large pericentric inversions considered here may become established in a different manner to small rearrangements, because they are potentially associated with both higher fitness costs and greater selective advantages than the more comprehensive set of inversions found in comparative genomic surveys.

In conclusion, our results generally support recombination suppression mechanisms that drive the increase in frequency of inversions. The presence of many within-species inversion polymorphisms in birds implies other mechanisms contribute to inversion accumulation beyond those driven by range overlap, but many of these mechanisms also likely involve recombination suppression. For example, female preferences for male traits are more likely to increase if the trait and preference are in strong linkage disequilibrium (Lande, 1981). Further, whatever the selective advantage, if favored inversions capture deleterious alleles when they first arise, they may not increase to fixation and result in stable polymorphisms (Kirkpatrick and Barton, 2006), as inferred for at least two bird species (Küpper et al., 2015; Lamichhaney et al., 2015; Tuttle et al., 2015). Two examples are known of the same inversion polymorphisms segregating in more than one species (Table S2), which may reflect introgression or preservation through the speciation event. Whether inversion polymorphisms have arisen by a different class of mechanisms than inversions fixed between species remains to be determined.

3 Chromosomal inversions and reproductive isolation in an avian hybrid zone[1]

3.1 Abstract

Hybrid zones are powerful natural systems with which to examine speciation as a process. Before reproductive isolation is absolute, a hybrid zone may act as semipermeable genetic barrier between diverging populations: universally favored mutations will often sweep between populations while alleles that are deleterious in the opposite genetic background do not. When the genomes of hybridizing taxa are enriched for variation that is deleterious in the genomic background of the other species, hybridization can generate a selective advantage for a recombination modifier, like a chromosome inversion, that maintains linkage between sets of differentially adapted genes. Using a combination of genomic (genotype-by-sequencing) and morphological analyses (bill color reflectance spectrometry), we analyze the hybrid zone between two subspecies of the long-tailed finch (*Poephila acuticauda*), which differ markedly in bill color and have a highly heterogeneous landscape of genetic divergence. Genomic differentiation between subspecies is observed to be low across the autosomes, except notably for a region on chromosome 8 that appears to be involved in bill color variation, and disproportionately concentrated onto the Z chromosome within a chromosomal inversion. We describe genomic evidence for this inversion on the Z and describe its geographic distribution in relation to the extent of reproductive isolation between subspecies. Strikingly, we observe that while the widths of genomic and morphological admixture in the long-tailed finch system are both narrow (118 and 146 km wide, respectively), their centers are displaced by 350 km from each other. This suggests that bill color, the principal morphological trait upon which subspecies were first described, may be entirely unlinked from reproductive isolation in the long-tailed finch.

[1] Portions of this chapter have been published as: Griffith SC and Hooper DM. 2017. Geographical variation in bill colour in the Long-tailed Finch: evidence for a narrow zone of admixture between sub-species. Emu – Austral Ornithology 117: 1-10.

3.2 Introduction

Hybrid zones allow a direct examination of the development or erosion of reproductive isolation between incipient species and can therefore enable the study of speciation as a process. While gene flow generally acts to homogenize differences between diverging populations it can, paradoxically, play a creative role in speciation by promoting the evolution of chromosome inversions that encompass and keep together sets of locally adapted genes – thereby accelerating the establishment of reproductive isolation (Navarro and Barton, 2003; Kirkpatrick and Barton, 2006; Dagilis and Kirkpatrick, 2016). Across the passerine birds, the rate of chromosome inversion fixation scales with the proportion of closely related species that are found in sympatry and sister species that overlap in range are more likely to differ by chromosome inversions than those in allopatry (see Chapters 1 and 2). These findings are consistent with a model in which gene flow following secondary contact establishes a selective advantage for inversions to spread to fixation. However, this has yet to be tested directly. Here, we examine the hybrid zone between two subspecies of the long-tailed finch (*Poephila acuticauda*, Estrildidae), a small passerine endemic to the top end of Australia, with chromosome inversions known to be segregating (Christidis, 1986a), in order to evaluate whether inversions are involved in maintaining subspecies as independently evolving populations.

The long-tailed finch comprises two populations that differ principally in bill color with a prominent phenotypic difference (yellow in the west and red in the east) across their geographic distribution over the tropical savannahs of northern Australia. Indeed this difference in bill color contributed to their division into two subspecies as long ago as 1900 when Heinroth (1900) named the *hecki* subspecies. The exact nature of variation in bill color over the entire range of the species, however, remains unclear. At the two extreme ends of the range it is well established that in the west *Poephila acutiacuada acuticauda* has a yellow bill and in the east individuals of *P. a. hecki* have red bills (Higgins et al., 2006). The literature presents two alternative positions with respect to the geographic center and extent of bill color admixture between subspecies. In the

first, bill color follows a geographic pattern of gradual variation from yellow, through shades of orange to red along a fairly constant longitudinal gradient from west to east (Immelmann, 1965; Mayr et al., 1968). In the alternative, there is a more abrupt geographic transition between two distinct, and diagnostic forms with little to no evidence of admixture (Keast, 1958; Harrison, 1974; Boles, 1988). The distinction is important as a wide and gradual bill color cline width provides little support for the existence of two evolutionarily distinct lineages while a narrow and abrupt bill color cline width is more consistent with a hybrid zone between evolutionarily distinct populations whereby selection acting against hybrids and/or the parentals sets the extent of admixture (Barton and Hewitt, 1985; Cracraft, 1986; Barton and Gale, 1993).

The geographic location of the phenotypic boundary between long-tailed finch subspecies has also been the subject of considerable discussion. First, with Keast (1958) suggesting that the nominate race was confined to the Derby area with orange-billed birds everywhere else. Harrison (1974) later suggested that the divide is around the Western Australian border with the Northern Territory. In Cracraft's (1986) paper, his Figure 1, suggests that the boundary between the two is on the west side of the Cambridge Gulf (and around the longitude of Wyndham, Western Australia). In his Figure 5, Ford (1987a) places the division between the two subspecies slightly to the east, and the line roughly bisects the town of Kununurra, Western Australia.

Many pairs of closely related Australian species and subspecies have ranges with coincident overlapping range boundaries across prominent biogeographic breaks and along clinal environmental gradients (Cracraft, 1986, Ford, 1987a, Ford, 1987b). These coincident biogeographic breaks, a likely product of repeated bouts of widespread aridification and habitat fragmentation throughout the Pleistocene, have resulted in many taxon pairs that vary conspicuously in color (in birds, plumage or bill color) and often hybridize where their ranges meet: as seen in the eastern yellow robin *Eopsaltria australis* (Ford, 1979) or the chestnut quail-thrush *Cinclosoma castanotum*; Ford, 1981). More recent studies of species such as the red-backed fairy-wren (*Malurus melanocephalus*; Baldassarre et al., 2013; 2014) have taken advantage of field portable optical spectrometers to quantitatively examine fine scale variation in color variation. This is particularly useful for the characterization of colored parts such as skin and mandibles because the color of these parts degrades relatively quickly after death and is not reliably measured on museum skins, unlike plumage coloration that may maintain its color for many

decades (Dale et al., 2015). As conspicuous color displays are often the product of sexual selection, hybridization between taxa that differ in such traits enables a direct investigation of divergence in color preference and production as well as the importance of such traits to the emergence of reproductive isolation: both pre- and post-zygotic in nature.

Beyond the primary difference in bill color, the long-tailed finch also shows subspecific differences in song (Zann, 1976) and sperm morphology (Rowe et al., 2015) – traits known in birds to contribute to pre-mating and post-mating pre-zygotic isolation (Price, 2008). The presence of chromosome inversions, together with the availability of traits that may be involved in both pre- and post-zygotic isolation between hybridizing subspecies, makes the long-tailed finch an ideal target with which to examine the contribution of chromosome inversions to

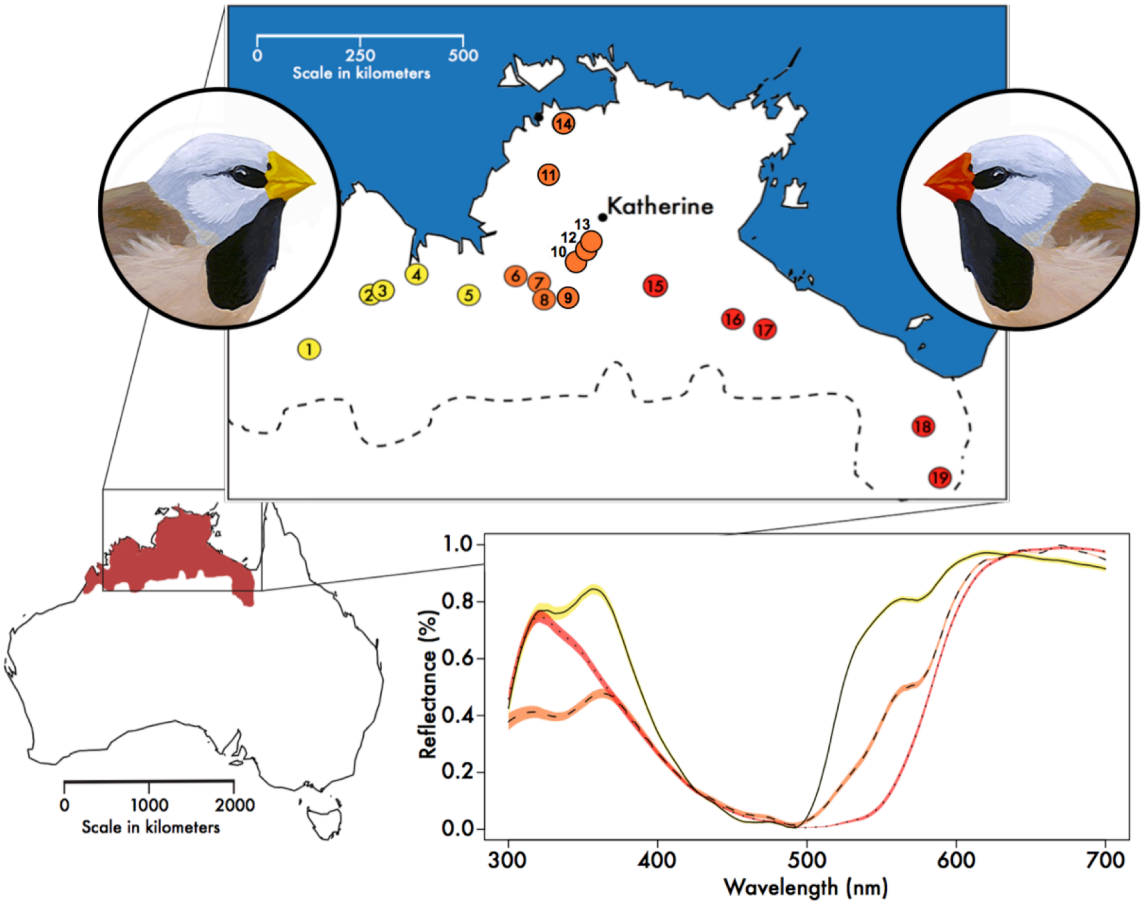

Figure 6 | Long-tailed finch (*Poephila acuticauda*) range, population sampling, and bill reflectance spectrometry curves. Clockwise from bottom-left: Geographic range of the long-tailed finch, map inset with geographic locations of the 19 populations sampled in this study – details in Table 5. Lower right, example reflectance spectra for populations of yellow (solid line), red (dotted line), and orange-billed individuals (dashed line) presented as mean and standard error.

reproductive isolation in an avian system. The intentions of this study were to 1) characterize the nature of contemporary variation in bill color and identify the genetic basis of this defining trait, 2) assess the extent of genomic differentiation between subspecies and locate the center and extent of genetic admixture between them, and 3) to find genetic evidence of chromosomal inversions and evaluate whether they contribute to reproductive isolation.

3.3 Materials and Methods

3.3.1 Study system and sampling

We captured long-tailed finches in the dry season (between late August and October), in three years 2009, 2010, and 2015. Birds were targeted with mist nets as they visited watering points (mostly in the early morning). All individuals were banded with a numbered metal band supplied by the Australian Bird and Bat Banding Scheme. We captured 784 adult individuals across 18 sites and that span nearly the entire longitudinal distribution of the species (1500 of 1800 km). The range of the species extends about a further 300km west of the westernmost sample that we took (Mt. House; Figure 6), but was not sampled for logistical reasons. Bill color was measured for all 784 of these adult individuals. Blood samples for genomic analysis were taken from the brachial vein of adult and juvenile individuals and stored on EDTA-treated FTA cards or placed directly into 90% ethanol and stored long-term at -20°C. Blood samples of the long-tailed finch from an additional site and tissue and blood materials from congeneric outgroup taxa used in order to root genetic analyses (both subspecies of the black-throated finch *Poephila cincta cincta*, *Poephila cincta atropygialis*; and both subspecies of the masked finch *Poephila personata personata*, and *Poephila personata leucotis*) were sourced from the Australian National Wildlife Collection (ANWC). Details for all sampled populations are presented in Table 5.

3.3.2 Bill color quantification and analyses

We quantified bill color via spectral reflectance of the upper mandible taken in three consecutive scans from the center of the bill using a USB2000 + Miniature Fiber Optic spectrophotometer

(Ocean Optics Inc., Dunedin, FL, USA), a xenon light source PX-2 (Ocean Optics Inc.) with a fiber-optic cable held at an angle of 90° to the bill and about 10mm from the surface of the mandible with a plastic sheath that excluded ambient light. Reflectance data were captured using the program AVASOFT 7 (Avantes, Eerbeek, Netherlands). We did not include juvenile individuals with immature black colored bills or juveniles with partially colored bills that still had a clear black or grey section, indicative of incompletely developed coloration, in the analyses presented.

In order to remove noisy or flat reads, all reflectance spectra were first checked by eye using the R package *pavo* (Maia et al., 2013). After 47 individuals were removed following quality filtering, reflectance spectra from a total of 737 adult individuals were included in the present analyses (Table 5). We utilized the processing functions of *pavo* to average the three replicate reflectance spectra for each individual and to loess-smooth the averaged spectra curves. Following Cuthill et al. (1999) we normalized spectra by maximum and minimum reflectance values and centred spectra to a mean reflectance of zero in order to remove bill brightness as a dominant variable. We analyzed geographic variation in bill color in two ways. First, to focus attention on variation between long-tailed finch bills across the yellow-red part of the visual spectrum, we restricted analyses to reflectance measurements between 450-650 nm. Following Montgomerie (2006), we quantified bill coloration for all individuals as chroma (S5, a measure of color saturation; Peters et al., 2004) based on the average reflectance using the summary.rspec function in *pavo*. Second, we assessed the main axes of color variation through principal component analysis of reflectance measurements between 300-650 nm after centering spectra to a mean of zero and binning spectra to 17 nm intervals using the procspec function in *pavo*. Together, PC1 and PC2 explained 70.8% of variation in bill color across samples (PC1: 39.5%; PC2: 31.3%). Loadings for PC2, however, most directly correspond to variation between yellow and red-billed individuals. As results using PC loadings for bill color were statistically identical to results based on chroma (S5), I here present only the results of the latter (see full results in Griffith and Hooper, 2017).

No.	Name	Latitude	Longitude	Distance (km)	Sampling Date	Ancestry	Bill Chroma S5	Hybrid Index (HI_A)	Hybrid Index (HI_Z)	Bill Color *N*	Genetic *N*
1	Mt. House	17.1°S	125.6°E	0	09/2009	*acuticauda*	0.18 ± 0.05	0.068	0.006	89	20
2	Ellenbrae	16.0°S	127.1°E	205	09/2009	*acuticauda*	0.18 ± 0.04	0.054	0.002	12	15
3	Nelson	15.8°S	127.5°E	246	09/2009	*acuticauda*	0.11 ± 0.05	0.294	0.022	48	14
4	Wyndham	15.6°S	128.1°E	317	05 and 09/2009	Admixed	0.15 ± 0.08	0.425	0.218	79	15
5	Newry	16.1°S	129.1°E	389	08 and 09/2009	Admixed	0.17 ± 0.05	0.531	0.738	16	15
6	Auvergne	15.6°S	130.3°E	523	09/2015	*hecki*	0.25 ± 0.08	0.874	0.997	92	20
7	Coolibah	15.8°S	130.8°E	571	09/2015	*hecki*	0.28 ± 0.06	0.837	1.000	68	20
8	Kidman Springs	16.1°S	130.9°E	574	09/2015	*hecki*	0.32 ± 0.05	0.895	0.999	18	17
9	Mooloolo	16.1°S	131.4°E	632	09/2015	*hecki*	0.18 ± 0.05	0.844	0.997	6	8
10	Willeroo	15.3°S	131.6°E	670	09/2015	*hecki*	0.35 ± 0.08	0.905	0.999	33	20
11	Tipperary	13.6°S	131.0°E	695	09/2015	*hecki*	0.57 ± 0.08	0.943	0.999	55	19
12	Stapleton – Mathison	15.1°S	131.8°E	697	09/2015	*hecki*	0.47 ± 0.12	0.917	0.999	59	20
13	Stapleton – Bullyard	14.9°S	131.9°E	710	09/2015	*hecki*	0.46 ± 0.09	N/A	N/A	6	0
14	Koolpinyah	12.7°S	131.2°E	779	10/2002	*hecki*	N/A	0.959	1.000	0	6
15	Maryfield	15.8°S	133.4°E	844	09/2010	*hecki*	0.83 ± 0.05	0.981	0.999	27	15
16	October Creek	16.6°S	134.9°E	988	09/2010	*hecki*	0.82 ± 0.05	0.992	1.000	27	14
17	McArthur River	16.5°S	135.9°E	1096	09/2010	*hecki*	0.86 ± 0.05	0.990	0.996	32	14
18	Chidna	19.4°S	139.4°E	1486	09/2010	*hecki*	0.90 ± 0.04	0.998	0.999	70	19
19	Leichardt	20.3°S	139.7°E	1530	09/2010	*hecki*	N/A	0.998	0.999	0	14
	Total									737	285

Table 5 | Sampling transect across the range of the long-tailed finch. Sampling locations (from west to east, with distance from Mt. House), dates and sample sizes (individuals with spectrometric data and genetic data), as well as average and standard deviation for bill chroma (S5), between 450-650nm, and hybrid indices (HI_A and HI_Z), respectively.

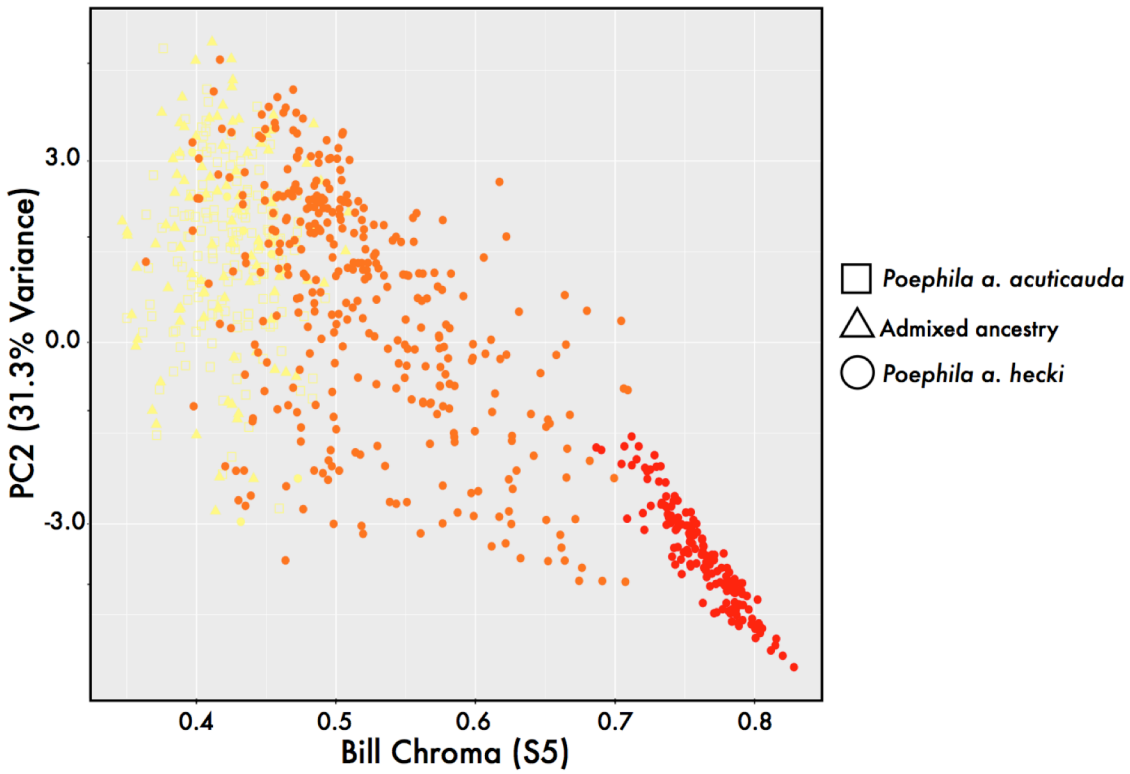

Figure 7 | Bill color and ancestry variation across the range of the long-tailed finch. Bill color represented both as chroma (S5) from 450-650 nm and individual loading for PC2 (31.3% variation) from 300-650 nm for all 737 individuals analyzed. Individuals have been represented in two ways. First, colored according to the average standardized bill chroma (S5) at their population of origin: yellow, bill chroma below 0.2 (pops. 1 – 5 and 9); red, bill chroma above 0.8 (pops. 15 – 18), and orange, bill chroma between 0.2 and 0.8 (pops. 6 – 8 and 10-13). Second, symbolized according to the average HI_Z Q score at their population of origin: squares, Q below 0.1 (subspecies *acuticauda*, pops. 1 – 3); circles, Q above 0.9 (subspecies *hecki*, pops. 6 – 19); and triangles, Q between 0.1 and 0.9 (admixed ancestry, pops. 4 and 5).

3.3.3 Genomic library preparation, sequencing, and variant calling

DNA was extracted from blood and tissue materials using the Qiagen Gentra Puregene Tissue Kit (Qiagen) following manufacturer's instructions with slight modifications. Samples were incubated in a 55°C shaking incubator (500 rpm) overnight in 225 µl of cel lysis buffer with 2-4 µl of proteinase K. Genomic DNA was quantified using a Qubit (Thermo Fisher Scientific); samples were diluted to ~100 ng/µl when initially greater than this concentration.

Genomic libraries were created following the MSG protocol previously described in Andolfatto et al. (2011) and Schumer et al. (2014). Briefly, 200 ng of DNA was digested with

the restriction enzyme MseI; following digestion, custom barcodes were ligated to each sample. To each sample, 5 µl of sodium acetate and 50 µl of isopropanol were added to each sample and samples were pooled in groups of 96 or 64 and precipitated overnight at -20°C. Following overnight precipitation, samples were extracted and re-suspended in TE (pH 8.0) and purified through a phenol-chloroform extraction and Agencourt bead purification (Beckman Coulter Inc., Brea, CA). Pooled libraries were run on a Blue Pippin 1.5% agarose gel cassette (Sage Science) and fragments between 250-300 bp were selected for and purified. 3-8 ng of each pooled sampled was amplified for 11-13 PCR cycles with custom indexed primers (generously shared by members of the Andolfatto lab) and 100 bp paired-end sequenced upon one Illumina HiSeq 4000 lane. A total of 354 individual samples were sequenced across six Illumina HiSeq 4000 lanes (*Poephila acuticauda*, N =285; *P. cincta*, N = 40; *P. personata*, N = 30; Tables 5 and 6).

Raw reads from the six pooled genomic libraries were first de-multiplexed by an individual specific barcode, trimmed for restriction enzyme overhang, and quality filtered to remove reads with more than seven bases below Q20 using ipyrad v.0.6.11 (http://github.com/dereneaton/ipyrad). Following de-multiplexing, individual reads were mapped to the zebra finch reference genome assembly taeGut1, otherwise known as WUGSC 3.2.4 (ftp://hgdownload.cse.ucsc.edu/goldenPath/taeGut1/chromosomes/), using BWAmem v.0.7.12 (Li, 2013). Sequence divergence between the long-tailed finch, as well as the two other *Poephila* taxa, and the zebra finch is low, about 1.6% (Singhal et al., 2015), and on average 98% of reads for the three *Poephila* species successfully mapped to a unique position in the zebra finch reference assembly.

Following initial alignment, nucleotide variants were called across the entire zebra finch reference assembly using the GATK v3.7 HaplotypeCaller (McKenna et al., 2010). We integrated variant data calculated individually across all samples into a combined VCF file using the CombineGVCF and GenotypeGVCF modules in GATK. SNPs were pruned from this initial variant call set via hard quality filters in GATK as follows: variant confidence by depth (QD < 2.0), strand bias (FS > 60.0), mapping quality across samples (MQ < 40.0), mapping quality of heterozygous variants (MQRankSum < -12.5), and distance from read ends for variant calls (ReadPosRankSum < -8.0). Moreover, SNP variants in known repetitive regions in the zebra finch genome and SNPs in regions with exceptionally high coverage were masked as to

avoid including error-prone variants and variants from genomic regions that are likely to be collapsed duplicates in a genome assembly, respectively. We masked SNPs at sites where coverage was greater than 5× the species average and SNPs at sites that overlapped the repeat annotation for the zebra finch comes from the RepeatMasker Repeat Library (Smit et al., 1996-2010; http://www.repeatmasker.org). Finally, this quality-filtered variant set was further refined using vcftools v0.1.14 to exclude singletons (--mac 2), variants missing coverage in more than 50% of samples (--max-missing 0.5), and samples with less than 60% of the remaining genotyped variable sites. One set of the remaining 79,428 quality-filtered variants included only long-tailed finch samples and a second included SNP data from all three *Poephila* taxa.

Finally, in order to accurately estimate sample sizes for clinal analyses and evaluate haplotype clustering in principal component analyses, below, all 285 long-tailed finch samples sequenced for this project were sexed to male or female by amplifying the sex-linked CHD gene using primers 2550F and 2718R (Fridolfsson and Ellegren, 1999) and visualizing the PCR product upon a gel following electrophoresis. Samples were scored as male from the presence of a single PCR band (homozygous, ZZ) or as female from the presence of two bands of different size (heterozygous, ZW).

3.3.4 Population structure analyses

We first used our quality-filtered set of SNP variants to evaluate the extent and distribution of genomic differentiation between long-tailed finch subspecies by computing averaged F_{ST} for i) all autosomal chromosomes together and ii) the Z chromosome for each pair of populations sampled. While averaged pairwise F_{ST} for the autosomes is low ($F_{ST} \approx 0.0$) between all populations, we observe two highly differentiated ($F_{ST} \approx 0.4$) population pools based on the averaged pairwise F_{ST} for the Z chromosome that we define as: subspecies *acuticauda*, populations 1-3, (N = 49); subspecies *hecki*, populations 6-19, (N = 206); and two populations of mixed ancestry (pops. 4-5, N = 30, Table 5).

Outlier regions in scans of genomic differentiation can result from processes other than divergent selection and resistance to gene flow, notably shared background selection and regions of low recombination. In order to identify regions of the genome significantly differentiated

across the long-tailed finch hybrid zone resulting from differential selection, we built an empirical null model of differentiation across the genome for allopatric control populations belonging to the same subspecies and bill color (following Vijay et al., 2016). Using two control comparisons (see Figure 8) we first determined outlier windows at the 99th percentile of the Z-transformed F_{ST} distribution (F_{ST}'), with differentiation represented in units of standard deviation relative to the mean. These outlier regions in control comparisons are likely to be the result of processes other than divergent selection in our hybrid zone. We next evaluated outlier regions in our focal comparison (between populations 3 and 6) in the same way. Finally, we subtracted the maximum value of orthologous windows in control comparisons from our focal hybrid zone comparison (Figure 8) and identified outliers at the 99th percentile for this net genetic differentiation statistic (ΔF_{ST}'). Outlier windows for in the focal comparison for F_{ST}' but not for ΔF_{ST}' are interpreted as regions of differentiation produced from processed shared across the entire species. However, outlier regions in the focal comparison present in both F_{ST}' and ΔF_{ST}' were considered to be resistant to gene flow and under divergent selection between subspecies.

In order to examine the geographic extent of genetic admixture between long-tailed finch subspecies, we analyzed our set of variants in two ways: first, using only autosomal SNPs and, second, using a subset of Z chromosome SNPs drawn from the quality filtered set of variants described above and found to be at an allele frequency ≥ 0.9 or ≤ 0.1 in subspecies *acuticauda* (pops. 1 – 4) and ≤ 0.1 or ≥ 0.9 in subspecies *hecki* (pops. 14 – 19), respectively. Each subset of SNP loci consisted of 481 and 3814 markers, respectively. We used the Bayesian clustering approach implemented in STRUCTURE v2.3.4 (Pritchard et al., 2000; Falush et al., 2003) in order to assign individual samples to genetic groups. We first set the hypothesis about the number of genetic clusters (*K*) equal to 2 as we seek to investigate the hybrid zone between subspecies. Moreover, increasing *K*, or setting *K* to 1, did not result in a superior fit to the data as determined by log likelihood comparison. We ran 10 iterations for each expectation of *K*, using the admixture model with correlated allele frequencies, and a burn-in period of 100,000 MCMC replicates. Results across iterations of *K* were concatenated and summarized using the program CLUMPP (Jakobsson and Rosenberg, 2007). Following Singhal and Moritz (2013), we assigned a hybrid index score to each sample based upon the probability (*Q*) each sample was assigned by

STRUCTURE to the eastern *hecki* subspecies. Accordingly, two hybrid indices were generated for each sample: one using the autosomal set of 481 diagnostic SNPs (hereafter HI_A) and one using the Z chromosome set of 3814 diagnostic SNPs (hereafter HI_Z). Finally, all individuals were assigned to a hybrid category (i.e. pure parental or admixed) based upon their hybrid index *Q* (Aboim et al., 2010; Taylor et al., 2012; Baldassarre et al., 2014). Individuals were classified as pure *hecki* if $Q \geq 0.9$, pure *acuticauda* if $Q \leq 0.1$, and admixed ancestry if $0.1 < Q < 0.9$.

As an additional, and more direct, assessment of the spatial structure of reproductive isolation and admixture between long-tailed finch subspecies, we estimated the effective migration surface between our sampling populations using EEMS (Estimated Effective Migration Surfaces; Petkova et al., 2016). The EEMS platform utilizes a population genetic model to infer departures from isolation by distance (IBD) and effective migration rates given the geographic and genetic distances between a set of geo-referenced genotyped individuals. Given the heterogeneous landscape of genomic differentiation between the autosomes and the Z chromosome, we used EEMS for these regions independently and together. In contrast to the subset of high frequency difference SNPs used in STRUCTURE analyses, we calculated pairwise genetic distance between individuals using the *bed2diffs_v1* function in EEMS with the entire set of quality-filtered SNPs for the autosomes (5,107,878 SNPs and 241 individuals), Z chromosome (122,013 SNPs and 234 individuals), and entire genome (5,230,057 SNPs and 241 individuals), respectively. We performed each EEMS run for 5 million generations (numMCMCIter), a 500 thousand generation burn-in (numBurnIter), iteratively between 100, 300, and 500 demes (nDemes); and with all other tuning parameters set to defaults given appropriate sampling of parameter space during the MCMC. The fit of each model was assessed visually by comparing the relationship between fitted and observed dissimilarities between demes.

3.3.5 Geographic cline analyses

In order to assess the geographic structure of genetic and bill color variation across the hybrid zone between long-tailed finch subspecies, we fit the mean and variance of the two hybrid indices (HI_A and HI_Z) and bill chroma (S5) at each of the 18 sampling sites with genetic data

and the 17 sampling sites with color data to a series of equilibrium geographic cline models using the Metropolis-Hastings Markov chain Monte Carlo algorithm employed in the R package *HZAR* (Derryberry et al., 2013). Distances between sampling sites were estimated from their latitude and longitude in Google Earth and are cumulative from the most western site (Mt. House; Table 5). In order to evaluate the best-fit cline model to the data, we ran 5 separate models that varied in the number of cline shape parameters estimated. All models estimated cline center (distance from sampling location 1, c) and width (1/maximum slope, w), but varied in their estimation of different combinations of the exponential decay curve parameters δ and τ (no tails, right tail only, left tail only, mirrored tails, or both exponential tails estimated individually). Parameters delta (δ) and tau (τ) correspond to the distance from the cline center to the exponential tail and the slope of that tail, respectively (Gay et al., 2008; Derryberry et al., 2013). Cline models for individual SNP loci also varied as to whether or not they estimated allele frequencies at the ends of each cline (p_{min} and p_{max}) or had these values fixed at 0 and 1. Support for alternative cline models was then evaluated using AIC corrected for small sample size (AICc) and the model with the lowest AICc score selected as the best-supported model.

We next evaluated the support for a coincidence in the location of cline center between the genetic and bill color clines. We first compared the two log-likelihood unit confidence intervals (CIs) around cline center location for the best supported genetic and bill color models and considered them to significantly differ if CIs did not overlap. Second, following Baldassarre et al. (2014), we re-fit the best-supported bill color cline model but fixed cline center (c) to the estimated cline center for the genetic clines. We compared AICc scores between the unconstrained and each fixed-center bill color model and considered the genetic and bill color clines to be non-coincident if the fixed cline models differed in AICc score by more than two points.

3.3.6 Quantifying selection in the hybrid zone

To evaluate the relative contributions of neutral diffusion and natural selection in maintaining the observed width of the genetic and bill color clines requires information regarding the number of generations since secondary contact between long-tailed finch subspecies occurred and the

root mean square natal dispersal distance (Barton and Gale, 1993). Following Barton and Gale (1993), assuming a Gaussin model of dispersal, the width of a cline (w) under neutral diffusion is the product of the number of generations since secondary contact (t) and the root mean square of natal dispersal distance (σ):

$$w = 2.51 \sigma \sqrt{t}$$

Secondary contact (t) between long-tailed finch subspecies likely occurred most recently sometime between 21 kya and 14 kya, following the end of peak aridity across the Australasian region and the re-establishment of the tropical monsoon cycle in northern Australia, respectively (Fitzsimmons et al., 2013; Reeves et al., 2013a; 2013b). This corresponds to between 12,000 – 8,000 generations given a 1.75-year generation time for the long-tailed finch (van Rooij and Griffith, 2011). In lieu of a direct estimate of natal dispersal, we can make use of two indirect proxies for dispersal distance. First, we can make an inference based on the relationship between direct measures of natal dispersal and body mass using data from 75 British bird species (Paradis et al., 1998). Second, we can estimate natal dispersal distance from patterns of linkage disequilibrium calculated from our genomic data. Linkage disequilibrium (D) was estimated for each sampling site based upon the observed variance in the autosomal hybrid index (HI_A) across loci using the method established by Barton and Gale (1993). In order to estimate D at the hybrid zone center, we regressed D onto the average allele frequencies (pq) over the 481 diagnostic autosomal hybrid index SNP loci at each site and then setting $pq = 0.25$. Following Syzmura and Barton (1986), σ was estimated as:

$$\sigma = \sqrt{rDw^2}$$

where w is the HI_A cline width and r is the recombination rate, here set to 0.5. We next compare the inferred cline widths from the best-supported hybrid index and bill color models with the neutral cline width expectation and consider them to be significantly different if the 95% CIs do not overlap. Last, in order to quantify the degree of selection acting within the hybrid zone, we estimated the selection pressure (s) upon each individual diagnostic SNP locus based on the

observed cline width and dispersal distance, following Barton (1979), as:

$$w = \sigma\sqrt{(8/s)}$$

3.3.7 Genome-wide mapping of bill color loci

We estimated the association between genotype and bill color phenotype using the subset of all genotyped long-tailed finch samples with associated bill color data (264 samples in total). We used a linear regression of bill color on SNP genotype, examining each biallelic SNP in the quality-filtered SNP set, in PLINK v1.07 (Purcell et al., 2007) where association significance is scored as an asymptotic p-value. Sample phenotype was scored and independently evaluated as bill chroma (S5, from 450-650nm), individual loading for PC2 (from 300-650nm), and as a dichotomous variable (0 = pure *acuticauda* yellow or 1 = pure *hecki* red or admixed orange).

The significant genetic structure that exists between long-tailed finch populations, especially those with different bill colors, can result in an enrichment of spurious associations in genome wide association studies (GWAS). Therefore, in order to control for the confounding influence of population stratification, additional association mapping of bill color was performed using the EIGENSTRAT module in EIGENSOFT v6.1.4 wherein association mapping is carried out following a principal components analysis correction to the data (Patterson et al., 2006; Price et al., 2006).

3.3.8 Principal components analysis and inversion haplotype inference

Chromosome inversion polymorphisms, by virtue of rarely recombining, leave characteristic patterns of genomic substructure that can be detected by principal components analysis (PCA). When an inversion segregates within a population, we can expect to find that genetic variation on that chromosome sorts into independent clusters of individuals whose membership depends on their karyotype. Indeed, for an inversion polymorphism at an equilibrium frequency of 0.5, we can expect to observe three clusters of individuals along principal component 1 (PC1): two clusters comprising individuals homozygous for the alternative configurations, respectively, and a

third cluster in between these comprising individuals heterozygous for the inversion. As such, all individuals can be scored as either homozygous for the inverted or ancestral state or as being heterozygous (Ma and Amos, 2012; Knief et al., 2016).

The patchiness of the MSG dataset generated for this study is not amenable for most PCA approaches that rely on little to no missing genotype data across individuals sampled. We therefore use the *trace* module of the program LASER v2.04 (Locating Ancestry from SEquence Reads; Wang and Zhan et al., 2014) that utilizes a projection Procrustes analysis to place patchily genotyped samples into the PCA space established from a set of high-quality reference panel individuals. We use the quality-filtered SNP set from 20 whole-genome sequenced long-tailed finch samples (10 from each subspecies) as the *trace* reference panel (ENA Study: PRJEB10586; Singhal et al., 2015). We analyzed each chromosome independently (mapping inferred from the zebra finch) on the quality-filtered SNP set of 285 individuals. We infer inversion haplotypes from the clustering of individuals across principal components space.

3.4 Results

3.4.1 Bill color quantification and analyses

We collected and analyzed color data from the bills of 737 adult long-tailed finches from 17 sites spread across nearly 1500 km in the present study (Figure 6; Table 5). Reflectance spectra from yellow-billed and red-billed long-tailed finches are well differentiated between 500-600 nm: most of the light in this range of wavelengths is reflected by birds with yellow bills and absorbed by birds with red bills (Figure 6). Compared to yellow and red-billed birds, long-tailed finches with 'orange' bills are found to exhibit intermediate degrees of light reflectance/absorbance within the range of 500-600 nm. Long-tailed finch bills also appear to differentially reflect light in the ultraviolet spectrum (300-400 nm). While yellow-billed birds have a reflectance peak at approximately 360 nm, red-billed birds have a reflectance peak at 320 nm (Figure 6).

Evaluating variation in bill color from reflectance spectra either as the second principal component of variation (PC2) in reflectance spectra between 300-650 nm or as bill chroma (S5) between 450-650 nm well represented the transition in bill color from west to east across the

range of the long-tailed finch (Figure 7). Scores for each colorimetric measure were highly negatively correlated across individuals (r = -0.8) however, only bill chroma fully differentiated yellow-billed from red-billed birds, with no overlap between groups, and individuals from populations (pops. 6 – 13, hereafter 'center') where orange-billed birds were observed together span the range of variation between each color type (Figure 7).

3.4.2 Genomic library preparation, sequencing, and variant calling

Across the 285 long-tailed finch individuals sequenced in this study, approximately 1.11 billion 100bp reads were generated in total with an average of 3.78 million reads per sample (median of 2.41 million reads per sample; Table 6). From an initial variant call set of 24.55 million SNPs, filtering by quality and coverage across samples, and masking by depth of coverage and repeat regions, resulted in a final quality-filtered dataset of 79,428 SNPs (3797 or 4.8% of which are located on chromosome Z) for 285 of 293 samples sequenced for use in subsequent analyses (Table 7).

3.4.3 Population structure analyses

In accordance with results from a previous study (Singhal et al., 2015), we observe that genomic differentiation between long-tailed finch subspecies is highly heterogeneous: F_{ST} is generally low across the autosomes, apart from a few areas of high F_{ST}, but greatly elevated upon the Z chromosome (Figure 8, Table 8). While the averaged F_{ST} for the autosomes between phenotypically 'pure' populations of either subspecies was 0.01, the Z chromosome averaged F_{ST} was 0.40. After filtering for quality and coverage, nearly all of the 4917 SNPs observed to be fixed differences, given the sample size, between subspecies (populations 1 and 2 against populations 18 and 19) were located upon the Z chromosome (99%, 4874 of 4917 fixed differences).

Analysis of genetic clustering and admixture across the range of the long-tailed finch using the program STRUCTURE for both the autosomal and Z chromosome datasets best

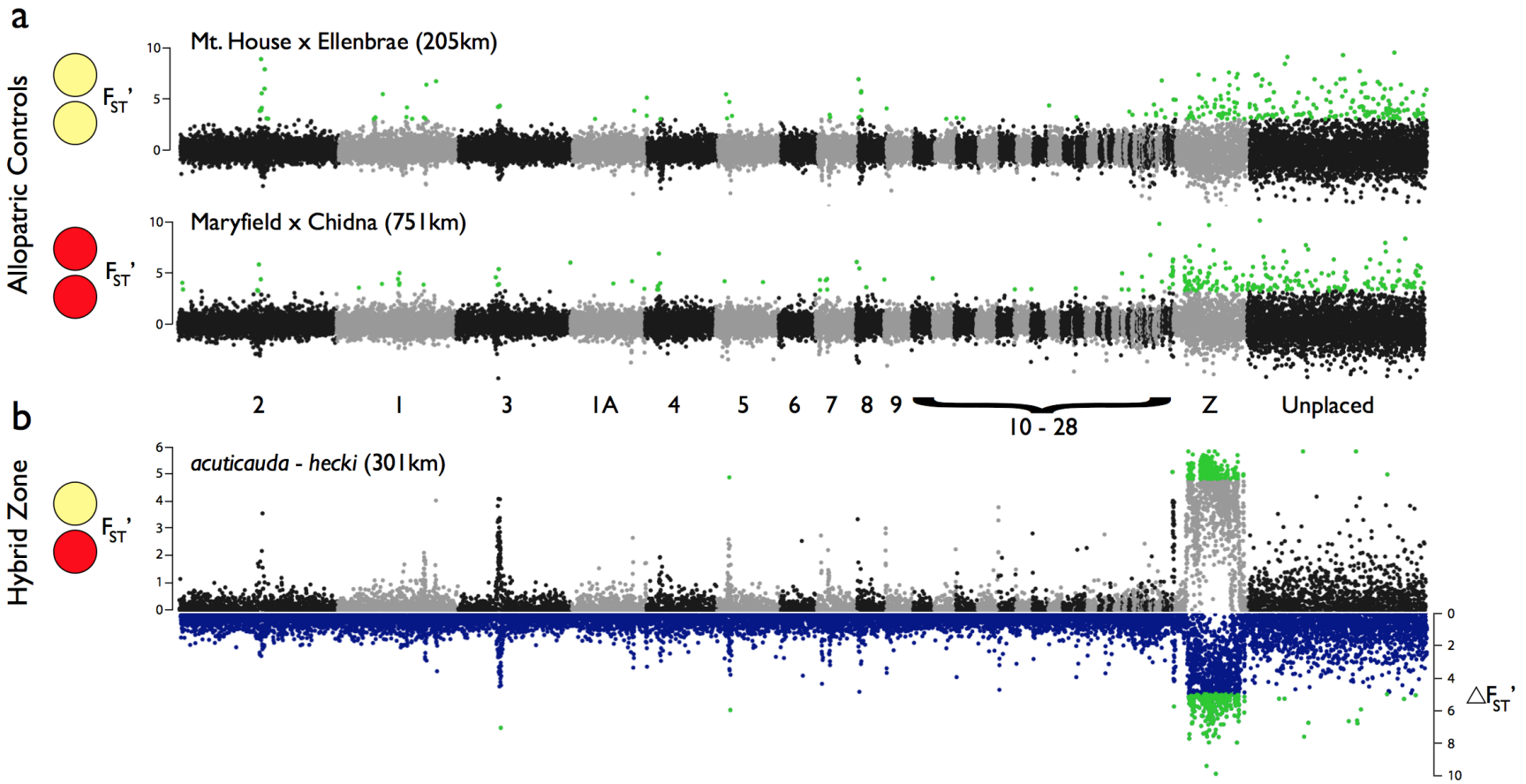

Figure 8 | Genomic differentiation (F_{ST}) between populations of the long-tailed finch. **a)** standardized genetic differentiation F_{ST}' calculated in 50kb sliding windows across the genome (colors alternate black and gray between chromosomes) between individuals from two control population comparisons of the same subspecies and bill color (see Table 5). The y-axis shows standard deviations of a normal distribution. Geographic distance between populations is given in kilometers. **b)** standardized genetic differentiation F_{ST}' (black and grey, positive axis) and net genetic differentiation ΔF_{ST}' (blue, mirrored to the negative axis) in 50kb sliding windows across the genome for focal comparison across the hybrid zone between subspecies *acuticauda* (population 3, Nelson) and subspecies *hecki* (population 6, Auvergne). Genomic regions of extreme differentiation (>99th percentile) are shown in green for both F_{ST}' and ΔF_{ST}'.

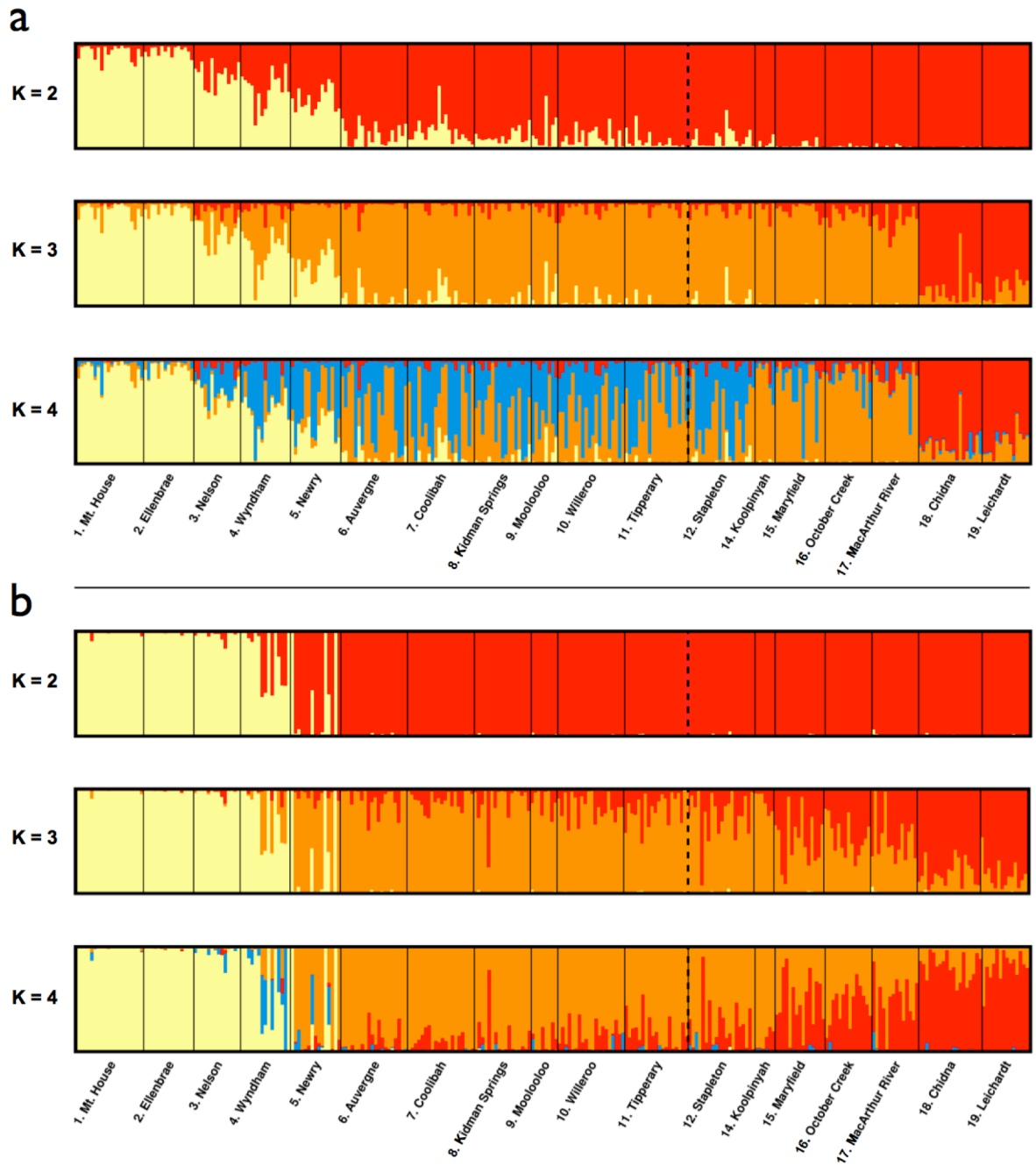

Figure 9 | Genetic structure across the range of the long-tailed finch. For K = 2, Bayesian assignment probability (y-axis) from STRUCTURE to either the western *acuticauda* genetic cluster or the eastern *hecki* genetic cluster are shown in yellow and red, respectively. Assignment results are shown for **a)** the 481 SNP HI_A dataset and the **b)** 3814 SNP HI_Z dataset. Each vertical column represents an individual sample with black bars separating populations ordered as in Figure 6 from west to east. The dashed vertical line represents the approximate location of the bill color contact zone. Sample sizes in Table 5.

supports the occurrence of two differentiated genetic clusters (K = 2), corresponding to the described subspecies, with a clear geographic center of hybridization between them (Figure 9). The presence of admixed individuals using the autosomes was far more extensive than for the Z chromosome. We first present results for the autosomes and then for the Z chromosome:

For the autosomes (Figure 9a), the majority of individuals from populations 1 and 2 (25 of 35 samples) were supported as members of the *acuticauda* genetic cluster (*Q* value ≤ 0.1, mean = 0.062 ± SD 0.063) and the majority of individuals from populations 10 – 19 (122 of 141 samples) were supported as members of the *hecki* genetic cluster (*Q* value ≥ 0.9, mean = 0.961 ± SD 0.067). However, the majority of individuals from populations 3 – 9 (77 of 109 samples) were admixtures of the autosomal variation unique to either subspecies (*Q* value between 0.1 and 0.9, mean = 0.685 ± SD 0.258).

On the Z chromosome, in contrast, admixture patterns were far more restricted to a narrow geographic area (Figure 9b). The majority of individuals from populations 1 through 3 (48 of 49 samples) were supported as members of the *acuticauda* genetic cluster (*Q* value ≤ 0.1, mean = 0.009 ± SD 0.026) and all individuals belonging to populations 6 – 19 (206 of 206 samples) were supported as members of the *hecki* genetic cluster (*Q* value ≥ 0.9, mean = 0.999 ± SD 0.005). However, individuals from populations 4 and 5 were comprised of admixed (8 of 30

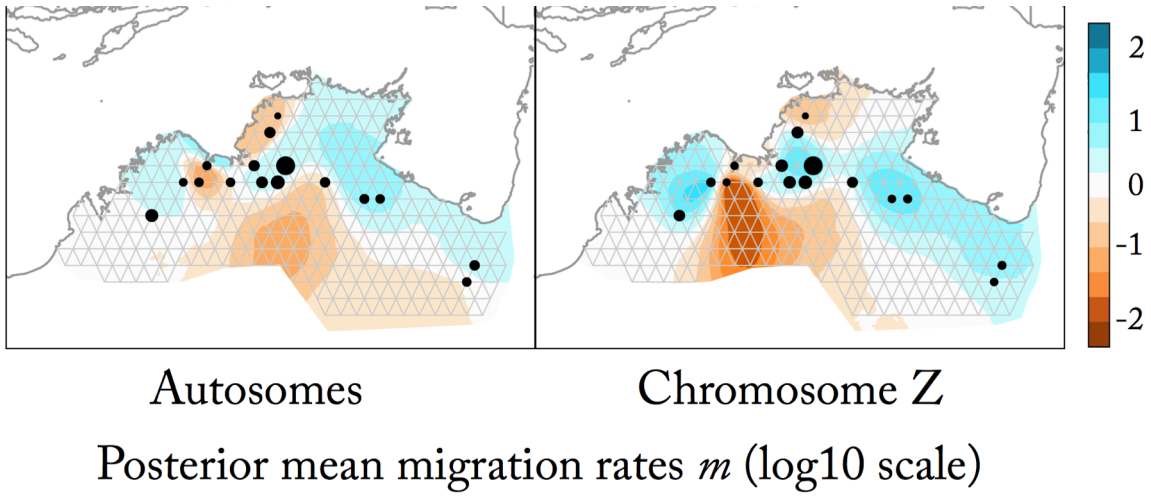

Figure 10 | Estimated effective migration surfaces (EEMS) for the autosomes (left) and chromosome Z (right). Migration rates (*m*) are color contoured on a $\log_{10}$ scale with cooler and warmer colors indicating migration rates greater than or less than the average expected under isolation-by-distance, respectively. A value of -1, for instance, indicates an effective migration rate tenfold slower than average.

samples), *acuticauda* (12 of 30 samples), or *hecki* ancestry (10 of 30 samples). The proportion of individuals of admixed, *acuticauda* and *hecki* ancestry (0.27, 0.40, and 0.33) in these populations is suggestive of a trimodal contact zone between subspecies where both hybrids and migrants co-occur but hybrids are selected against or recombination otherwise inhibited (Gay et al., 2008).

Results from estimated effective migration surfaces (EEMS) analysis support the occurrence of a significant barrier to effective gene flow between subspecies in both the autosomal and Z chromosome data (Figure 10). This barrier runs roughly north to south just west of the Western Australia – Northern Territory border. A potential landscape feature limiting gene flow in this area is the Ord River that flows through this area around the town of Kununnura, WA. A potential secondary barrier to migration appears to occur in the north between populations 11 and 14 and may represent a barrier between coastal and inland populations. Consistent with both STRUCTURE (Figure 9) and clinal analyses (see below, Figure 11), this barrier to gene flow is stronger for the Z chromosome than for the autosomes. Notably, within the ranges of each subspecies, the estimated effective migration rates are greater than expected by a pure isolation by distance model, suggesting that natal dispersal of long-tailed finches *per se* is not limiting gene flow between populations.

3.4.4 Geographic cline analyses

The best-fitting cline model for bill chroma inferred via ΔAICc model comparison was the full model that estimated cline width, center, and independent shape parameters for left and right exponential tails (Table 6). This cline has a center 702 (698 – 708, two log-likelihood support limits) km east of our westernmost sampled population and is inferred to roughly transect Stapleton Station, NT, in between sampling sites 12 and 13 (Figures 6, 11; Table 5). The inferred bill color cline width is 146 (122.6 – 207.3) km wide. Exponential tail shape parameters differed significantly between the left and right tails indicating an asymmetry in movement of this trait. The left exponential tail, on the west-side of the contact zone, begins closer to the cline center than the right exponential tail, on the east-side of the contact zone, ($\delta_L < \delta_R$) and has a greater slope ($\tau_L > \tau_R$) (Figure 11). Moreover, while variation in bill chroma was greatest in populations within the contact zone ($var_H = 0.0081$), individuals from yellow-billed populations

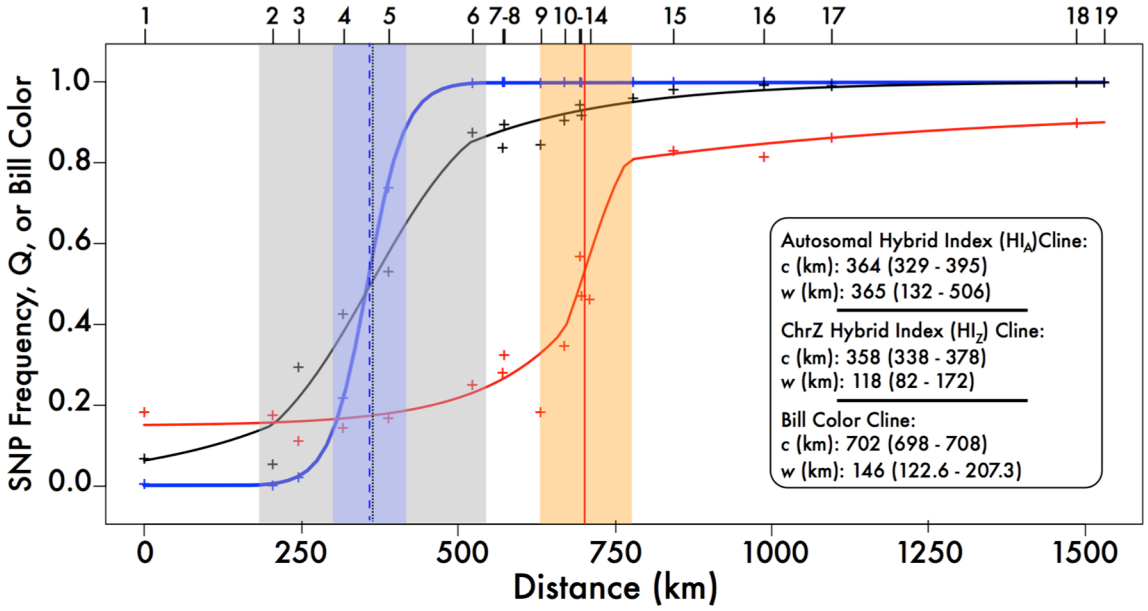

Figure 11 | Maximum likelihood HI_A, HI_Z, and bill color clines, 95% credible confidence interval, and cline shape parameters as estimated from HZAR. Distance in kilometers (km) from westernmost site (population 1, Mt. House) with greater values for Q and bill chroma (S5) corresponding to a higher proportion of genetic ancestry from subspecies *hecki* and more red bills, respectively. The inferred widths of the HI_A, HI_Z, and bill color clines are represented in light grey, blue, and orange, respectively.

were an order of magnitude more variable (var_L = 0.0043) than red-billed populations (var_R = 0.00041).

In contrast to bill color, both of the hybrid index clines were inferred to be centered ~350 km west of the center of bill color admixture. The best-fitting cline model for the autosomal hybrid index (HI_A) inferred via ΔAICc model comparison was a model that estimated cline width, center, mirrored shape parameters for both left and right exponential tails, and fixed p_{min}/p_{max} at 0 and 1 (Table 7). This HI_A cline has an inferred center 364 (329 – 395) km east of Mt. House, and lies between populations 4 and 5 just across the Western Australia – Northern Territory border around the location of the Ord River and the town of Kununurra, Western Australia (Figures 6, 11; Table 5). The inferred width of autosomal admixture in this model was 365 (132 – 506) km. The best-fitting model for the Z chromosome hybrid index (HI_Z) cline had the same parameter set as the autosomal hybrid index: exponential tails mirrored across the hybrid center (Table 8). In the best-supported model, the HI_Z cline was estimated to be located 358 (338 -378) km west of Mt. House and 118 (82 – 172) km in width (Figure 11).

3.4.5 Quantifying selection in the hybrid zone

In order to produce a neutral cline coincident in width to that observed for bill color (w = 146 km) or either hybrid index (HI_A, w = 365 km; HI_Z, w = 118 km), natal dispersal would need to be between 0.32 and 1.0 km per generation if secondary contact took place 21 kya; the most conservative estimate given available paleoclimate data (Fitzsimmons et al. 2013; Reeves et al. 2013a; 2013b). Given our field experience with the long-tailed finch, we believe these estimates for natal dispersal distance (σ) are too low to be biologically reasonable for the species, suggesting a role for selection in maintaining the extent of bill color admixture (Griffith *pers. obs.*). As no direct estimates of natal dispersal distance are available, we rely on two alternative indirect measures. First, for birds of similar body mass to the long-tailed finch (13.2 g ± 0.97, N = 302 wild-caught adults; Griffith and Hooper, 2017) average natal dispersal distance would be 6.5 km (2.7 – 15.6, N = 5; Paradis et al., 1998). The expected cline widths under neutral diffusion given σ estimated from body mass would be 1460 km wide. This estimate is well outside the two log-likelihood support intervals for both the cline widths of bill color and each hybrid index (Tables 8 and 9). Second, using information from patterns of linkage disequilibrium across long-tailed finch populations, we infer σ to be 41.5 km (Figure 12). While this indirect estimate is an order of magnitude greater than the estimate based on body size, we believe it to be reasonable and is

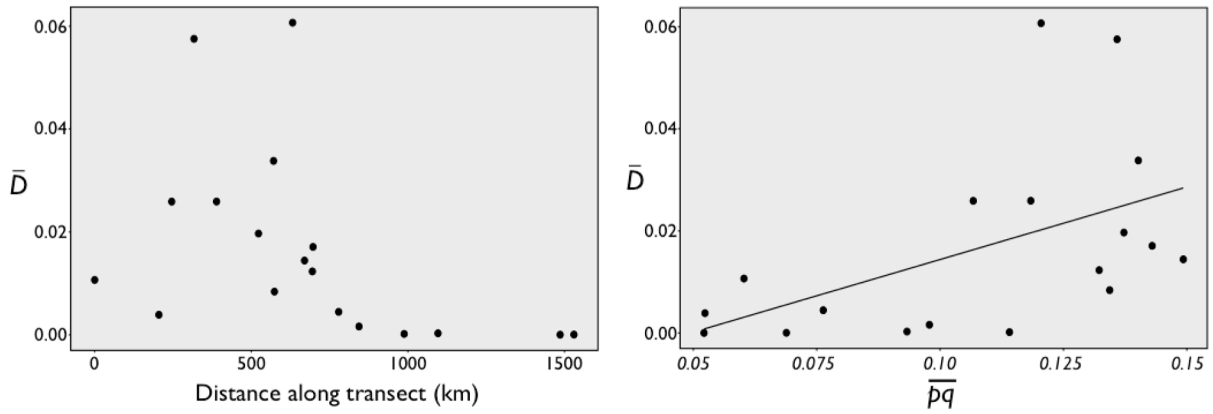

Figure 12 | Distance along sampling transect from Mt. House against average linkage disequilibrium (D) across 481 diagnostic autosomal SNPs in each population (left). Average allele frequencies (pq) in each population against linkage disequilibrium (right). Linear regression line shown.

Model	c (km)	w (km)	δ_L	τ_L	δ_R	τ_R	AICc	ΔAIC
Exponential tails, independent	702 (698 – 708)	146 (122.6 – 207.3)	31.9 (24.8 – 44.9)	0.245 (0.19 – 0.4)	59.7 (48 – 93.6)	0.071 (0.05 – 0.14)	-1729.3	-
Exponential tails, mirrored[1]	698 (695.8 – 702.3)	129 (105.1 – 172.1)	29.2 (22.8 – 47)	0.199 (0.15 – 0.3)	29.2 (22.8 – 47)	0.199 (0.15 – 0.3)	-1718.7	-10.68
Right tail only	713 (706.3 – 722.2)	332 (301.2 – 351.4)	None	None	132 (120.5 – 157.4)	0.154 (0.1 – 0.27)	-1713.7	-15.64
Left tail only	699 (695 – 703.4)	178 (141.8 – 241.5)	31.9 (23.4 – 50.6)	0.318 (0.24 – 0.49)	None	None	-1692.7	-36.63
Uniform, no tails	708 (699.1 – 715.9)	343 (306.5 – 369.9)	None	None	None	None	-1687.7	-41.69

Table 6 | Bill color cline model comparison in *HZAR*. Parameter estimates and two log-likelihood support limits are shown in parentheses. Cline center (c) is in kilometers (km) from population 1 (Mt. House), width (w) is 1/maximum slope, and δ and τ are shape parameters for the exponential tails. [1] Exponential shape parameters δ_M and τ_M are presented here as identical left and right tail shape parameters for simplicity.

Model	c (km)	w (km)	δ_L	τ_L	δ_R	τ_R	AICc	ΔAIC
Exponential tails, mirrored[1]	363.5 (329.4 – 394.5)	364.8 (131.6 – 505.5)	159.7 (0.07 – 907.1)	0.439 (0.0 – 0.99)	159.7 (0.07 – 907.1)	0.439 (0.0 – 0.99)	14.83	-
Uniform, no tails	368.8 (331.2 – 402.8)	480.5 (405.7 – 576.5)	None	None	None	None	15.14	-0.31
Right tail only	361.4 (324.5 – 396.1)	420.7 (299.9 – 546.1)	None	None	159.3 (1.52 – 2999.9)	0.660 (0.0 – 0.99)	16.87	-2.04
Left tail only	373.8 (334.2 – 407.1)	463.6 (391.0 – 568.7)	202.4 (10.7 – 2999.9)	0.581 (0.0 – 0.99)	None	None	18.61	-3.78
Exponential tails, independent	366.5 (338.4 – 393.6)	360.8 (297.3 – 502.0)	208.0 (10.8 – 2998.5)	0.296 (0.0 – 0.99)	123.5 (0.60 – 2913.1)	0.609 (0.002 – 0.99)	18.83	-4.01
Null model	N/A	N/A	N/A	N/A	N/A	N/A	315.9	-301.07

Table 7 | Autosomal hybrid index (HI_A) cline model comparison in *HZAR*. Parameter estimates and two log-likelihood support limits are shown in parentheses. Cline center (c) is in kilometers (km) from population 1 (Mt. House), width (w) is 1/maximum slope, and δ and τ are shape parameters for the exponential tails. [1] Exponential shape parameters δ_M and τ_M are presented here as identical left and right tail shape parameters for simplicity

Model	c (km)	w (km)	δ_L	τ_L	δ_R	τ_R	AICc	ΔAIC
Exponential tails, mirrored[1]	357.9 (338.0 – 377.6)	117.6 (81.7 – 172.0)	181.8 (79.4 – 415.2)	0.004 (0.0 – 0.57)	181.8 (79.4 – 415.2)	0.004 (0.0 – 0.57)	8.73	-
Right tail only	356.7 (337.0 – 377.4)	130.2 (89.2 – 181.0)	None	None	215.9 (57.1 – 623.3)	0.005 (0.0 – 0.73)	10.47	-1.74
Uniform, no tails	359.2 (336.9 – 382.4)	148.6 (125.8 – 203.9)	None	None	None	None	12.11	-3.38
Exponential tails, independent	355.7 (340.9 – 373.2)	123.6 (80.6 – 168.4)	166.9 (6.4 – 2999.7)	0.045 (0.0 – 0.99)	212.4 (34.8 – 567.2)	0.075 (0.0 – 0.68)	13.04	-4.31
Left tail only	357.3 (338.2 – 381.5)	138.7 (126.1 – 195.8)	167.3 (7.5 – 2999.9)	0.048 (0.0 – 0.99)	None	None	14.86	-6.13
Null model	N/A	N/A	N/A	N/A	N/A	N/A	399.45	-390.72

Table 8 | Chromosome Z hybrid index (HI_Z) cline model comparison in *HZAR*. Parameter estimates and two log-likelihood support limits are shown in parentheses. Cline center (c) is in kilometers (km) from population 1 (Mt. House), width (w) is 1/maximum slope, and δ and τ are shape parameters for the exponential tails. [1] Exponential shape parameters δ_M and τ_M are presented here as identical left and right tail shape parameters for simplicity

consistent with our EEMS results where rates of effective migration rates between populations within subspecies are greater than expected under a pure isolation-by-distance model.

Using the indirect estimate of natal dispersal (σ = 41.5 km/gen) from LD patterns in our long-tailed finch populations, we estimate effective selection upon bill color to be 0.7% (0.3-0.9%), HI_A to be 0.1% (0.05-0.8%), and HI_Z to be 1.0 (0.5-2.1%), respectively. We urge caution in interpreting these results as the calculations are highly sensitive to estimates of dispersal.

3.4.6 Genome-wide mapping of bill color loci

Association mapping was first performed using 5,140,028 quality-filtered genome-wide SNPs in 264 individuals with bill color scored in three ways: as bill chroma (S5, from 450-650nm), individual loading for PC2 (31.3% reflectance variation from 300-650nm), and as a dichotomous character state (0 = pure *acuticauda* yellow or 1 = pure *hecki* red or admixed orange). Across the three complementary color scores, two chromosomes were enriched for SNPs that showed strong associations with bill color variation: chromosome 8 and the Z chromosome (Figure 13).

Two regions on chromosome 8 were significantly associated with bill color variation in the long-tailed finch (Figure 13). The first region spans 21 markers located between 4.99 Mb and 5.19 Mb on chromosome 8. This region encompasses two protein coding genes on the zebra finch genome assembly belonging to the tyrosine phosphatase gene family: ENSTGUG00000004389 and ENSTGUG00000004404. This region is enriched for SNPs that are significantly associated with bill color in all three comparisons after Bonferroni correction however there is no known association between tyrosine phosphatase function and color expression.

The second region on chromosome 8 that is significantly associated with bill color when scored as a dichotomous character state, and trending significance for the two other bill color metrics, contains two SNPs located at 24,234,874 and 24,678,733. This region contains a cytochrome P450 gene cluster recently shown to be most strongly associated with the *yellowbeak* mutation in zebra finch (Mundy et al., 2016) and for red plumage expression in red-factor canaries (Lopes et al., 2016). Our strongly associated SNP at 24,678,733 is only 50 kbp upstream of the most significantly associated marker in the *yellowbeak* study (Mundy et al.,

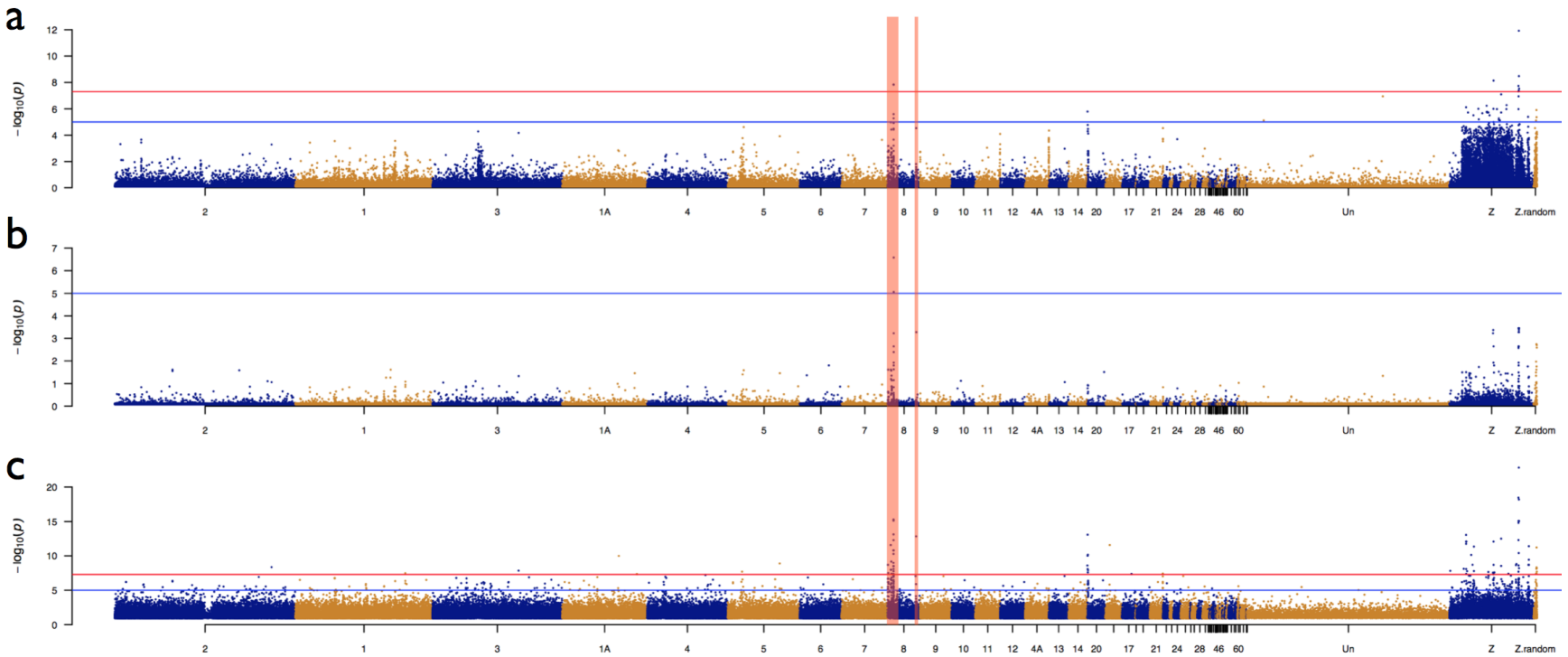

Figure 13 | Genome wide association mapping bill color in the long-tailed finch. Mapping performed using 285 genotyped long-tailed finches with associated bill color measures. Chromosomes alternate in color between blue and gold in order of descending size. Data points represent false-discovery rate (FDR)-adjusted *P* values for a total of 500 k SNPs on the y-axis. Bill color was evaluated across individuals in three ways: **a)** bill chroma (S5) between 450-650 nm, **b)** PC2 from a principal components analysis of reflectance variation between 300-750 nm (31.3% variation), and **c)** as a dichotomous variable (0 = pure *acuticauda* yellow or 1 = pure *hecki* red or admixed orange). See Section 3.3.2 and Table 5 for further explanation of quantifying color variation. Suggestive and genome-wide significance thresholds represented by blue and red horizontal lines, respectively. Two vertical orange bars highlights regions on chromosome 8 enriched for SNPs significantly associated with bill color in all three comparisons. The narrower of the two, containing a SNP a t 24,678,733 is located within the region recently shown to be associated with the *yellowbeak* mutation in the zebra finch (Mundy et al., 2016).

2016).

The Z chromosome was enriched for SNPs that were significantly associated with bill color variation in all three association mappings. The Z chromosome is likely to be enriched for false-positive associations, however, due to the considerable genetic structure between long-tailed finch populations on this chromosome that largely – but not perfectly – co-varies with bill color (see Figure 11). One region of significant association with bill color across all three comparisons, however, spans 11 SNP markers located between 59.67 Mb and 60.22 Mb and contains eight protein coding genes on the zebra finch genome assembly. Yet, none of these genes have any immediate functional relationship with carotenoid-based color expression.

3.4.7 Principal components analysis and inversion haplotype inference

Principal components analysis (PCA) was performed using 148,548 Z chromosome SNPs shared

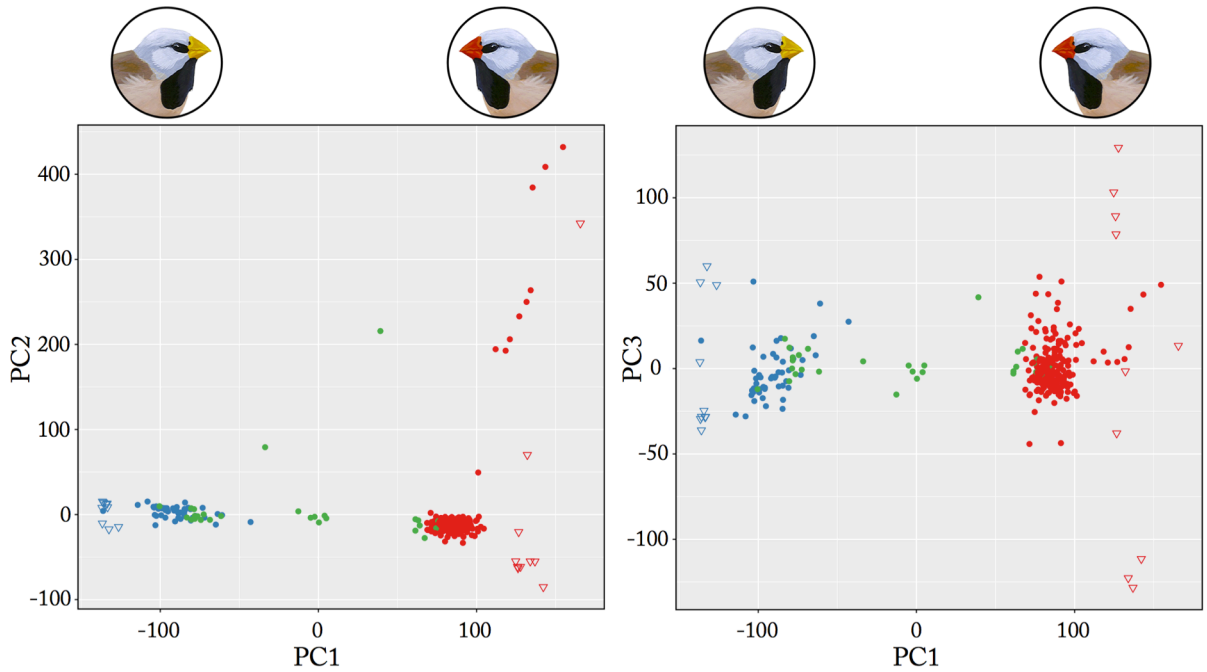

Figure 14 | PCA and Z chromosome clustering for 305 wild-caught long-tailed finches. Each point represents an individual color-coded by ancestry assignment from STRUCTURE analysis: subspecies *acuticauda* in blue (pops. 1 – 3, n = 59) and subspecies *hecki* in red (pops. 6 – 19, n = 216). Individuals from hybrid zone populations have been shown in green (pops. 4 and 5, n = 30). The 20 whole-genome sequenced reference panel individuals used to infer principal component space are represented with triangles. Each study sample was projected onto reference panel PCA space using Procrustes projection analysis based upon 148,548 shared SNPs.

between 285 study samples and 20 reference panel individuals with the *trace* module in LASER (Wang et al., 2014). Principal component 1 (PC1) grouped individuals into three discrete clusters that correspond to the two long-tailed finch subspecies and F1 subspecies hybrids (Figure 14). The discrete nature of each cluster of individuals suggests significant recombination suppression on the Z chromosome (previously reported in Singhal et al., 2015) that is consistent with a chromosomal inversion difference between long-tailed finch subspecies. Results from PCA analysis are in agreement with population assignment calls from a STRUCTURE analysis based on a subset of 3814 high-frequency difference SNP loci (see Figure 9 and section 3.4.3).

3.5 Discussion

Variation across the range of the long-tailed finch in bill color and genetic admixture fit steep clinal transitions between 1) yellow-billed finches in the west (historically subspecies *acuticauda*) and red-billed finches in the east (historically subspecies *hecki*) and 2) two highly differentiated Z chromosome types that constitute the majority of genomic differentiation between subspecies. The centers of these two clines, however, are displaced from each other by about 350 km. Strikingly, a yellow bill is not indicative of membership in subspecies *acuticauda* as the majority of yellow-billed birds at Newry (population 5) are more closely related to red-billed members of the *hecki* genetic cluster than they are to other yellow-billed birds in the *acuticauda* cluster (Figure 7; Table 5). These findings suggest that the genes underlying bill color in the long-tailed finch are decoupled from and subject to different evolutionary forces than the Z chromosome; where the majority of fixed differences between subspecies appear to reside in a chromosomal inversion.

Differentiation between long-tailed finch subspecies likely occurred during periods of allopatric divergence within two refugial populations as bouts of intense continental aridification during the Pleistocene created ecological barriers to dispersal from the Bonaparte gulf through the lowlands of the Victoria River (Cracraft, 1986; Ford, 1987a). Tropical woodland habitats across northern Australia, to which the long-tailed finch is restricted, likely began to fragment as the climate of the Australasian region became increasingly cooler and drier from 32 kya and achieved greatest fragmentation during the Last Glacial Maximum 21 kya (± 3 ka) when Australia was last at its coolest and driest (Reeves et al., 2013a; 2013b). Tropical woodland

habitats would subsequently have re-expanded as climatic conditions in northern Australia began to warm from 21 kya and become wetter with the reestablishment of the monsoon from 14 kya (Fitzsimmons et al., 2013; Reeves et al., 2013a; 2013b). Secondary contact between long-tailed finch subspecies likely occurred as temperature and precipitation increased across northern Australia after the Last Glacial Maximum and more favorable climatic conditions facilitated range expansion out of refugia.

The costs of hybridization between long-tailed finch subspecies following secondary contact appear to be heterogeneously distributed across the genome as admixture patterns exhibit considerable variation depending on genomic position. We first consider the genetic basis of bill color and the implications of bill color variation before focusing on wider patterns of genomic differentiation and admixture as they together relate to the extent of reproductive isolation between long-tailed finch subspecies.

Bill color mapping: A genome-wide association analysis of bill color variation in the long-tailed finch recovered statistically significant signal across three comparisons for three regions of the genome. The first region, on chromosome 8, contains 21 SNPs between 4.99 Mb and 5.19 Mb that are significantly associated with bill color after Bonferroni correction in all three comparisons (Figure 13). This region spans two protein-coding genes, both members of the tyrosine phosphatase gene family. The relevance of these genes with carotenoid-based color expression is unclear. Moreover, this region was also significantly differentiated, in the upper 99th percentile, of our standardized genetic differentiation (F_{ST}') metric between both population control comparisons of individuals of shared bill color; making this region more likely to be differentiated due to shared background selection rather than divergent selection processes (Figure 8). A second region, comprising most of the Z chromosome, was also observed to be significantly associated with bill color variation in the long-tailed finch. Much of this signal is likely to be a false-positive byproduct of the considerable genetic variation that resides on this chromosome that is tightly linked and largely co-varies with the bill color difference between subspecies. One area on the Z chromosome, however, spanning 11 SNPs located between 59.67 Mb and 60.22 Mb was found to be significantly differentiated, even for the Z chromosome, in all three comparisons and contains eight protein-coding genes. Yet the link between these genes

and color expression is again unclear and will require further examination.

The third region found to be associated with bill color across comparisons is more promising. This region is located on chromosome 8 between 24.23 Mb and 24.68 Mb and contained two SNPs significantly associated with bill color when scored as a character state even after Bonferroni correction (this region trended significant in the two other comparisons, Figure 13). This region is of immediate interest as it encompasses a group of cytochrome P450 genes that have previously been implicated as the oxidative ketolase agent responsible for converting yellow dietary carotenoids into red ketocarotenoids and are differentially expressed in yellow-red bills (Mundy et al., 2016) and yellow-red feathers (Lopes et al., 2016). While this is therefore the most compelling region found to be associated with bill color, it will require fine-scale mapping and gene expression analyses in future studies in order to map down to the causal mutations of interest and to validate its importance for the expression of this defining trait within the long-tailed finch.

Bill color admixture: We find that bill color variation is greatest within a narrow contact zone 146 km wide and centered ~50 km to the west of Katherine, Northern Territory. This stands in contrast to a pattern of extensive intergradation of bill color across a wide geographic area, as had been previously suggested (Immelmann 1965; Mayr 1968). Indeed, over broad geographic distances (about 390 km in the west and 640 km in the east) yellow-billed finches in the west (pops. 1 – 5) and red-billed finches in the east (pops. 14 – 17), respectively, show little variation in bill coloration (Figure 11; Table 5). Despite the low variation in bill color in areas of allopatry, and the narrow area of maximal bill color admixture, the best-fit cline model suggests that introgression of bill color outside the contact zone has occurred and is substantial (Figure 11; Table 6). A previous analysis of the bill color variation in isolation from genetic data suggested that the best-fit geographic cline model suggested that introgression of this trait was asymmetrical in nature with "red alleles" moving from east to west (Figure 11; Table 6; Griffith and Hooper, 2017). We hereafter refer to this model as 'asymmetrical-red'. Below, we consider alternative explanations for the observed pattern of bill color admixture in light of our genomic analyses.

First, the displacement of the bill color cline center 350 km east of both autosomal and Z chromosome hybrid index cline centers might have resulted instead from an asymmetrical movement of "yellow alleles" from *acuticauda* eastward into the genomic background of the *hecki* subspecies. If individuals of both long-tailed finch subspecies favor yellower bills, sexual selection for this trait could facilitate the adaptive introgression of "yellow alleles" out of the zone of initial secondary contact. In this 'asymmetrical-yellow' model, secondary contact first took place near the town of Kununurra, Western Australia, and while most of genomic variation has remained centered there, variation for yellower bills has moved asymmetrically east due to sexual selection. While genetic admixture is highly restricted on the Z chromosome to a narrow area of geographic contact, the geographic extent of autosomal admixture between subspecies is far more extensive (Figures 9 and 11). Indeed, the eastern extent of genetic variation from subspecies *acuticauda* sits approximately at the center of bill color admixture, perhaps suggesting that one genetic contribution of subspecies *acuticauda* east of the center of genomic admixture between subspecies is the genetic variation underlying yellower bills (Figures 9 and 11). Association mapping for bill color in part supports this prediction as variation for this trait is linked to SNPs on autosomal chromosome 8, including SNPs in a region previously shown to be involved in the carotenoid based red-yellow bill color variation in the zebra finch (Figure 13; Mundy et al., 2016).

Bill coloration in the zebra finch (*Taeniopygia guttata*), a close relative of the long-tailed finch, is a well-studied sexually selected ornamental trait (Blount et al., 2003). However, bill color in the long-tailed finch does not appear to be under strong sexual selection and is thus unlikely to be introgressing adaptively between subspecies. For instance, in a population at Wyndham (population 4), bill color is a poor signal of sex, condition, and reproductive success (van Rooij and Griffith, 2012). Variation in bill color was only weakly related to gender with 25% of males being misclassified as females by a discriminant function test using this trait alone (by contrast only 11% were incorrectly misclassified using tail streamer length; van Rooij and Griffith, 2010). In the same population there was no evidence for assortative mating in relation to bill color, nor any evidence that variation in bill color was related to whether individuals bred or not, the success of reproductive attempts, or the condition of individuals (van Rooij and Griffith, 2012). However, the significance of bill color to reproductive success in admixed

populations, where bill color variation is greatest, remains to be tested. Indeed, variation in bill color within the range center (pops. 6 – 13) is inferred to be 2× greater than in yellow-billed populations (pops. 1 – 5) and nearly 20× greater than in red-billed populations (pops. 15 – 19), and may provide ample variation for selection to act upon.

In a second alternative to the 'asymmetrical-red' model, the geographic discordance between the centers of genomic and bill color admixture may have resulted instead from differences in the nature and targets of selection acting on hybrids. Indeed, the discordance in cline centers could result if 1) strong frequency dependent selection is acting upon bill color such that local variation in this trait is limited and maintained in the area of initial secondary contact, the current location of the bill color cline center, and 2) asymmetrical reproductive success favors *hecki* males over *acuticauda* males in inter-subspecific crosses. Genomic variation, when decoupled from loci involved in bill color production, would proceed to move west to where the center of genetic admixture currently resides, largely leaving bill color behind in a stable morphological contact zone. We refer to this as the 'asymmetrical-*hecki*' model. We note that this model is entirely consistent with the evidence presented above for the 'asymmetrical-yellow' model and aspects of the reproductive biology in this system may further grant it additional support.

For instance, sperm morphology differs between subspecies of the long-tailed finch with males of subspecies *acuticauda* having significantly longer sperm with narrower head widths and a lower midpiece:flagellum ratio than males of subspecies *hecki* (Rowe et al., 2015). Across animals, sperm morphology evolution tends to co-evolve with and track the evolution of the female reproductive environment (Kleven et al., 2009; Higginson et al., 2012) and the strength of post-mating pre-zygotic reproductive isolation increases quickly between populations as these traits diverge (Miller and Pitnick, 2002). Indeed, males of subspecies *acuticauda* appear to have lower reproductive success when paired with females of subspecies *hecki* but, critically, fecundity is not lower for males of subspecies *hecki* in the reciprocal cross (Griffith, *pers. comm.*). This asymmetry in reproductive success, in favor of *hecki* males, may well result in the western movement of genomic variation from subspecies *hecki* to the current center of genetic admixture between subspecies and leave bill color variation largely behind due to frequency dependent selection on this trait.

A final alternative explanation for the discordance between the centers of bill color and genomic admixture results from ecological variation across the range of the long-tailed finch. As carotenoid based colors in birds require a dietary input in order to be expressed, geographic variation in the bill color of the long-tailed finch could be a byproduct not of genetic variation but rather of variation in the environmental availability of carotenoid rich resources (Hill, 1992). We can largely discount this hypothesis out of hand, however, as environmental variation across the range of the long-tailed finch is minimal (extrapolated from the minimal ecological variation observed across the range of the sympatric red-backed fairy-wren; Baldassarre et al., 2013; Morton et al., 2011), because bill color is known to be heritable, and – as discussed above – is significantly associated in association comparisons with SNPs on chromosome 8 and the Z chromosome.

Genomic differentiation: The landscape of genomic differentiation between subspecies of the long-tailed finch is a mosaic of mostly low-differentiated regions interspersed with a few peaks of significantly elevated divergence (Figure 8). In order to identify regions of the genome that are resistant to gene flow and thereby important to the maintenance of subspecies, we employed a metric of net genetic differentiation (ΔF_{ST}') that is able to disentangle the confounding influence of background selection shared across extant populations, or the ancestral population, from the influence of divergent selection on loci resistant to gene flow between focal populations (see Vijay et al., 2016; Irwin et al., 2016). This approach highlights the striking differentiation of the Z chromosome between long-tailed finch subspecies (Figure 8). Compared to the autosomes, the Z chromosome has an elevated proportion of 50 kb windows in the 99th percentile of the F_{ST}' distribution in both control comparisons. However, even after controlling for this background differentiation, the Z chromosome retains the disproportionate enrichment of net genomic differentiation (ΔF_{ST}') in the focal comparison across the long-tailed finch hybrid zone (Figure 8). This strongly suggests that the Z chromosome is differentiated because it is resistant to gene flow and actively involved in reproductive isolation between long-tailed finch subspecies.

Further analyses of genomic admixture across the range of the long-tailed finch support the significant role of the Z chromosome in reproductive isolation. In both STRUCTURE and EEMS analyses, the Z chromosome is found, compared to the autosomes, to be more resistant

to admixture and a greater barrier to effective migration between subspecies (Figures 9 and 10). Indeed, while EEMS analysis supports a migration barrier between subspecies in both the autosomal and Z chromosome data, the strength of this barrier is an order of magnitude stronger for the Z chromosome (Figure 10). Geographic clinal analyses of hybrid indices using a subset of SNP loci nearly fixed between subspecies at opposite ends of their range on the autosomes (HI_A) and the Z chromosome (HI_Z) recover indistinguishable centers of genetic admixture but a threefold wider area of admixture for the autosomes (w = 365 km, 329 – 395 km, 2 log-likelihood support limits) compared to the Z chromosome (w = 118 km, 82 – 172 km; Figure 11; Tables 7 and 8). Given a natal dispersal distance (σ) of 41.5 km/generation for the long-tailed finch this would result in a roughly tenfold greater strength of selection on the Z chromosome compared to selection across the autosomes as a whole (Figure 12).

Across studies of avian hybrid zones, the Z chromosome is often found to be more resistant to genetic admixture than the autosomes (see Price, 2008). Might processes other than divergent selection produce this signal? One such process is related to a difference in natal dispersal distance between the sexes; with females dispersing farther than males do. As the Z chromosome spends ⅔ of its time in males and only ⅓ of its time in females, if females have a greater natal dispersal distance than males, the Z chromosome will exhibit a greater influence of isolation-by-distance than the autosomes. We find this explanation to be unconvincing in the long-tailed finch. While a direct examination of sex-biased dispersal distances has not been performed in this system, we observe no difference in the inferred rates of effective migration in EEMS analysis between the Z chromosome and the autosomes (Figure 10). A second alternative process to selection relates to the difference in relative effective population size between the Z chromosome and the autosomes. There are, at equilibrium, three copies of the Z chromosome for every four copies of any autosomal chromosome. Thus, this 3:4 equilibrium ratio of relative effective population size of the Z to the autosomes is theoretically expected to result in faster rates of genetic drift on the Z chromosome, elevated further as variation in male mating success increases, which could result in a greater degree of differentiation across hybrid zones for the Z compared to the autosomes (Mank and Ellegren, 2007; Mank et al., 2010a; Wright et al., 2015). Evidence for this phenomena are mixed in the long-tailed finch. Despite the enrichment of 50 kb windows in the 99th percentile of the ΔF_{ST}' distribution, suggesting a signature of divergent

selection, we also observe an elevated proportion of 50 kb windows on the Z chromosome in the 99th percentile of the F_{ST}' distribution compared to the autosomes in both control comparisons (Figure 8). Together this suggests that both drift and selection may be responsible for the elevated differentiation on the Z chromosome.

We argue, however, for a strong contribution of selection in elevating the role of the Z chromosome in the differentiation between long-tailed finch subspecies. Compared to the autosomes, the Z chromosome is often disproportionately involved in reproductive isolation between species: the so-called 'large-X' or in this case 'large-Z effect' (Coyne 1992; Coyne and Orr, 1989). In birds, the Z chromosome is both enriched for male-biased genes and, as observed in the Galloanserae, is also the location of faster rates of female-biased gene expression divergence (Dean et al., 2015). Together these two phenomena will result in many fitness costs in hybrids to be Z-linked. As such, divergent selection may often be the most important process behind the frequent observation in avian hybrid zone studies that genetic differentiation and the inferred strength of reproductive isolation are greater on the Z chromosome than the autosomes.

Indeed, an enrichment of genes subject to divergent selection, linked together within a chromosome inversion, may explain the observed disproportionate loading of genomic differentiation between long-tailed finch subspecies onto the Z chromosome. Previous cytological work with the long-tailed finch discovered alternative forms of the Z chromosome, products of chromosomal inversion, segregating in this species (Chrstidis, 1986a). In addition to the discovery of an elevated bloc of genetic differentiation on the Z chromosome, we find evidence via principal components analysis for three principal clusters of genetic variation on the Z chromosome corresponding to individuals belonging to subspecies *acuticauda*, subspecies *hecki*, and hybrid individuals from the zone of admixture that are equally intermediate between these two clusters (Figure 14). An area of approximately 57 Mb in size (between 12 Mb and 69 Mb) constitutes a protracted bloc of net genomic differentiation (ΔF_{ST}') in the 99th percentile of this distribution and matches the location of a recombination desert observed in a mixed sample of individuals from both subspecies (Singhal et al., 2015). Critically, recombination rates are observed to be equivalent with similarly sized autosomes in the 12 Mb and 4 Mb flanking the telomeres of the Z chromosome (Singhal et al., 2015) and these regions contain no regions of elevated net genomic differentiation across the long-tailed finch hybrid zone. Together these

findings are consistent with a chromosomal inversion on the Z chromosome that is enriched for loci resistant to gene flow between subspecies.

Given the observed difference in sperm morphology between long-tailed finch subspecies and the costs of inter-subspecific mating (see above), an inversion that suppressed recombination between genes involved in sperm morphology, the female reproductive environment, and/or mate choice disequilibrium would be favored. Two recent studies in the zebra finch observe that inversion polymorphisms on the Z chromosome are acting as a supergene for alternative sperm morphologies that result in substantial fitness variation across males (Kim et al., 2017; Knief et al., 2017). A similar situation may be at play in the long-tailed finch, whereby the inversion on the Z chromosome between subspecies is involved in the observed sperm variation and nascent reproductive isolation between subspecies. This will require further investigation. One trait, however, that appears to not be strongly linked with the Z chromosome, despite its potential advantage as a target of mate choice and thus its ability to be involved in pre-zygotic isolation, is bill color.

Future Works

As with any scientific pursuit, this dissertation has motivated a host of questions that could not hope to have been addressed fully or at all during my time as a graduate student. The results from comparative cytological studies in Chapters 1 and 2 suggest that i) speciation with gene flow has occurred regularly in birds and ii) that the costs of this frequent hybridization have often selected for chromosome inversions to decrease recombination between divergently evolving populations. Within the Australian grassfinches, species often differ by pericentric inversions and in Chapter 3 I investigated how inversions on the Z chromosome are involved in reproductive isolation across a hybrid zone between subspecies of the long-tailed finch. The extent to which speciation in this clade has involved repeated bouts of allopatry and secondary contact that together promote chromosome inversion evolution remains unknown and will require further investigation.

A holistic understanding of speciation as a process should endeavor to examine both the structural and functional context in which it takes place. In future efforts, I would like to expand work in the grassfinch system through an integrative program of study between genome structure (inversions) and function (gene expression). Indeed, the elevated rate of both structural and functional evolution on the Z chromosome relative to the autosomes, which appears to be common in birds, remains to be thoroughly examined. The relative significance of genetic drift versus natural selection on the large-Z effect in birds has recently been qualified with respect to protein coding (Harrison et al., 2015; Wright et al., 2015) and gene expression evolution (Dean et al., 2015), respectively, but we know little about the generality of these results; and even less about the evolutionary forces underlying chromosome inversion fixation. While arguments can be made for the primary role of genetic drift or natural selection in driving faster rates of structural evolution on the Z chromosome, akin to those made for the large-Z effect in functional divergence, they also remain to be explicitly tested. The Australian grassfinches would provide a good system with which to examine all of these questions.

One route to evaluating these issues is to utilize the new emerging approaches to *de novo* genome assembly so as to bypass reference biases in the detection of structural variants. I would like to 1) generate *de novo* diploid genome assemblies for members of the Australian grassfinch

clade – including both subspecies of the long-tailed finch hybrid system - and 2) sequence full phased transcriptomes from somatic and gonadal tissues for males and females of these same taxa. These data can be used to characterize species-specific patterns of sex-bias in gene expression, the divergence history of sex-biased expression within the clade, map chromosome rearrangement differences between taxa at a resolution not previously possible, and establish the genomic landscape of expression evolution as it relates to chromosome rearrangement. More specifically, I can ask: whether rates of i) protein coding and ii) expression divergence for Z-linked genes relative to their autosomal counterparts are more consistent with divergence by drift or selection, iii) if genes located within chromosome inversion differences between taxa show elevated rates of expression divergence relative to those in collinear genomic regions, and iv) the extent to which hybrid dysfunction between long-tailed finch subspecies, and the architecture of that dysfunction, is caused by differentially expressed genes.

Data Accessibility

Rates of karyotypic evolution in Estrildid finches differ between island and continental clades

- *Publication*: (Hooper and Price, 2015)
- *Geographic and Sample Data*: Supplementary Information

Chromosomal inversion differences correlate with range overlap in passerine birds

- *Publication*: (Hooper and Price, *In Press*)
- *DNA Sequences*: GenBank Accession numbers: MF458370-MF458470
- *Geographic and Sample Data*: Supplementary Information

Chromosomal inversions and reproductive isolation in an avian hybrid zone

- *Publication*: (Griffith and Hooper, 2017)

References

Anderson, A. R., A. A. Hoffmann, S. W. Mckechnie, P. A. Umina, and A. R. Weeks. 2005. The latitudinal cline in the In (3R) Payne inversion polymorphism has shifted in the last 20 years in Australian *Drosophila melanogaster* populations. Molecular Ecology 14:851-858.

Arnaiz-Villena, A., V. Ruiz-del-Valle, P. Gomez-Prieto, R. Reguera, C. Parga-Lozano, and I. Serrano-Vela. 2009. Estrildinae Finches (Aves, Passeriformes) from Africa, South Asia and Australia: a Molecular Phylogeographic Study. The Open Ornithology Journal 2:29-36.

Aslam, M. L., J. W. Bastiaansen, R. P. Crooijmans, A. Vereijken, H. J. Megens, and M. A. Groenen. 2010. A SNP based linkage map of the turkey genome reveals multiple intrachromosomal rearrangements between the turkey and chicken genomes. BMC Genomics 11:647.

Axelsson, E., N. Smith, H. Sundstrom, S. Berlin, and H. Ellegren. 2004. Male-biased mutation rate and divergence in autosomal, Z-linked and W-linked introns of chicken and turkey. Mol Biol Evol 21:1538–1547.

Ayala FJ, and M. Coluzzi. 2005. Chromosome speciation: Humans, Drosophila, and mosquitoes. Proc. Natl. Acad. Sci. USA 102:6535–42

Ayala, D., R. F. Guerrero, and M. Kirkpatrick. 2012. Reproductive isolation and local adaptation quantified for a chromosome inversion in a malaria mosquito. Evolution 67:946-958.

Ayers, K. L., N. M. Davidson, D. Demiyah, K. N. Roeszler, F. Grützner, A. H. Sinclair, A. Oshlack, and C. A. Smith. 2013. RNA sequencing reveals sexually dimorphic gene expression before gonadal differentiation in chicken and allows comprehensive annotation of the W-chromosome. Genome Biol. 14:R26.

Backström, N., W. Forstmeier, H. Schielzeth, H. Mellenius, K. Nam, E. Bolund, M. T. Webster, T. Ost, M. Schneider, B. Kempenaers, et al. 2010. The recombination landscape of the zebra finch *Taeniopygia guttata* genome. Genome Research 20:485-495.

Balakrishnan, C. N., and S. V. Edwards. 2009. Nucleotide variation, linkage disequilibrium and founder-facilitated speciation in wild populations of the zebra finch (*Taeniopygia guttata*). Genetics 181:645-660.

Baldassarre, D. T., and M. S. Webster. 2013. Experimental evidence that extra-pair mating drives asymmetrical introgression of a sexual trait. Proceedings of the Royal Society of London B: Biological Sciences 280:20132175.

Baldassarre, D. T., H. A. Thomassen, J. Karubian, and M. S. Webster. 2013. The role of ecological variation in driving divergence of sexual and non-sexual traits in the red-backed

fairy-wren (*Malurus melanocephalus*). BMC Evolutionary Biology 13:75.

Baldassarre, D. T., T. A. White, J. Karubian, and M. S. Webster. 2014. Genomic and morphological analysis of a semipermeable avian hybrid zone suggests asymmetrical introgression of a sexual signal. Evolution 68:2644-2657.

Barton, N. H., and G. M. Hewitt. 1985. Analysis of hybrid zones. Annual review of Ecology and Systematics 113-148.

Barton, N. H., and K. S. Gale. 1993. Genetic analysis of hybrid zones. Conference: *Symposium on Hybrid zones and the evolutionary process*, pp 13-45. Ed Harrison, R. G. at the 4th International Congress of Systematic and Evolutionary Biology (ICSEB).

Baudat, F. and B. de Massy. 2007. Regulating double-stranded DNA break repair towards crossover or non-crossover during mammalian meiosis. Chromosome Resarch 15:565–577.

Bartoń, K. 2013. MuMIn: multi-model inference. *R package version 1. 5*.

Baudat, F., and B. de Massy. 2007. Regulating double-stranded DNA break repair towards crossover or non-crossover during mammalian meiosis. Chromosome Research 15:565-577.

Bed'Hom, B., P. Coullin, Z. Guillier-Gencik, S. Moulin, A. Bernheim, and V. Volobouev. 2003. Characterization of the atypical karyotype of the black-winged kite *Elanus caeruleus* (Falconiformes: *Accipitridae*) by means of classical and molecular cytogenetic techniques. Chromosome Research 11:335-343.

Blount, J. D., N. B. Metcalfe, K. E. Arnold, P. F. Surai, G. L. Devevey, and P. Monaghan. 2003. Neonatal nutrition, adult antioxidant defences and sexual attractiveness in the zebra finch. Proceedings of the Royal Society of London B: Biological Sciences 270:1691-1696.

Boles, W. E. 1988. Comments on the subspecies of Australian native and introduced finches. Emu 88:20-24.

Bollback, J. P. 2006. SIMMAP: stochastic character mapping of discrete traits on phylogenies. BMC bioinformatics 71: 88.

Brown K. M., L. M. Burk, L. M. Henagan, and M. A. F. Noor. 2004. A test of the chromosomal rearrangement model of speciation in *Drosophila pseudoobscura*. Evolution 58:1856–60.

Castiglia, R. 2014. Sympatric sister species in rodents are more chromosomally differentiated than allopatric ones: implications for the role of chromosomal rearrangements in speciation. Mammal Review 44:1-4.

Charlesworth, B. 1991. The evolution of sex chromosomes. Science 251:1030–1033.

Charlesworth, D., and B. Charlesworth. 1979. Selection on recombination in clines. Genetics 91:581-589.

Charlesworth, B., and D. Charlesworth. 2000. The degeneration of Y chromosomes. Philosophical Transactions: Biological Sciences 355:1563–1572.

Charlesworth, B., J. A. Coyne, and N. H. Barton. 1987. The relative rates of evolution of sex chromosomes and autosomes. American Naturalist, 113-146.

Chen, N., D. W. Bellott, D. C. Page, and A. G. Clark. 2012. Identification of avian W-linked contigs by short-read sequencing. BMC genomics 13:183.

Christidis, L. 1983. Extensive chromosomal repatterning in two congeneric species: *Pytilia melba*, and *Pytilia phoenicoptera* (Swainson *Estrildidae*); Aves. Cytogenetic and Genome Research 364:641-648.

—. 1986a. Chromosomal evolution within the family *Estrildidae* Aves I. The Poephilae. Genetica 712:81-97.

—. 1986b. Chromosomal evolution within the family *Estrildidae* Aves II. The Lonchurae. Genetica 712:99-113.

—. 1987. Chromosomal evolution within the family *Estrildidae* Aves III. The Estrildae waxbill finches. Genetica 722:93-100.

—.1990. Aves, Pages 116 in B. John, ed., Animal Cytogenetics. Berlin and Stuttgart, Gebrüder Bornträger.

Claramunt, S., and J. Cracraft. 2015. A new time tree reveals Earth historys imprint on the evolution of modern birds. Science Advances 1:e1501005–e1501005.

Cole, C. T. 2003. Genetic variation in rare and common plants. Annual Review of Ecology, Evolution, and Systematics, 213-237.

Coyne, J. A. 1992. Genetics and speciation. Nature 355:511.

Coyne, J.A., and H. A. Orr. 1989. Two rules of speciation. In *Speciation and Its Consequences* (Otte, D. and Endler, J., eds), pp. 180–207, Sinauer Associates.

Coyne, J. A., and H. A. Orr. 2004. Speciation (Vol. 37). Sunderland, MA: Sinauer Associates.

Cracraft, J. 1986. Origin and evolution of continental biotas: speciation and historical congruence within the Australian avifauna. Evolution 40:977-996.

Cruickshank, T. E., and M. W. Hahn. 2014. Reanalysis suggests that genomic islands of speciation are due to reduced diversity, not reduced gene flow. Molecular ecology 23:3133-3157.

Cui, R., M. Schumer, K. Kruesi, R. Walter, P. Andolfatto, and G. G. Rosenthal. 2013. Phylogenomics reveals extensive reticulate evolution in *Xiphophorus* fishes. Evolution 67:2166-2179.

Cuthill, I. C., A. T. D. Bennett, J. C. Partridge, and E. J. Maier. 1999. Plumage reflectance and the objective assessment of avian sexual dichromatism. American Naturalist 153:183-200

Dagilis, A. J. and M. Kirkpatrick. 2016. Prezygotic isolation, mating preferences, and the evolution of chromosomal inversions. Evolution 70:1465–1472.

Dalloul, R. A., J. A. Long, A. V. Zimin, L. Aslam, K. Beal, L. A. Blomberg, P. Bouffard, D. W. Burt, O. Crasta, R. P. M. A. Crooijmans. 2010. Multi-platform next-generation sequencing of the domestic turkey (*Meleagris gallopavo*): genome assembly and analysis. PLoS biology 8: e1000475.

de Massy, B. 2013. Initiation of meiotic recombination: how and where? Conservation and specificities among eukaryotes. Annu. Rev. Genet. 47:110711-155423.

de Oliveira E. H. C., F. A. Habermann, O. Lacerda, I. J. Sbalqueiro, J. Wienberg, and S. Muller. 2005. Chromosome reshuffling in birds of prey: the karyotype of the worlds largest eagle (Harpy eagle, *Harpia harpyja*) compared to that of the chicken (*Gallus gallus*). Chromosoma 114:338-343.

del Hoyo, J., A. Elliott, and A. D. Christie. 2003-2011. *Handbook of the Birds of the World. Vols 8–16*. (Lynx Edicions).

Derryberry, E. P., G. E. Derryberry, J. M. Maley, and R. T. Brumfield. 2014. HZAR: hybrid zone analysis using an R software package. Molecular Ecology Resources 14:652-663.

Dobzhansky, T. 1951 Genetics and the origin of species (eds N. Eldredge and S. J. Gould), 3rd edn. New York, NY: Columbia University Press.

Drummond, A. J., and A. Rambaut. 2007. BEAST: Bayesian evolutionary analysis by sampling trees. BMC evolutionary biology, 71: 214.

Drummond, A. J., M. A. Suchard, D. Xie, and A. Rambaut. 2012. Bayesian phylogenetics with BEAUti and the BEAST 1.7. Molecular biology and evolution 29:1969-1973.

Dumont, B. L., and B. A. Payseur. 2008. Evolution of the genomic rate of recombination in mammals. Evolution 62:276-294.

Dumont, B. L., and B. A. Payseur. 2011. Evolution of the genomic recombination rate in murid rodents. Genetics 187:643-657.

Dunning, J. B. 1993. *Handbook of avian body masses.* (CRC, Boca Raton).

Eaton, D. A., and R. H. Ree. 2013. Inferring phylogeny and introgression using RADseq data: an example from flowering plants (*Pedicularis*: *Orobanchaceae*). Systematic Biology 62:689-706.

Ellegren, H. 2009. Genomic evidence for a large-Z effect. Proceedings of the Royal Society B: Biological Sciences 276:361-366.

—. 2010. Evolutionary stasis: the stable chromosomes of birds. Trends in Ecology and Evolution 255:283-291.

—. 2013. The evolutionary genomics of birds. Annual Review of Ecology, Evolution, and Systematics 44:239-259.

Ellegren, H. and A. K. Fridolfsson. 1997. Male–driven evolution of DNA sequences in birds. Nature Genetics 17:182–184.

Faria, R., and A. Navarro. 2010. Chromosomal speciation revisited: rearranging theory with pieces of evidence. Trends in Ecology and Evolution 25:660-669.

Feder, J. L., R. Gejji, T. H. Powell, and P. Nosil. 2011. Adaptive chromosomal divergence driven by mixed geographic mode of evolution. Evolution 658:2157-2170.

Fishman, L., A. Stathos, P. M. Beardsley, C. F. Williams, and J. P. Hill. 2013. Chromosomal rearrangements and the genetics of reproductive barriers in *Mimulus* (monkey flowers). Evolution 67:2547-2560.

Fitzsimmons, K. E., T. J. Cohen, P. P. Hesse, J. Jansen, G. C. Nanson, J. H. May, T. T. Barrows et al. 2013. Late Quaternary palaeoenvironmental change in the Australian drylands. Quaternary Science Reviews 74:78-96.

Ford, J. 1979. Speciation or Subspeciation in the Yellow Robins? Emu 79:103-106.

—. 1981. Geographical variation in Cinclosoma castanotum and its historical significance. Emu 81:185-192.

—. 1987a. Minor isolates and minor geographical barriers in avian speciation in continental Australia. Emu 87:90-102.

—. 1987b. Hybrid zones in Australian birds. *Emu*, 87:158-178.

Gay, L., P. A. Crochet, D. A. Bell, and T. Lenormand. 2008. Comparing clines on molecular and phenotypic traits in hybrid zones: a window on tension zone models. Evolution 62:2789-2806.

Goodwin, D., and M. Woodcock. 1982. Estrildid finches of the world. London: British Museum Natural History.

Grafen, A. 1989. The Phylogenetic Regression. *Philos. Trans. R. Soc. Lond. Ser. B–Biol. Sci.* 326:119–157.

Grant, P. R., and B. R. Grant. 2011. How and why species multiply: the radiation of Darwin's finches. Princeton University Press.

Graves, J. A. M. 2014. Avian sex, sex chromosomes, and dosage compensation in the age of genomics. Chromosome Research 22:45-57.

Griffin, D. K., L. B. Robertson, H. G. Tempest, B. M. and Skinner. 2006. The evolution of the avian genome as revealed by comparative molecular cytogenetics. Cytogenetic and genome research 117: 64-77.

Griffith, S. C., and D. M. Hooper. 2017. Geographical variation in bill colour in the Long-tailed Finch: evidence for a narrow zone of admixture between sub-species. Emu 117:1-10.

Haldane, J., 1927 A mathematical theory of natural and artificial selection. Part V: selection and mutation. Math. Proc. Camb. Philos. Soc. 3:607–615.

Hansmann, T., I. Nanda, V. Volobouev, F. Yang, M. Schartl, T. Haaf, and M. Schmid. 2009. Cross-species chromosome painting corroborates microchromosome fusion during karyotype evolution of birds. Cytogenetic and genome research 126:281-304.

Hansson, B., M. Ljungqvist, D. A. Dawson, J. C. Mueller, J. Olano-Marin, H. Ellegren, and J. Å. Nilsson. 2009. Avian genome evolution: insights from a linkage map of the blue tit (*Cyanistes caeruleus*). Heredity 104:67-78.

Hedrick, P. W. 1981. The establishment of chromosomal variants. Evolution: 322-332.
Hirschi, M., Hauschteck-Jungen, E. and V. Zigwild. 1972. Karyotypen von zwei Vogelarten, *Euodice cantans* (*Estrildidae*) und *Emberiza flaviventris* (*Pyrrhuloxiidae*, Emberizinae). Cytologia 37:525-529.

Heinroth, O. 1900. Ornithologische Monatsberichte 8:22-23.

Higgins, P. J., J. M. Peter, and S. J. Cowling. (Eds). 2006. Handbook of Australian, New Zealand and Antarctic Birds. Vol. 7: Boatbill to Starlings. (Oxford University Press: Melbourne).

Higginson, D. M., K. B. Miller, K. A. Segraves, and S. Pitnick. 2012. Female reproductive tract form drives the evolution of complex sperm morphology. Proceedings of the National Academy of Sciences 109:4538-4543.

Hill, G. E. 1992. Proximate basis of variation in carotenoid pigmentation in male house finches. Auk 109:1-12.

Hoffmann, A. A., and L. H. Rieseberg. 2008. Revisiting the impact of inversions in evolution: from population genetic markers to drivers of adaptive shifts and speciation?. Annual review of ecology, evolution, and systematics 39:21-42.

Hooper, D. M., and T. D. Price. 2015. Rates of karyotypic evolution in Estrildid finches differ between island and continental clades. Evolution 69:890–903.

Hooper, D. M., and T. D. Price. 2017. Chromosomal inversion differences correlate with range overlap in passerine birds. Nature ecology and evolution *In Press*.

Hudson, E. J., and T. D. Price. 2014. Pervasive reinforcement and the role of sexual selection in biological speciation. Journal of Heredity 105:821–833.

Immelmann, K. 1965. Australian Finches in Bush and Aviary. (Angus and Robertson: Sydney).

Irwin, D. E., M. Alcaide, K. E. Delmore, J. H. Irwin, and G. L. Owens. 2016. Recurrent selection explains parallel evolution of genomic regions of high relative but low absolute differentiation in a ring species. Molecular ecology 25:4488-4507.

Itoh, Y., and A. P. Arnold. 2005. Chromosomal polymorphism and comparative painting analysis in the zebra finch. Chromosome Research 131:47-56.

Jaenike, J. 2001. Sex chromosome meiotic drive. Annual Review of Ecology and Systematics 25-49.

Jenks, G. F. 1967. The data model concept in statistical mapping. International Yearbook of Cartography 7:186–190.

Jones, F. C., M. G. Grabherr, Y. F. Chan, P. Russell, E. Mauceli, J. Johnson, R. Swofford et al. 2012. The genomic basis of adaptive evolution in threespine sticklebacks. Nature 484:55-61.

Joron, M., L. Frezal, R. T. Jones, N. L. Chamberlain, S. F. Lee, C. R. Haag, A. Whibley et al. 2011. Chromosomal rearrangements maintain a polymorphic supergene controlling butterfly mimicry. Nature 477:203-U102.

Kandul, N. P., V. A. Lukhtanov, and N. E. Pierce. 2007. Karyotypic diversity and speciation in *Agrodiaetus* butterflies. Evolution, 613:546-559.

Kawakami, T., L. Smeds, N. Backström, A. Husby, A. Qvarnström, C. F. Mugal, P. Olason, and H. Ellegren. 2014. A high-density linkage map enables a second-generation collared flycatcher genome assembly and reveals the patterns of avian recombination rate variation and chromosomal evolution. Molecular ecology 23:4035-4058.

Keast, A. 1958. Intraspecific variation in the Australian finches. Emu 58:219-246.

Kim, K. W., C. Bennison, N. Hemmings, L. Brookes, L. L. Hurley, S. C. Griffith, T. Burke, T. R. Birkhead, and J. Slate. 2017. A sex-linked supergene controls sperm morphology and swimming speed in a songbird. Nature ecology and evolution 1.

Kimura, M. 1962. On the probability of fixation of mutant genes in a population. Genetics 47:713.

King, M. 1993. Species Evolution: The Role of Chromosomal Change. Cambridge University Press, Cambridge, UK.

—. 1987. Chromosomal rearrangements, speciation and the theoretical approach. Heredity 59:1–6.

Kirkpatrick, M., and N. H. Barton. 2006. Chromosome inversions, local adaptation and speciation. Genetics 173:419-434.

Kirkpatrick, M. 2010. How and why chromosome inversions evolve. PLoS biology, 8:e1000501.

Kleven, O., F. Fossøy, T. Laskemoen, R. J. Robertson, G. Rudolfsen, and J. T. Lifjeld. 2009. Comparative evidence for the evolution of sperm swimming speed by sperm competition and female sperm storage duration in passerine birds. Evolution 63:2466-2473.

Knief, U., G. Hemmrich-Stanisak, M. Wittig, A. Franke, S. C. Griffith, B. Kempenaers, and W. Forstmeier. 2016. Fitness consequences of polymorphic inversions in the zebra finch genome. Genome biology 17:199.

Knief, U., W. Forstmeier, Y. Pei, M. Ihle, D. Wang, K. Martin, P. Opatová et al. 2017. A sex-chromosome inversion causes strong overdominance for sperm traits that affect siring success. Nature ecology and evolution 1.

Krasikova, A., A. Daks, A. Zlotina, and E. Gaginskaya. 2009. Polymorphic heterochromatic segments in Japanese quail microchromosomes. Cytogenetic and genome research 126:148-155.

Kunte, K., W. Zhang, A. Tenger-Trolander, D. H. Palmer, A. Martin, R. D. Reed, S. P. Mullen, and M. R. Kronforst. 2014. Doublesex is a mimicry supergene. Nature 507:229-232.

Lamichhaney, S., G. Fan, F. Widemo, U. Gunnarsson, D. S. Thalmann, M. P. Hoeppner, S. Kerje et al. 2016. Structural genomic changes underlie alternative reproductive strategies in the ruff (*Philomachus pugnax*). Nature Genetics 48:84.

Lande, R. 1979. Effective deme sizes during long-term evolution estimated from rates of chromosomal rearrangement. Evolution 33:234–251.

—. 1981. Models of speciation by sexual selection on polygenic traits. Proc Nat Acad Sci USA 78:3721–3725.

—. 1985. The fixation of chromosomal rearrangements in a subdivided population with local extinction and recolonisation. Heredity 54:323–332.

Lee, J. Y., and S. V. Edwards. 2008. Divergence across Australia's Carpentarian Barrier: Statistical phylogeography of the red-backed fairy wren (*Malurus melanocephalus*). Evolution 62:3117-3134.

Leffler, E. M., K. Bullaughey, D. R. Matute, W. K. Meyer, L. Segurel, A. Venkat, P. Andolfatto, and M. Przeworski. 2012. Revisiting an old riddle: what determines genetic diversity levels within species? PLoS Biology 10: e1001388.

Lemaitre, C., M. D. Braga, C. Gautier, M. F. Sagot, E. Tannier, and G. A. Marais. 2009. Footprints of inversions at present and past pseudoautosomal boundaries in human sex chromosomes. Genome Biology and Evolution 1:56-66.

Levan, A., K. Fredga, and A. A. Sandberg. 1964. Nomenclature for centromeric position on chromosomes. Hereditas 52:201-220.

Lithgow, P. E., R. O'Connor, D. Smith, G. Fonseka, A. Al Mutery, C. Rathje, R. Frodsham, P. O'Brien, F. Kasai, M. A. Ferguson-Smith, et al. 2014. Novel tools for characterising inter and intra chromosomal rearrangements in avian microchromosomes. Chromosome Res. 22:85-97.

Lopes, R. J., J. D. Johnson, M. B. Toomey, M. S. Ferreira, P. M. Araujo, J. Melo-Ferreira, L. Andersson, G. E. Hill, J. C. Corbo, and M. Carneiro. 2016. Genetic basis for red coloration in birds. Current Biology 26:1427-1434.

Lowery, R. K., G. Uribe, E. B. Jimenez, M. A. Weiss, K. J. Herrera, M. Regueiro, and R. J. Herrera. 2013. Neanderthal and Denisova genetic affinities with contemporary humans: Introgression versus common ancestral polymorphisms. Gene 530:83-94.

Lowry, D. B., and J. H. Willis. 2010. A widespread chromosomal inversion polymorphism contributes to a major life-history transition, local adaptation, and reproductive isolation. PLoS Biology 8:1-14.

Maddison, W. P., and D. R. Maddison. 2015. Mesquite: a modular system for evolutionary analysis. Version 3.02 http://mesquiteproject.org

Maia, R., C. M. Eliason, P. P. Bitton, S. M. Doucet, and M. D. Shawkey. 2013. pavo: an R package for the analysis, visualization and organization of spectral data. Methods in Ecology and Evolution 4:906-913.

Mank, J. E., and H. Ellegren. 2007. Parallel divergence and degradation of the avian W sex chromosome. Trends in Ecology and Evolution, 22:389-391.

Mank, J. E., K. Nam, and H. Ellegren. 2010a. Faster-Z evolution is predominantly due to genetic drift. Molecular biology and evolution, 27:661-670.

Mank, J. E., B. Vicoso, S. Berlin, and B. Charlesworth. 2010b. Effective population size and the Faster-X effect: empirical results and their interpretation. Evolution 64:663-674.

Marshall, O. J., A. C. Chueh, L. H. Wong, and K. H. Choo. 2008. Neocentromeres: new insights into centromere structure, disease development, and karyotype evolution. The American Journal of Human Genetics 82:261-282.

Martin, P. R., R. Montgomerie, and S. C. Lougheed. 2015. Color patterns of closely related bird species are more divergent at intermediate levels of breeding range sympatry. American Naturalist 185:443–451.

Masabanda, J. S., D. W. Burt, P. C. O'Brien, A. Vignal, V. Fillon, P. S. Walsh, H. Cox, H. G. Tempest, J. Smith, F. Habermann, et al. 2004. Molecular cytogenetic definition of the chicken genome: the first complete avian karyotype. Genetics 166:1367-1373.

Mayr, E., J. R. A. Paynter, and M. A. Traylor. 1968. Family Estrildidae. Pp. 306–390 *in* J. R. A. Paynter, ed. Check-list of birds of the world, vol. 14. Museum of Comparative Zoology, Cambridge, MA.

McCarthy, E. M. 2006. *Handbook of Avian Hybrids of the World*. (Oxford University Press).

Miller, G. T., and S. Pitnick. 2002. Sperm-female coevolution in Drosophila. Science 298:1230-1233.

Mittal, O.P., and V. L. Sharma. 1993. Karyotypes of three species of passerine birds (Estrildidae) Res. Bull. Punjab Univ. 43:105-115.

Moghadam, H. K., M. A. Pointer, A. E. Wright, S. Berlin, and J. E Mank. 2012. W chromosome expression responds to female-specific selection. Proc. Natl. Acad. Sci. USA 109:8207-8211.

Montgomerie, R. 2006. Analyzing colors. *Bird coloration*, *1*, 90-147. Eds G. E. Hill, and K. J. McGraw, Harvard University Press, Cambridge, MA.

Mundy, N. I., J. Stapley, C. Bennison, R. Tucker, H. Twyman, K. W. Kim, T. Burke, T. R. Birkhead, S. Andersson, and J. Slate. 2016. Red carotenoid coloration in the zebra finch is controlled by a cytochrome P450 gene cluster. Current Biology 26:1435-1440.

Nanda I., E. Karl, V. Volobouev, D. K. Griffin, M. Schartl, and M. Schmid. 2006. Extensive gross genomic rearrangements between chicken and Old World vultures (Falconiformes: *Accipitridae*). Cytogenet. Genome Res. 112:286-295.

Nanda, I., E. Karl, D. K. Griffin, M. Schartl, and M. Schmid. 2007. Chromosome repatterning in three representative parrots (Psittaciformes) inferred from comparative chromosome painting. Cytogenetic and genome research 117:43-53.

Navarro, A., and N. H. Barton. 2003. Accumulating postzygotic isolation genes in parapatry: a new twist on chromosomal speciation. Evolution 57:447-459.

Nevo, E., A. Beiles, and R. Ben-Shlomo. 1984. The evolutionary significance of genetic diversity: ecological, demographic and life history correlates (pp. 13-213). Springer Berlin Heidelberg.

Nie, W., P. C. O'Brien, B. L. Ng, B. Fu, V. Volobouev, N. P. Carter, M. A. Ferguson-Smith, and F. Yang. 2009. Avian comparative genomics: reciprocal chromosome painting between domestic chicken (*Gallus gallus*) and the stone curlew (*Burhinus oedicnemus*, Charadriiformes)—An atypical species with low diploid number. Chromosome Research 17:99-113.

Nishida, C., J. Ishijima, A. Kosaka, H. Tanabe, F. A. Habermann, D. K. Griffin, and Y. Matsuda. 2008. Characterization of chromosome structures of Falconinae (*Falconidae*, Falconiformes, Aves) by chromosome painting and delineation of chromosome rearrangements during their differentiation. Chromosome Research 16:171-181.

Nishida, C., S. Ishishita, K. Yamada, D. K. Griffin, and Y. Matsuda. 2014. Dynamic chromosome reorganization in the osprey (*Pandion haliaetus, Pandionidae*, Falconiformes): relationship between chromosome size and the chromosomal distribution of centromeric repetitive DNA sequences. Cytogenetic and genome Research 142:179-189.

Noor, M. A. F. 1997. How often does sympatry affect sexual isolation in Drosophila? American Naturalist 149:1156–1163.

Noor, M. A. F., L. A. Grams, L. A. Bertucci, Y. Almendarez, J. Reiland, and K. R. Smith. 2001. The genetics of reproductive isolation and the potential for gene exchange between *Drosophila pseudoobscura* and *D. persimilis* via backcross hybrid males. Evolution 55:512-521.

Ohno, S. 1967. *Sex chromosomes and sex-linked genes*. (Springer).

Ohta, T. 1972. Population size and rate of evolution. Journal of molecular evolution 1:305-314.

Ortiz-Barrientos D., J. Reiland, J. Hey, and M. A. F. Noor. 2002. Recombination and the divergence of hybridizing species. Genetica 116:167–78.

Paradis, E., S. R. Baillie, W. J. Sutherland, and R. D. Gregory. 1998. Patterns of natal and breeding dispersal in birds. Journal of Animal Ecology 67:518-536.

Patterson, N., A. L. Price, and D. Reich. 2006. Population structure and eigenanalysis. PLoS genetics 2:e190.

Payseur, B.A., and L. H.Rieseberg. 2016. A genomic perspective on hybridization and speciation. Molecular ecology 25:2337-2360.

Pebesma, E. J., and R. S. Bivand. 2016. sp: classes and methods for spatial data. R package version 0.9-44.

Peischl, S., and M. Kirkpatrick. 2012. Establishment of new mutations in changing environments. Genetics 191:895-906.

Peters, A., A. G. Denk, K. Delhey, and B. Kempenaers. 2004. Carotenoid-based bill colour as an indicator of immunocompetence and sperm performance in male mallards. Journal of evolutionary biology, 17:1111-1120.

Petkova, D., J. Novembre, and M. Stephens. 2016. Visualizing spatial population structure with estimated effective migration surfaces. Nature genetics 48:94-100.

Pinheiro, J., D. Bates, S. DebRoy, D. Sarkar, and R. C. Team. 2014. *nlme: Linear and nonlinear mixed effects models. R package version 3.1-117, http://CRAN.R-project.org/package=nlme*.

Poelstra, J. W., N. Vijay, C. M. Bossu, H. Lantz, B. Ryll, I. Mueller, V. Baglione, P. Unneberg, M. Wikelski, M. G. Grabherr, et al. 2014. The genomic landscape underlying phenotypic integrity in the face of gene flow in crows. Science 344:1410-1414.

Posada, D. 2008. jModelTest: phylogenetic model averaging. Molecular biology and evolution, 25: 1253-1256.

Puig, M., M. Cáceres, and A. Ruiz. 2004. Silencing of a gene adjacent to the breakpoint of a widespread Drosophila inversion by a transposon-induced antisense RNA. Proc Natl Acad Sci USA, 101:9013-9018.

Prasad, R., and S. C. Patnaik. 1977. Karyotypes of five passerine birds belonging to family *Ploceidae*. Caryologia 30:361-368.

Price, A. L., N. J. Patterson, R. M. Plenge, M. E. Weinblatt, N. A. Shadick, and D. Reich. 2006. Principal components analysis corrects for stratification in genome-wide association studies. Nature genetics 38:904-909.

Price, T. 2008. Speciation in birds. Roberts. Boulder CO.

Price, T. D., and M. M. Bouvier. 2002. The evolution of F1 postzygotic incompatibilities in birds. Evolution 56:2083–2089.

Price, T. D., D. M. Hooper, C. D. Buchanan, U. S. Johansson, D. T. Tietze, P. Alström, U. Olsson, M. Ghosh-Harihar, F. Ishtiaq, S. K. Gupta, et al. 2014. Niche filling slows the diversification of Himalayan songbirds. Nature 509:222-225.

Pritchard, J. K., M. Stephens, and P. Donnelly. 2000. Inference of population structure using multilocus genotype data. Genetics 155:945-959.

Prum, R. O., J. S. Berv, A. Dornburg, D. J. Field, J. P. Townsend, E. M. Lemmon, and A. R. Lemmon. 2015. A comprehensive phylogeny of birds (Aves) using targeted next-generation DNA sequencing. Nature 526:569-U247.

Purcell, S., B. Neale, K. Todd-Brown, L. Thomas, M. A. R. Ferreira, D. Bender, J. Maller et al. 2007. PLINK: a tool set for whole-genome association and population-based linkage analyses. The American Journal of Human Genetics 81:559-575.

R Core Team 2014. R: A language and environment for statistical computing. R Foundation for Statistical Computing, Vienna, Austria. ISBN 3-900051-07-0, URLhttp://www.R-project.org/.

Rambaut, A., and A. J. Drummond. 2007. Tracer v1. 4.

Ray-Chaudhuri, R. 1976. Cytotaxonomy and chromosome evolution in Passeriformes (Ayes). Journal of Zoological Systematics and Evolutionary Research, 14: 299-320.

Reeves, J. M., T. T. Barrows, T. J. Cohen, A. S. Kiem, H. C. Bostock, K. E. Fitzsimmons, J. D. Jansen et al. 2013a. Climate variability over the last 35,000 years recorded in marine and terrestrial archives in the Australian region: an OZ-INTIMATE compilation. Quaternary Science Reviews 74:21-34.

Reeves, J. M., H. C. Bostock, L. K. Ayliffe, T. T. Barrows, P. De Deckker, L. S. Devriendt, G. B. Dunbar et al. 2013b. Palaeoenvironmental change in tropical Australasia over the last 30,000 years–a synthesis by the OZ-INTIMATE group. Quaternary Science Reviews 74:97-114.

Rieseberg, L. H. 2001. Chromosomal rearrangements and speciation. Trends in Ecology and Evolution 16:351-358.

Rowe, M., S. C. Griffith, A. Hofgaard, and J. T. Lifjeld. 2015. Subspecific variation in sperm morphology and performance in the Long-tailed Finch (*Poephila acuticauda*). Avian Research 6:23.

Rutkowska, J., M. Lagisz, and S. Nakagawa. 2012. The long and the short of avian W chromosomes: no evidence for gradual W shortening. Biology Letters 8:636–638.

Schielzeth, H. 2010. Simple means to improve the interpretability of regression coefficients. Methods in Ecology and Evolution 1:103–113.

Schnute, J. T., N. Boers, R. Haigh, and A. Couture-Beil. 2015. PBSmapping: PBS Mapping 2.59. R package version. *cran.r-project.org*.

Shaw, K. L., and S. P. Mullen. 2014. Speciation continuum. Journal of Heredity 105:741-742.

Shields, G. F. 1982. Comparative avian cytogenetics: a review. Condor, 45-58.

Singhal, S., E. M. Leffler, K. Sannareddy, I. Turner, O. Venn, D. M. Hooper, A. I. Strand et al. 2015. Stable recombination hotspots in birds. Science 350:928-932.

Skinner, B. M., and D. K. Griffin. 2011. Intrachromosomal rearrangements in avian genome evolution: evidence for regions prone to breakpoints. Heredity 1081:37-41.

Smit A., R. Hubley, and P. Green. 1996–2010. RepeatMasker Open-3.0. www.repeatmasker.org.

Smukowski, C. S., and M. A. F. Noor. 2011. Recombination rate variation in closely related species. Heredity 107:496-508.

Sorenson, M. D., and R. B. Payne. 2001. A single ancient origin of brood parasitism in African finches: Implications for host-parasite coevolution. Evolution 55:2550-2567.

Sorenson, M. D., C. N. Balakrishnan, and R. B. Payne. 2004. Clade-limited colonization in brood parasitic finches (*Vidua* spp.). Systematic Biology 53:140-153.

Sousa, V., and J. Hey. 2013. Understanding the origin of species with genome-scale data: modelling gene flow. Nature Reviews Genetics 14:404-414.

Spirito, F. 1998. in *Endless forms: Species and speciation* (eds. Howard, D. J. and Berlocher, S. H.) 320–329 (Oxford Univ. Press).

Stapley, J., T. R. Birkhead, T. Burke, and J. Slate. 2008. A linkage map of the zebra finch *Taeniopygia guttata* provides new insights into avian genome evolution. Genetics 179:651-667.

Stebbins, G. L. 1958. The inviability, weakness and sterility of interspecific hybrids. Adv. Gen. 9:147–215.

Sturtevant, A. H. 1921. A case of rearrangement of genes in Drosophila. Proceedings of the National Academy of Sciences 7:235-237.

Szymura, J. M., and N. H. Barton. 1986. Genetic analysis of a hybrid zone between the fire-bellied toads, *Bombina bombina* and *B. variegata*, near Cracow in southern Poland. Evolution 40:1141-1159.

Takagi N. 1972. A comparative study of the chromosome replication in 6 species of birds. Japanese Journal of Genetics, 47: 115-123.

Takagi, N., and M. Sasaki. 1974. A phylogenetic study of bird karyotypes. Chromosoma 46: 91-120.

Turelli, M., and H. A. Orr. 2000. Dominance, epistasis and the genetics of postzygotic isolation. Genetics 154:1663–1679.

Tuttle, E. M., A. O. Bergland, M. L. Korody, M. S. Brewer, D. J. Newhouse, P. Minx, M. Stager et al. 2016. Divergence and functional degradation of a sex chromosome-like supergene. Current Biology 26:344-350.

van Rooij, E. P., and S. C. Griffith. 2010. Are monomorphic species really sexually indistinguishable: No evidence in wild Long-tailed Finches (*Poephila acuticauda*). Ethology 116:929-940.

van Rooij, E. P., and S. C. Griffith. 2011. Breeding ecology of an Australian estrildid, the Long-tailed Finch (*Poephila acuticauda*). Emu 111:297-303.

van Rooij, E. P., and S. C. Griffith. 2012. No evidence of assortative mating on the basis of putative ornamental traits in Long-tailed Finches *Poephila acuticauda*. *Ibis* 154:444-451.

Vicoso, B., and B. Charlesworth. 2009. Effective population size and the faster-X effect: an extended model. Evolution 63:2413-2426.

Vijay, N., C. M. Bossu, J. W. Poelstra, M. H. Weissensteiner, A. Suh, A. P. Kryukov, and J. B. W. Wolf. 2016. Evolution of heterogeneous genome differentiation across multiple contact zones in a crow species complex. Nature communications 7: 13195.

Völker, M., N. Backström, B. M. Skinner, E. J. Langley, S. K. Bunzey, H. Ellegren, and D. K. Griffin. 2010. Copy number variation, chromosome rearrangement, and their association with recombination during avian evolution. Genome Research 20:503-511.

Walsh, J. B. 1982. Rate of accumulation of reproductive isolation by chromosome rearrangements. American Naturalist 120:510–532.

Wang, C., X. Zhan, J. Bragg-Gresham, H. M. Kang, D. Stambolian, E. Y. Chew, K. E. Branham et al. 2014. Ancestry estimation and control of population stratification for sequence-based association studies. Nature genetics 46:409-415.

Warren, W. C., D. F. Clayton, H. Ellegren, A. P.Arnold, L. W. Hillier, A. Künstner, A., S. Searle, S. White, A. J. Viella, S. Fairley, et al. 2010. The genome of a songbird. Nature 464:757-762.

Weir, J. T., and T. D. Price. 2011. Limits to speciation inferred from times to secondary sympatry and ages of hybridizing species along a latitudinal gradient. American Naturalist 177:462–469.

Wesley, C. S., and W. F. Eanes. 1994. Isolation and analysis of the breakpoint sequences of chromosome inversion In (3L) Payne in Drosophila melanogaster. Proceedings of the National Academy of Sciences 91:3132-3136.

White, M. J. D. 1969. Chromosomal rearrangements and speciation in animals. Annu. Rev. Genet. 3:75–98.

—. 1978. Modes of speciation. San Francisco, CA: W.H. Freeman.

White, E. P., S. K. M. Ernest, A. J. Kerkhoff, and B. J. Enquist. 2007. Relationships between body size and abundance in ecology. Trends in Ecology and Evolution 22:323–330.

Whitlock, M. C., R. Bürger, and U. Dieckmann. 2004. Fixation of new mutations in small populations. Evolutionary conservation biology 155-170.

Wilson, M. A., and K. D. Makova. 2009. Genomic Analyses of Sex Chromosome Evolution. Annual Review of Genomics and Human Genetics 10:333–354.

Wright, A. E., and J. E. Mank. 2013. The scope and strength of sex-specific selection in genome evolution. Journal of evolutionary biology, 26:1841-1853.

Wright, A. E., P. W. Harrison, S. H. Montgomery, M. A. Pointer, and J. E. Mank. 2014. Independent stratum formation on the avian sex chromosomes reveals inter-chromosomal gene conversion and predominance of purifying selection on the W chromosome. Evolution 68:3281-3295.

Wright, A. E., P. W. Harrison, F. Zimmer, S. H. Montgomery, M. A. Pointer, and J. E. Mank. 2015. Variation in promiscuity and sexual selection drives avian rate of Faster-Z evolution. Molecular ecology 24:1218-1235.

Yan, L., Z. Liqing, Z. Dexiang, Z. Xiquan, and L. Xuemei. 2010. Faster evolution of Z-linked duplicate genes in chicken. Journal of Genetics and Genomics 37:695-702.

Yu, G., and T. T. Y. Lam. ggtree: a phylogenetic tree viewer for different types of tree annotations.

Zann, R. A. 1976. Variation in the songs of three species of estrildine grassfinches. Emu 76:97-108.

Zhang, G., C. Li, Q. Li, B. Li, D. M. Larkin, C. Lee, J. F. Storz, A. Antunes, M. J. Greenwold, R. W. Meredith, et al. 2014. Comparative genomics reveals insights into avian genome evolution and adaptation. Science 346:1311-1320.

Zlotina, A., S. Galkina, A. Krasikova, R. P. Crooijmans, M. A. Groenen, E. Gaginskaya, and S. Deryusheva. 2012. Centromere positions in chicken and Japanese quail chromosomes: de novo centromere formation versus pericentric inversions. Chromosome Research 20:1017-1032.